الجمهورية الجزائرية الديمقراطية الشعبية
People's democratic Republic of Algeria
وزارة التعليم العالي والبحث العلمي
Ministry of Higher Education and Scientific Research
جامعة الشهيد الشيخ العربي التبسي- تبسة
Echahid Cheikh Larbi Tebessi- Tebessa University
Faculty of Science and Technology

Civil Engineering Department

Master's Thesis

Presented for obtaining the Academic Master's degree

In: Civil Engineering

Specialty: Geotechnics

By: Brik Sajda

Title

Seismic bearing capacity and failure patterns of shallow foundation resting on cohesive-frictional (C-φ) soils containing single and double underground voids

Presented and publicly defended on 08/06/2026, before the jury composed of:

M/HOUAM Abdelkader	Pr	Président
M/Athamnia Brahim	MCA	Supervisor
M/Boufarh Rafik	Pr	Supervisor
M/ABDI Abdelmadjid	MCB	Examiner

Promotion : 2025/2026

Acknowledgements

First and foremost, we thank Almighty God for granting us the strength and guidance to complete this work.

We would like to express our deepest gratitude and sincere appreciation to our first supervisor **Athamnia Brahim** for his invaluable guidance, continuous support, constructive advice, and encouragement throughout the preparation of this dissertation.

We would also like to extend our heartfelt thanks to our second supervisor **Boufarh Rafik** for his valuable suggestions, insightful comments, and constant assistance, which greatly contributed to the successful completion of this work.

Our sincere appreciation is also extended to the honorable **members of the examination committee** for agreeing to evaluate this dissertation and for their valuable comments and recommendations that will undoubtedly enrich this research.

Finally, we would like to thank everyone who contributed, directly or indirectly, to the completion of this work. Their support, assistance, and encouragement have been greatly appreciated.

Dedication

In the name of Allah, the Most Gracious, the Most Merciful.

First and foremost, I dedicate this work to **my beloved father**, whose sacrifices, guidance, and unwavering support have been a constant source of strength throughout my academic journey.

To **my dear mother**, whose endless love, patience, prayers, and encouragement have always inspired me to persevere and achieve my goals. No words can truly express my gratitude for everything she has done for me.

To **my brothers**, for their love, understanding, and continuous support during every stage of my studies.

To all **my family members**, near and far, who have always believed in me and supported me with their prayers and encouragement.

To **my classmates, colleagues, and friends**, with whom I shared unforgettable moments, challenges, and achievements throughout these years of study.

To **everyone** who contributed, directly or indirectly, to the completion of this work.

To **all** those who extended a helping hand, offered valuable advice, encouragement, or support whenever I needed it.

With sincere gratitude and appreciation.

Abstract;

Underground cavities can significantly influence the performance of shallow foundations, particularly when seismic forces are involved. This study examines the effect of subsurface cavities on the seismic bearing capacity of a strip footing founded on cohesive soil. Particular attention is given to the influence of soil cohesion, cavity depth, cavity eccentricity, and the spacing between adjacent cavities on the overall response of the soil–foundation system.

A review of the literature was first conducted to examine conventional bearing-capacity theories and the methods commonly employed to assess foundation performance under earthquake loading. Previous investigations concerning underground cavities were also evaluated to identify the principal factors governing foundation stability in cavity-prone ground.

To investigate these effects, a numerical model was developed using the finite element method in PLAXIS 2D. Soil behaviour was simulated under the seismic excitation recorded during the Kobe earthquake. Three cavity arrangements were considered in the analysis: a single cavity, two symmetrically positioned cavities, and two parallel cavities.

The numerical results show that cavities located close to the footing lead to a marked reduction in seismic bearing capacity. The negative influence of cavities becomes less pronounced as cavity depth, cavity eccentricity, or the distance between adjacent cavities increases. In addition, higher soil cohesion was found to improve the resistance of the soil–foundation system and enhance its performance under seismic loading.

The study demonstrates that the interaction between foundations and underground cavities should be incorporated into geotechnical design procedures in earthquake-prone regions. The findings contribute to a better understanding of failure mechanisms and guide the design of foundations constructed above ground containing natural or artificial cavities.

Keywords: Seismic bearing capacity, shallow foundations, underground cavities, cohesive soil, Kobe earthquake, PLAXIS 2D, soil–foundation interaction, cavity depth, cavity eccentricity, cavity spacing.

Résumé ;

Les cavités souterraines peuvent influencer significativement le comportement des fondations superficielles, notamment en présence de sollicitations sismiques. Cette étude examine l'effet des cavités souterraines sur la capacité portante sismique d'une semelle filante reposant sur un sol cohérent. Une attention particulière est accordée à l'influence de la cohésion du sol, de la profondeur des cavités, de leur excentricité et de l'espacement entre cavités adjacentes sur la réponse globale du système sol-fondation.

Une revue de la littérature a d'abord été menée pour examiner les théories conventionnelles de la capacité portante et les méthodes couramment utilisées pour évaluer la performance des fondations sous chargement sismique. Des études antérieures relatives aux cavités souterraines ont également été analysées afin d'identifier les principaux facteurs régissant la stabilité des fondations dans les terrains sujets aux cavités.

Pour étudier ces effets, un modèle numérique a été développé à l'aide de la méthode des éléments finis dans PLAXIS 2D. Le comportement du sol a été simulé sous l'excitation sismique enregistrée lors du séisme de Kobe. Trois configurations de cavités ont été considérées dans l'analyse : une cavité unique, deux cavités disposées symétriquement et deux cavités parallèles.

Les résultats numériques montrent que les cavités situées à proximité de la semelle entraînent une réduction marquée de la capacité portante sismique. L'influence négative des cavités s'atténue à mesure que la profondeur, l'excentricité ou la distance entre cavités adjacentes augmentent. Par ailleurs, une cohésion plus élevée du sol améliore la résistance du système sol-fondation et renforce ses performances sous chargement sismique.

Cette étude démontre que l'interaction entre les fondations et les cavités souterraines doit être prise en compte dans les procédures de dimensionnement géotechnique dans les régions sismiques. Les résultats contribuent à une meilleure compréhension des mécanismes de rupture et orientent la conception des fondations établies au-dessus de terrains renfermant des cavités naturelles ou artificielles.

.

Mots-clés : : Capacité portante sismique, cavités souterraines, semelle filante, interaction sol–fondation, sol cohérent, PLAXIS 2D, éléments finis, séisme de Kobe.

Abstract

الملخص

تشكل التجاويف الجوفية أحد التحديات التي قد تؤثر في أداء الأساسات السطحية، خاصة في المناطق التي تتعرض للنشاط الزلزالي. ويزداد هذا التأثير عندما تكون التجاويف قريبة من الأساس أو تقع ضمن المنطقة المتأثرة بالإجهادات الناتجة عنه. لذلك تهدف هذه الدراسة إلى تقييم سلوك أساس شريطي مرتكز على تربة متماسكة في وجود تجاويف جوفية وتحت تأثير الأحمال الزلزالية، مع التركيز على عدد من العوامل التي يمكن أن تغير من استجابة النظام الترابي بشكل واضح.

في البداية، تم التطرق إلى المفاهيم الأساسية المرتبطة بالقدرة التحميلة للأساسات تحت الظروف الزلزالية، ثم مراجعة أهم الدراسات التي تناولت مشكلة التجاويف الجوفية وتأثيرها في استقرار المنشآت. بعد ذلك، أُنجز نموذج عددي باستعمال برنامج PLAXIS 2D لمحاكاة سلوك التربة والأساس أثناء التعرض لزلزال قوي. وشملت الدراسة ثلاث حالات مختلفة، تمثلت في وجود تجويف واحد، وتجويفين متناظرين، وتجويفين متوازيين، بهدف مقارنة تأثير كل حالة على أداء الأساس.

أظهرت النتائج أن وجود التجاويف يؤدي إلى تراجع القدرة التحميلة للأساس، ويكون هذا التراجع أكثر وضوحًا عندما تقع التجاويف بالقرب من منطقة تحميل الأساس. كما تبين أن زيادة عمق التجويف أو زيادة بعده عن محور الأساس تساهم في الحد من تأثيره. كذلك لوحظ أن زيادة المسافة الفاصلة بين التجاويف تقلل من التداخل بين تأثيراتها، مما ينعكس إيجابًا على استقرار التربة.

ومن جهة أخرى، بينت الدراسة أهمية تماسك التربة في تحسين مقاومتها للأحمال الزلزالية، حيث ساعد ارتفاع قيمة التماسك على تقليل التشوهات وتحسين قدرة النظام المكون من التربة والأساس على تحمل التأثيرات الديناميكية. وتؤكد هذه النتائج ضرورة مراعاة وجود التجاويف الجوفية عند تصميم الأساسات في المناطق المعرضة للزلازل، لما لذلك من دور في تجنب المشكلات المرتبطة بالهبوط أو فقدان الاستقرار، والمساهمة في الوصول إلى تصاميم أكثر أمانًا وموثوقية.

الكلمات المفتاحية: القدرة التحميلة الزلزالية، الأساس الشريطي، التجاويف الجوفية، التربة المتماسكة، الزلازل، العناصر المحدودة

List of Symbols and Acronyms

Symbol/ Acronym	Description	Unit
q_u	Ultimate bearing capacity	kPa
q_n	Net ultimate bearing capacity	kPa
Fy	Seismic bearing capacity	KN/m
γ	Unit weight of soil	kN/m³
c	Soil cohesion	kPa
φ	Internal friction angle	°
ψ	Dilatancy angle	°
E	Young's modulus	kN/m²
ν	Poisson's ratio	–
K_o	Coefficient of earth pressure at rest	–
FS	Factor of safety	–
Nc	Bearing capacity factor related to cohesion	–
Nq	Bearing capacity factor related to surcharge	–
Nγ	Bearing capacity factor related to unit weight	–
Sc	Shape factor related to cohesion	–
Sq	Shape factor related to surcharge	–
Sγ	Shape factor related to unit weight	–
dc	Depth factor related to cohesion	–
dq	Depth factor related to surcharge	–
dγ	Depth factor related to unit weight	–
ic	Inclination factor related to cohesion	–
iq	Inclination factor related to surcharge	–
iγ	Inclination factor related to unit weight	–
SPT	Standard Penetration Test	–
B	Width of the foundation	m
D	Depth of foundation	m
α	Cavity depth	**–**
β	Cavity eccentricity	**–**
S	Cavity spacing	**–**

List of Tables

Table I.1: Comparative summary of pseudo-static, pseudo-dynamic, and time-history methods for seismic bearing capacity assessment…….. 19
Table II.1 : Influence of void geometry parameters on foundation bearing capacity……35
Table II.2 : Mitigation measures for void-induced bearing capacity loss…….. 37
Table II.3 : Thematic grouping of key studies on foundation-void interaction…… 41
Table III.1: Bearing capacity factor Nc for varying void depth coefficients α…… 70

List of Figures

Figure I.1: Cross-sectional view of a continuous (strip) foundation……5
Figure I.2: Cross-sectional view of an isolated (pad) foundation……6
Figure I.3: Cross-sectional view of a raft ……6.
Figure I.4: Classification of foundation types (shallow, semi-deep, and deep)……7
Figure I.5: Load–settlement curve of a shallow foundation ……8.
Figure I.6: Types of shear failure: (a) general shear failure, (b) local shear failure, (c) punching shear……9.
Figure I.7: .Prandtl slip-line failure mechanism……10.
Figure I.8: Terzaghi's bearing capacity factors (Nc, Nq, Nγ) as a function of friction angle ……11
Figure I.9: Meyerhof's bearing capacity coefficients as a function of friction angle φ' ……11
Figure I.10: Types of seismic waves and associated particle motions Seismic ……13
Figure I.11: bearing capacity factors N^L as a function of φ and kh (Richards et al., I993) ……15
Figure II.1 : Schematic representation of a cavity beneath a shallow footing……..22
Figure II.2 : Centered strip footing above a continuous underground void (Baus & Wang, 1983)……24
Figure II.3 : Numerical model — FEM (Baus & Wang, 1983)…….25.
Figure II.4 : Experimental model (Baus & Wang, 1983)……26
Figure II.5 : Comparison between FEM results and physical model test results (Baus & Wang, 1983)……26
Figure II.6 : Representation of a footing system above a square void (Kiyosumi et al., 2007)…….27
Figure II.7 : Variation of R as a function of void depth and eccentricity (Kiyosumi et al., 2007)……27……..
Figure II.8 : Soil rupture patterns for different X values at Y/B = 1.5 (Kiyosumi et al., 2007)……28…..
Figure II.9 : Failure mechanism (Kiyosumi et al., 2007)……28.
Figure II.10 : Comparison of critical failure mechanisms with experimental observations (Kiyosumi et al., 2007)…….30
Figure II.11 : Problem definition (Lee et al., 2014)……30
Figure II.12 : Typical finite element mesh and boundary conditions (Lee et al., 2014)……31
Figure II.13 : Critical void location curve under a strip footing (Lee et al., 2014)……..31
Figure II.14 : Load-settlement curve comparison (Lavasan et al., 2016)…….31

Figure II.15 : Failure mechanism with two underground voids beneath the footing (Lavasan et al., 2016)…….32
Figure II.16 : Comparison of Nc values from the optimised void configuration with results from previous studies (Zhou et al., 2018)……..32
Figure II.17 : Critical bearing capacity location (Zhou et al., 2018)…….33
Figure II.18 : Failure mechanism for a single underground void (Zhou et al., 2018)……33
Figure II.19 : Critical influence zone concept beneath a strip footing……33
Figure II.20 : Schematic showing the combined effects of void geometry and seismic loading on bearing capacity…….34
Figure II.21 : Karst cavity (cave system)……42
Figure II.22 : Volcanic lava tube cavity……....42
Figure II.23 : Erosional cavity (canyon formation)……43
Figure II.24 : Glacial cavity (subglacial hollow)……44
Figure II.25 : Underground quarry……..44
Figure II.26 : Underground mine tunnel…….45
Figure II.27 : Troglodyte dwellings…….45
Figure II.28 : Underground shelter and religious site (catacombs)…….46
Figure II.29 : Progressive collapse mechanism of an underground cavity……..47
Figure II.30 : Ground subsidence above an underground cavity……48
Figure II.31 : Principle of gravimetric measurement for cavity detection…….49
Figure II.32 : Principle of electrical resistivity measurement……....49
Figure II.33 : Electromagnetic survey configuration…….50
Figure II.34 : Illustration of the coring method…….51
Figure II.35 : The Cone Penetration Test (CPT)……..51
Figure II.36: Procedure for Ground Penetrating Radar ……..52
Figure III.1: Problem definition — (a) single void, (b) symmetrical dual voids, (c) parallel dual voids……..56
Figure III.2: Input window for soil model selection in PLAXIS 2D …….58
Figure III.3: Input window for general material data in PLAXIS ……..58
Figure III.4: Input window for mechanical properties in PLAXIS 2D ……61
Figure III.5: Model geometry in PLAXIS 2D ……..66
Figure III.6: Hydraulic conditions as defined in PLAXIS 2D …….63
Figure III.7: Load configuration in PLAXIS 2D …….64
Figure III.8: Node and stress point positions within a 15-node triangular soil element …65
Figure III.9: Generated finite element mesh in PLAXIS 2D ……..66
Figure III.10: Calculation phase settings in PLAXIS 2D …….68
Figure III.11: Total horizontal displacement …….69
Figure III.12: Total vertical ……70
Figure III.13: Comparison between Nc derived from the present study and Lee et al. (2014)……71
Figure IV.1: Time history of seismic accelerogram …….75
Figure IV.2: Aplication of the imposed settelement in the PLAXIS 2D…….76
Figure IV.3: Effect of soil cohesion on seismic bearing (β=0)……..77

Figure IV.4: Effect of soil cohesion on seismic bearing capacity (β=1, β=2),……..78
Figure IV.5: Effect of soil cohesion on seismic bearing capacity (β=3, β=4)…….79
Figure IV.6: Effect of soil cohesion on seismic bearing (S=1)…….80
Figure IV.7: Effect of soil cohesion on seismic bearing (S=2,S=3)…….82
Figure IV.8: Effect of soil cohesion on seismic bearing capacity(S=1) …….83
Figure IV.9: Effect of soil cohesion on seismic bearing(S=2,S=3) …….84
Figure IV.10: Effect of cavity depth on seismic bearing capacity (β=0)……..85
Figure IV.11: Effect of cavity depth on seismic bearing capacity(β=1, β=2)……..87
Figure IV.12: Effect of cavity depth on seismic bearing (β=3, β=4)……88
Figure IV.13: Effect of cavity depth on seismic bearing (S=1)……89
Figure IV.14: Effect of cavity depth on seismic bearing(S=2,S=3) ……..90
Figure IV.15: Effect of cavity depth on seismic bearing (S=1, S=2,S=3)……..92
Figure IV.16: Effect of cavity eccentricity on seismic bearing capacity (α=1,α=2)…….94
Figure IV.17: Effect of eccentricity depth on seismic bearing capacity (α=3,α=4)……95
Figure IV.18: Effect of cavity spacing on seismic bearing capacity(α=1)……96
Figure IV.189 Effect of cavity spacing on seismic bearing capacity(α=2, α=3)…….96
Figure IV.20: Effect of cavity spacing on seismic bearing (α=1)……96
Figure IV.21: Effect of cavity spacing on seismic bearing capacity (α=2, α=3)……98
FigureIV.22: Comparison between static and seismic bearing capacity β=0(α=1, α=2)……99
Figure IV.23: Comparison between static and seismic bearing capacity β=1(α=1, α=2)..100
Figure IV.24: Comparison between static and seismic bearing capacity S=1(α=1, α=2)….101
Figure IV.25: Comparison between static and seismic bearing capacity S=1(α=1, α=2)…102
Figure IV.26: seismic failure mechanism……104
Figure IV.27: static failure mechanism……107

Table of contents

Acknowledgment

Dedication

Abstract

Résumé

الملخص

List of figures

List of Tables

List of Symbols and acronyms

General Introduction

Chapter I : Bearing capacity theory

I.1 Introduction……5
I.2 Types of Foundation……..5
I.2.1 Shallow Foundations……5
I.2.1.1 Continuous (Strip) Foundation……..5
I.2.1.2 Isolated (Pad) Foundation……..5
I.2.1.3 Raft Foundation……..…6
I.2.2 Semi-Deep Foundation……..…6
I.2.3 Deep Foundation……..7
I.3 Failure Mechanisms of Shallow Foundations…….7
I.3.1 General Shear Failure…….8
I.3.2 Local Shear Failure…….8
I.3.3 Punching Shear Failure……..8
I.4 Static Bearing Capacity of Shallow Foundations……....9
I.4.1 Terzaghi's Method……10
I.4.2 Meyerhof's Method……11
I.4.3 Brinch Hansen's Method……..12
I.4.4 Bearing Capacity from In Situ Tests…….12
I.4.4.1 Plate Load Test……..12
I.4.4.2 Cone Penetration Test (CPT)……12
I.4.4.3 Standard Penetration Test (SPT)……12
I.5 Seismic Bearing Capacity of Shallow Foundations……..12
I.5.1 Origin and Propagation of Earthquakes……12
I.5.2 Factors Affecting Bearing Capacity Under Seismic Loading……..…13
I.5.3 Literature Review on Seismic Bearing Capacity Methods……..13
1.5.3.1 Pseudo-Static Methods……...14
- Meyerhof (1953) and Richards et al. (1993)……..14
- Paolucci & Pecker (1997)…….15
- Choudhury & Subba Rao (2005)……..15
- Cascone & Casablanca (2016)……..…16

I.5.3.2 Pseudo-Dynamic Methods……16
- Steedman & Zeng (1990): Original Formulation……..16

- Choudhury & Nimbalkar (2005): Application to Bearing Capacity…….17
- Ghosh (2008)……...17
- Limitations of the Pseudo-Dynamic Method…….....17

I.5.3.3 Time-History (Direct Dynamic) Methods……17

- Theoretical Basis……..17
- Fishman et al. (2003): FEM Dynamic Analysis……18
- Gerolymos & Gazetas (2006)……18
- Gazetas et al. (2013): Foundation Rocking……..18
- Conti et al. (2013): Centrifuge Tests and FEM ……..19

Selection of Input Motions

I.5.4 Comparative Summary of Seismic Bearing Capacity Methods.....19

I.6 Conclusion……20

Chapter II: Voids Analysis

II.1. Introduction……..22
II.2. Definition…….22
II.3. Literature Review……23
II.3.1. Baus and Wang (1983)……..23
II.3.2. Kiyosumi et al. (2007, 2011)……27
II.3.3. Lee et al. (2014)……30
II.3.4. Lavasan et al. (2016)……32
II.3.5. Zhou et al. (2018)…….33
II.3.6. Void Geometry Effects on Foundation Bearing Capacity……34
II.3.6.1. Types of Void Geometries Studied……35
II.3.6.2. Influence of Void Geometry on Bearing Capacity……..35.
II.3.6.3. Critical Influence Zone — Depth and Horizontal Offset……36
II2.3.7. Factors Controlling Bearing Capacity of Shallow Foundations on Voided Soils…...37
II.3.7.1. Void Geometry, Depth, and Horizontal Offset……37
II.3.7.2. Soil Type and Strength…….37
II.3.7.3. Reinforcement and Layering Effects……37
II.3.7.4. Static Bearing Capacity…….....38
II.3.7.5. Seismic Bearing Capacity…….38
II.3.8. Additional Recent Studies and Emerging Approaches……..39
II.3.8.1. Single and Twin Voids in Cohesive-Frictional and Clay Soils……..39
II.3.8.2. Layered and Reinforced Systems with Voids…….39
II.3.8.3. Seismic Bearing Capacity with Voids……40
II.3.8.4. Spatial and Geological Uncertainty……...40
II.4. Classification of Cavities……..41
II.4.1. Natural Cavities……41
II.4.1.1. Karst Cavities……42
II.4.1.2. Volcanic Cavities……...42
II.4.1.3. Erosional Cavities……...43
II.4.1.4. Glacial Cavities……..43
II.4.2. Anthropogenic Cavities……44
II.4.2.1. Underground Quarries……45
II.4.2.2. Underground Mines……45
II.4.2.3. Caves and Troglodyte Dwellings……46

II.4.2.4. Underground Shelters and Religious Sites……46
II.5. Geotechnical Risks Associated with Cavities……47
II.5.1. Collapse……47
II.5.2. Subsidence……47
II.5.3. Pollution and Contamination……48
II.6. Cavity Identification Methods……48
II.6.1. Geophysical Methods……48
II.6.1.1. Gravimetric Methods……48
II.6.1.2. Electrical Resistivity Method……49
II.6.1.3. Electromagnetic Method……49
II.6.2. Geotechnical Methods……50
II.6.2.1. Boreholes and Coring……50
II.6.2.2. Cone Penetration Test (CPT)……50
II.6.3. Optical and Radar Methods……51
II.6.3.1. Ground Penetrating Radar (GPR)……51
II.6.3.2. Cameras and Drones……52
II.7. Conclusion……52

Chapter III: Numerical Analysis

III.1. Introduction……55
III.2. Geometry……55
III.3. Material Properties and Constitutive Model……56
III.4. Dynamic Damping Parameters (Rayleigh Coefficients)……61
III.5. Boundary Conditions……63
III.6. Hydraulic Conditions……63
III.7. Applied Load……63
III.8. Meshing……64
III.9. Calculation Phases……66
III.9.1. Initial Phase……66
III.9.2. First Phase – Application of Foundation Load……66
III.9.3. Second Phase – Introduction of Cavities……66
III.9.4. Third Phase – Plastic Failure Analysis……67
III.10. Analysis of Mesh Deformation and Displacements……68
III.10.1. Mesh Deformation……68
III.10.2. Total Horizontal Displacement……69
III.10.3. Total Vertical Displacement……69
III.11. Bearing Capacity……70
III.12. Conclusion……72

Chapter IV :Parametric study

IV.1. Introduction……74
IV.2. Result analysis……76
IV.2.1. The effect of soil on the seismic bearing capacity……76
IV.2.2. Influance of cavity depth……84
IV.2.3. Influance of cavity eccentricity……92
IV.2.4. Influance of cavity spacing……94
IV.3. Comparative study……98
IV.4. Failure mécanisme……103
IV.5.conclusion ……107
General Conclusion……108
References……111

General Introduction

In recent years, rapid urbanization and the growing demand for infrastructure have led to the construction of numerous engineering projects in areas affected by geotechnical and seismic hazards. In such environments, ensuring the stability and safety of structures is a major concern. Among the different factors that influence structural performance, the behavior of shallow foundations plays a fundamental role because these foundations transfer loads directly to the supporting soil.

The bearing capacity of soil is one of the most important parameters considered in foundation design. However, the presence of underground cavities may considerably affect this capacity. Whether formed naturally through geological processes or created by human activities, cavities represent a significant source of risk for civil engineering structures. Their existence alters the stress distribution within the soil mass and can lead to excessive settlements, loss of stability, or even foundation failure.

The problem becomes more complex when seismic loading is taken into account. During an earthquake, the dynamic interaction between the soil, the foundation, and the cavity may generate additional stresses and deformations that are not observed under static conditions. As a result, cavities that appear harmless under normal loading may become critical when subjected to seismic excitation.

Although the influence of underground cavities on shallow foundations has been investigated by several researchers, many aspects of the soil–foundation–cavity interaction remain insufficiently understood, particularly under earthquake loading. In addition, the effects of cavity geometry and position have not yet been fully clarified. Therefore, further studies are required to improve the understanding of these mechanisms and to provide useful information for engineering practice.

The present work focuses on the behavior of strip footings resting on soils containing underground cavities. Particular attention is given to the changes in bearing capacity caused by different cavity configurations under both static and seismic conditions. Numerical simulations are carried out using PLAXIS 2D, which offers an efficient framework for analyzing complex geotechnical problems and evaluating the response of the system under various loading scenarios.

Several parameters are examined throughout the study. These include cavity depth, eccentricity, inclination, and the spacing between adjacent cavities. By varying these parameters, it becomes possible to identify the configurations that have the greatest influence on foundation performance and to determine the conditions that may lead to a significant reduction in bearing capacity.

To ensure the reliability of the numerical analyses, the developed model is validated by comparison with reference results available in the literature. Once validated, the model is used to perform a detailed parametric investigation. The seismic behavior of the system is assessed using the acceleration record of the Kobe earthquake, allowing a realistic evaluation of the response of the soil–foundation–cavity system under dynamic loading.

The findings of this research are expected to contribute to a better understanding of foundation behavior in the presence of underground cavities and to provide practical guidance for the design of shallow foundations in both static and seismic environments.

This thesis is organized into four chapters.

Chapter 1 presents the theoretical background on shallow foundations and bearing capacity under static and seismic loading conditions.

Chapter 2 reviews underground cavities, their classification, formation mechanisms, and the principal techniques used for their detection.

Chapter 3 describes the numerical methodology adopted in this work, including model development in PLAXIS 2D and the validation procedure.

Finally, **Chapter 4** presents the parametric study and discusses the influence of different cavity configurations on the static and seismic bearing capacity of strip footings. The results are analyzed to identify the most critical cases and to highlight the governing factors affecting system behavior.

CHAPTER I

BEARING CAPACITY THEORY

Static Methods, Dynamic Methods and Seismic Literature Review

I.1 Introduction

Foundations are an important element in the construction of all civil engineering structures; they are designed to transmit the loads of superstructures to the supporting soil. The type of foundation used depends on the soil type, water level, and the seismicity of the site. This chapter presents the different types of foundation, failure mechanisms, and methods for calculating the bearing capacity of shallow foundations under both static and seismic conditions.

The chapter is organized as follows: Section 1.2 classifies foundation types; Section 1.3 describes static failure mechanisms; Section 1.4 covers classical static bearing capacity methods; Section 1.5 introduces seismic bearing capacity, including a comprehensive literature review of pseudo-static, pseudo-dynamic, and time-history approaches; and Section 1.6 concludes with recommendations for method selection.

I.2 Types of Foundation

I.2.1 Shallow Foundations

Shallow foundations are those in which the embedment depth is small compared to the plan dimensions. They transmit loads to the near-surface soil layer. Three types are distinguished: continuous (strip) foundations, isolated (pad) foundations, and raft foundations.

I.2.1.1 Continuous Foundation

A continuous (strip) foundation is a long element whose length-to-width ratio is approximately L/B = 10. It is placed beneath a wall or a closely spaced row of columns and is used when loads are distributed linearly along the soil.

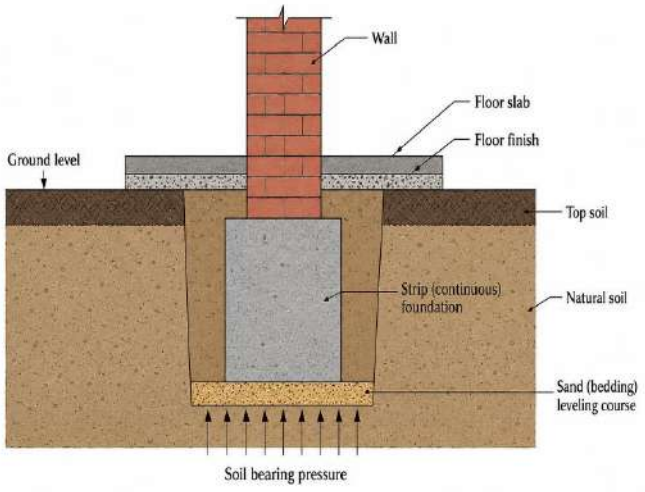


Figure I.*1: Cross-sectional view of a continuous (strip) foundation.*

I.2.1.2 Isolated Foundation

An isolated (pad) foundation is a square element with L/B ≈ 1, used when the load is concentrated at a single point, such as beneath a column.

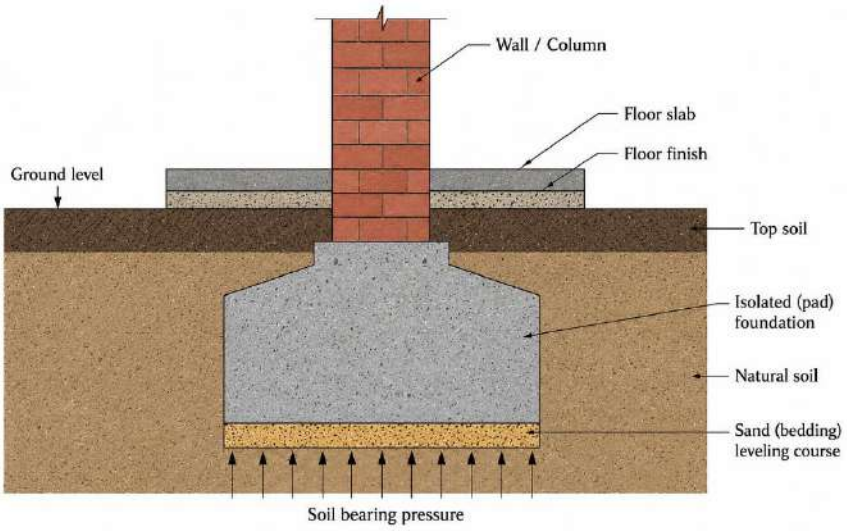


Figure I.*2: Cross-sectional view of an isolated (pad) foundation.*

I.2.1.3 Raft Foundation

A raft foundation consists of a reinforced concrete slab, typically 20 to 30 cm thick, covering the entire footprint of the structure. It is used when the soil contains underground cavities or when differential settlement must be minimized.

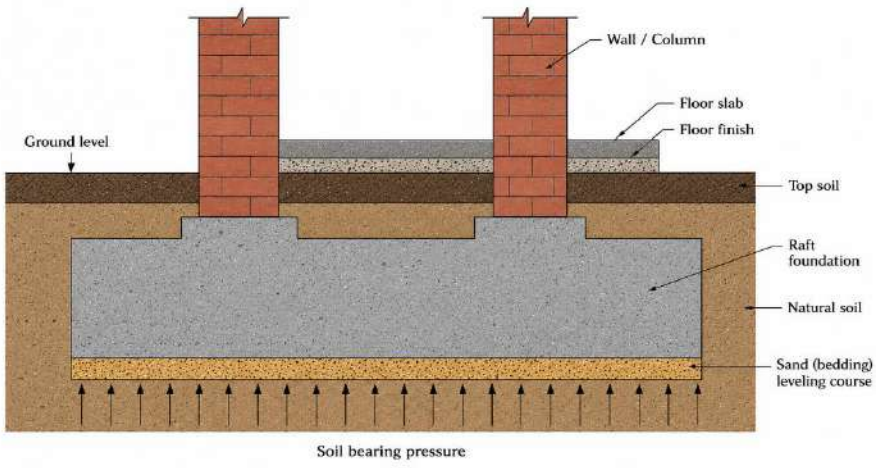


Figure I.*3: Cross-sectional view of a raft foundation.*

I.2.2 Semi-Deep Foundation

When shallow foundations are insufficient and deep foundations are not required, a semi-deep foundation is adopted. This type operates at a critical depth of 3 to 6 m and transmits loads to intermediate soil layers through lateral friction along the element.

I.2.3 Deep Foundation

Deep foundations are elements with an embedment depth greater than 6 m. They are used when the resistant soil layer lies at depth and transmit loads through end-bearing pressure and lateral skin friction

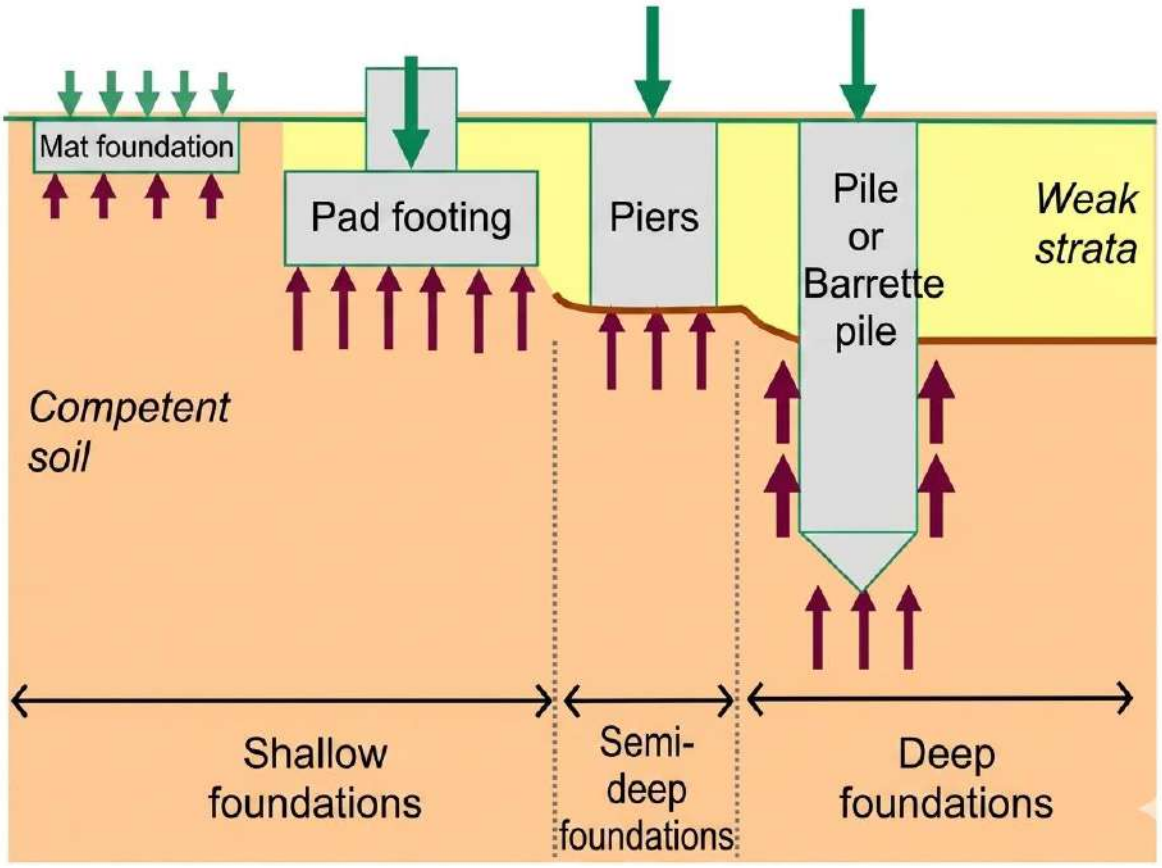


Figure I.*4: Classification of foundation types (shallow, semi-deep, and deep) [1].*

I.3 Failure Mechanisms of Shallow Foundations

During a shallow foundation load test, settlement initially increases proportionally with the applied load, indicating elastic behaviour. As the load continues to rise, settlements grow more rapidly even under small load increments, indicating that the soil is yielding. When the load reaches Q_l, punching failure occurs and the soil can no longer sustain additional loading. Beyond this point, large plastic deformations develop. The load Q_l represents the ultimate bearing capacity of the foundation.

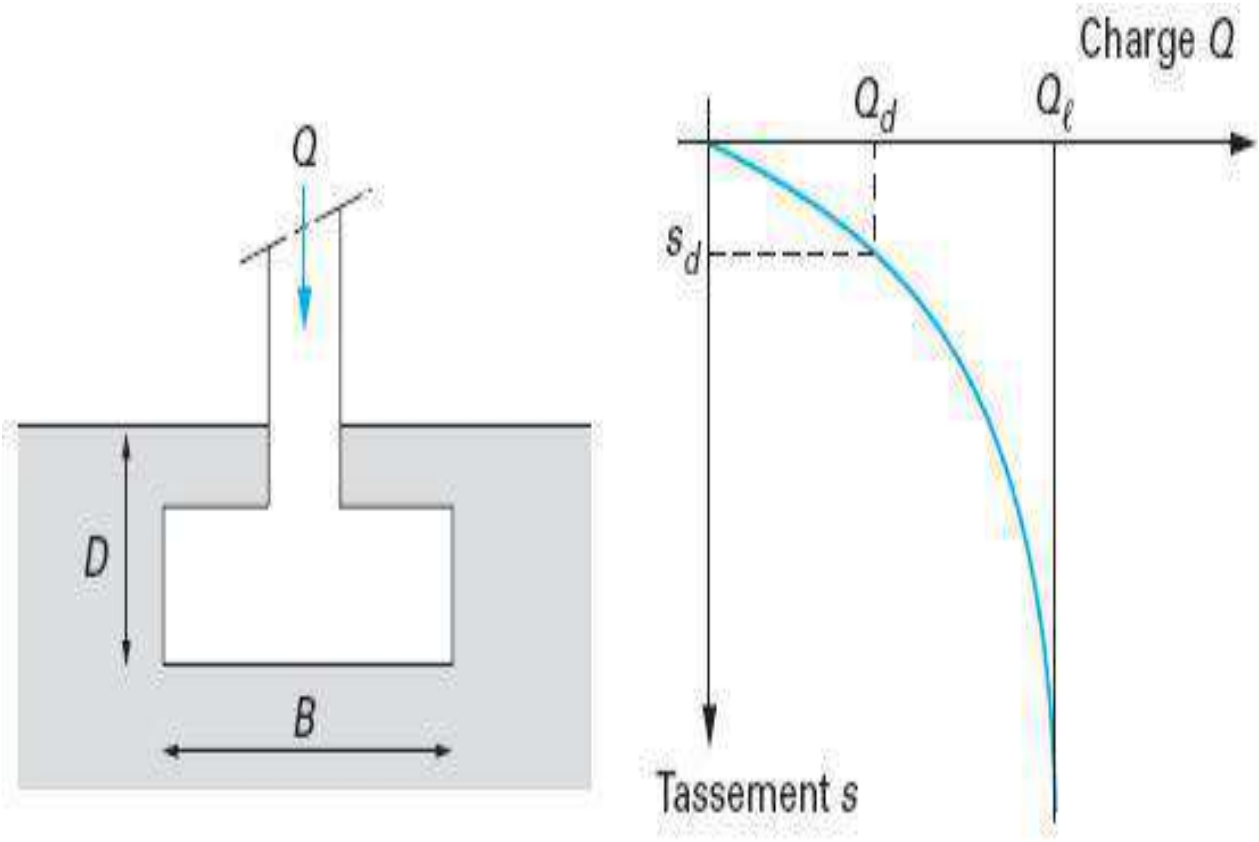


Figure I.*5: Load–settlement curve of a shallow foundation (Frank, Cuira&Burlon, 1999) [2].*

Three soil failure mechanisms are distinguished depending on the relative density of the soil.

I.3.1 General Shear Failure

This failure mode is characterised by the formation of a soil wedge beneath the footing, causing lateral displacement along shear surfaces extending to the ground surface. Failure is typically sudden. Soil heave may appear on both sides, but final collapse typically occurs on one side [3].

I.3.2 Local Shear Failure

In soils of medium relative density or intermediate consistency, slip surfaces develop only locally and do not extend to the ground surface. Some soil heave may appear on both sides of the foundation, usually after relatively large settlements [3].

I.3.3 Punching Shear Failure

In punching shear failure, the foundation sinks vertically with little disturbance to the surrounding soil. In cohesive soils, penetration is mostly undrained, while in granular soils, volume changes occur due to grain rearrangement [3].

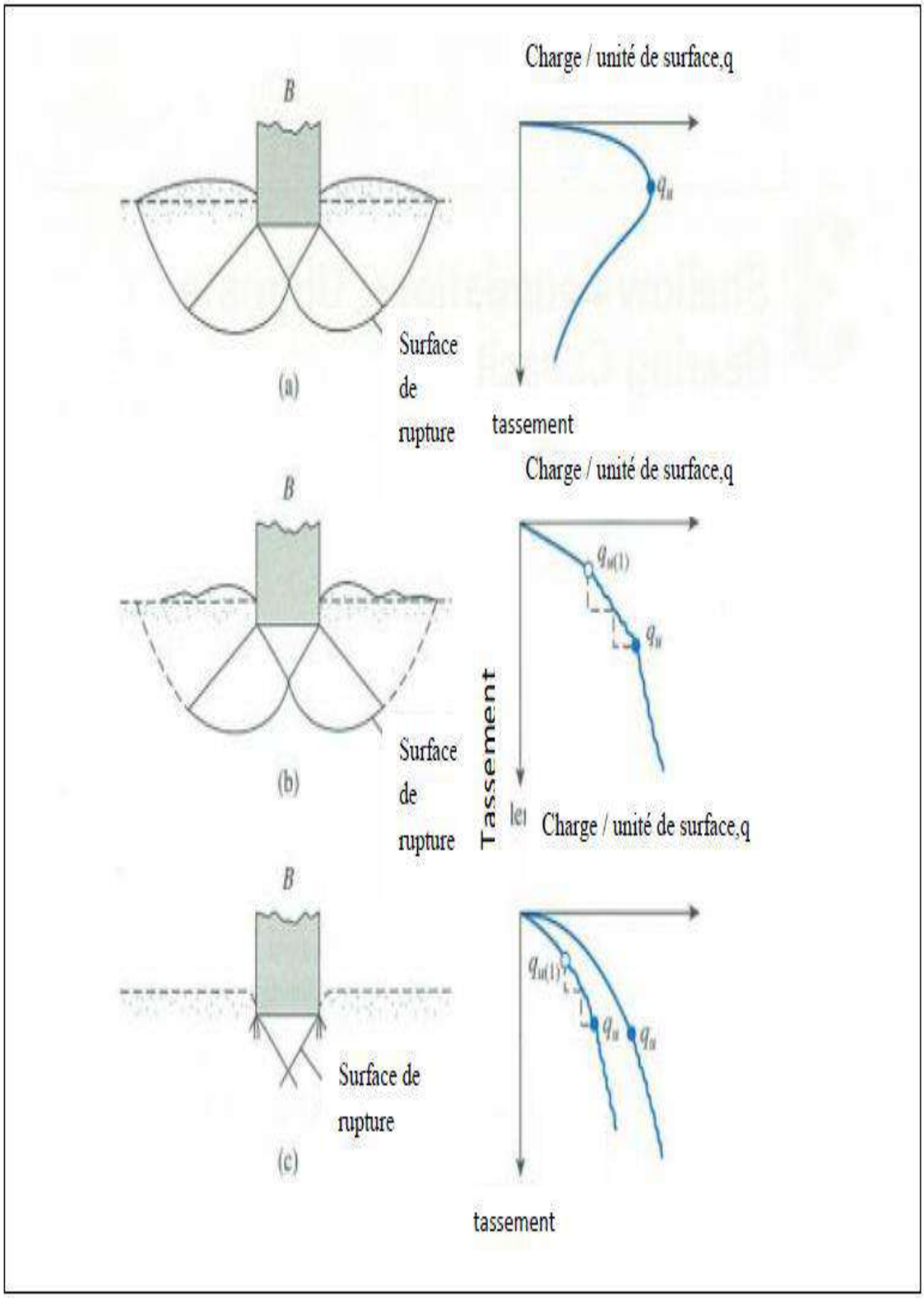


Figure I.6*: Types of shear failure: (a) general shear failure, (b) local shear failure, (c) punching shear failure [3].*

I.4 Static Bearing Capacity of Shallow Foundations

The evaluation of bearing capacity is one of the main challenges in geotechnical engineering. Several methods have been developed for this purpose, ranging from theoretical limit equilibrium solutions to empirical correlations derived from in situ tests.

I.4.1 Terzaghi's Method

According to Terzaghi (1943), the ultimate bearing capacity is calculated by superposing the contributions from soil cohesion, surcharge, and soil self-weight [4]:

$$qd = c \cdot Nc + q \cdot Nq + 0.5\gamma \cdot B \cdot N\gamma \quad \text{(I. 1)}$$

where:

$c = soil\ cohesion\ (kPa)$;

$q = overburden\ pressure\ (kPa)$;

$\gamma = unit\ weight\ \left(\frac{kN}{m^3}\right)$;

$B = footing\ width\ (m)$;

$Nc, Nq, N\gamma = dimensionless\ bearing\ capacity\ factors$.

The failure surface proposed by Prandtl (1921) consists of three zones: an active wedge (Region I) beneath the footing, a radial transition zone (Region II), and a passive zone (Region III) providing resistance.

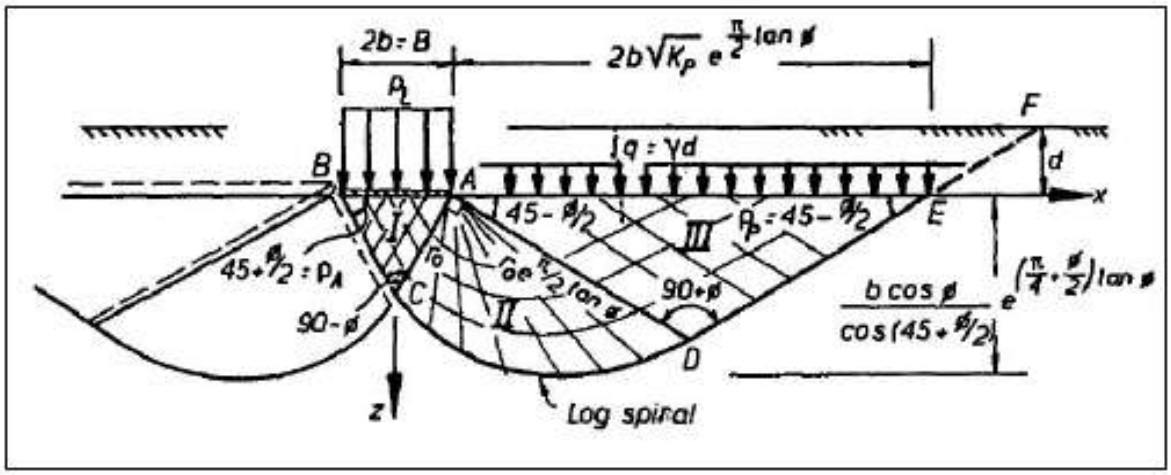


Figure I.*7: Prandtl slip-line failure mechanism (Richards et al., 1993) [5].*

ϕ'	N_c	N_q	N_γ*	ϕ'	N_c	N_q	N_γ*
0	5.70	1.00	0.00	26	27.09	14.21	9.84
1	6.00	1.10	0.01	27	29.24	15.90	11.60
2	6.30	1.22	0.04	28	31.61	17.81	13.70
3	6.62	1.35	0.06	29	34.24	19.98	16.18
4	6.97	1.49	0.10	30	37.16	22.46	19.13
5	7.34	1.64	0.14	31	40.41	25.28	22.65
6	7.73	1.81	0.20	32	44.04	28.52	26.87
7	8.15	2.00	0.27	33	48.09	32.23	31.94
8	8.60	2.21	0.35	34	52.64	36.50	38.04
9	9.09	2.44	0.44	35	57.75	41.44	45.41
10	9.61	2.69	0.56	36	63.53	47.16	54.36
11	10.16	2.98	0.69	37	70.01	53.80	65.27
12	10.76	3.29	0.85	38	77.50	61.55	78.61
13	11.41	3.63	1.04	39	85.97	70.61	95.03
14	12.11	4.02	1.26	40	95.66	81.27	115.31
15	12.86	4.45	1.52	41	106.81	93.85	140.51
16	13.68	4.92	1.82	42	119.67	108.75	171.99
17	14.60	5.45	2.18	43	134.58	126.50	211.56
18	15.12	6.04	2.59	44	151.95	147.74	261.60
19	16.56	6.70	3.07	45	172.28	173.28	325.34
20	17.69	7.44	3.64	46	196.22	204.19	407.11
21	18.92	8.26	4.31	47	224.55	241.80	512.84
22	20.27	9.19	5.09	48	258.28	287.85	650.67
23	21.75	10.23	6.00	49	298.71	344.63	831.99
24	23.36	11.40	7.08	50	347.50	415.14	1072.80
25	25.13	12.72	8.34				

I.*8: Terzaghi's bearing capacity factors (Nc, Nq, Nγ) as a function of friction angle φ' [4].*

I.4.2 Meyerhof's Method

Meyerhof (1951, 1963) extended Terzaghi's equation to account for foundation shape, load inclination, and embedment depth [6]:

$$ql = c \cdot Nc \cdot Sc \cdot dc \cdot ic + q \cdot Nq \cdot Sq \cdot dq \cdot iq + 0.5\gamma \cdot B' \cdot N\gamma \cdot S\gamma \cdot d\gamma \cdot i\gamma \quad (I.2)$$

The bearing capacity factors are:

- $Nc = (Nq - 1)\,cot\varphi$;
- $Nq = \exp(\pi\, tan\varphi)\, tan^2 45 + 2; = (Nq - 1)\, tan(1.4\varphi)$ [6].

Inclination factors:

- $ic = iq = \left(1 - \frac{\alpha}{90}^\circ\right)^2$;
- $i\gamma = (1 - \alpha/\varphi)^2$,

where α is the angle of the resultant load from the vertical axis.

Figure I.*9: Meyerhof's bearing capacity coefficients as a function of friction angle φ' [6].*

I.4.3 Brinch Hansen's Method

Brinch Hansen (1970) proposed a comprehensive generalized equation accounting for shape, depth, inclination, ground surface slope, and base tilt [7]:

$$qu = c \cdot Nc \cdot sc \cdot dc \cdot ic \cdot gc \cdot bc + q \cdot Nq \cdot sq \cdot dq \cdot iq \cdot gq \cdot bq + 0.5\gamma \cdot B' \cdot N\gamma \cdot s\gamma \cdot d\gamma \cdot i\gamma \cdot g\gamma \cdot b\gamma \quad (I.3)$$

I.4.4 Bearing Capacity from In Situ Tests

I.4.4.1 Plate Load Test

In accordance with NF P94-117-1, the plate load test evaluates bearing capacity from the load–settlement curve of a 600 mm rigid plate. The allowable capacity is: $qadm = qu / Fs$, with a safety factor Fs typically between 2 and 3.

I.4.4.2 Cone Penetration Test (CPT)

The CPT provides a continuous profile of tip resistance qc and sleeve friction fs without sample disturbance, enabling soil classification and bearing capacity estimation [8].

I.4.4.3 standard Penetration Test (SPT)

SPT N-values corrected for overburden (Liao & Whitman, 1985) and groundwater effects give $Ncor$. Meyerhof (1956, 1974) allowable bearing capacity [9]:

$$qa = (12/25) \cdot Se \cdot Ncor \cdot kd \quad (B \leq 1.22\,m) \quad (I.4a)$$

$$qa = (8/25) \cdot Se \cdot Ncor \cdot [(B + 0.305)/B]^2 \cdot kd \quad (B > 1.22\,m) \quad (I.4b)$$

$$kd = 1 + 0.33(D/B) \leq 1.33 \quad (I.4c)$$

I.5 Seismic Bearing Capacity of Shallow Foundations

Seismic loading introduces additional horizontal inertia forces and may trigger excess pore pressure in saturated soils, both of which reduce the bearing capacity of shallow foundations compared to the static case. The assessment of seismic bearing capacity requires not only quantification of the seismic forces but also a sound understanding of how those forces modify the failure mechanism and the mobilized soil resistance.

Three principal analytical frameworks have been developed to address this problem, in increasing order of rigour: the pseudo-static method, the pseudo-dynamic method, and the time-history (direct dynamic) method. The following section presents the theoretical basis of each approach, together with a critical review of the corresponding literature.

I.5.1 Origin and Propagation of Earthquakes

An earthquake results from the sudden release of elastic strain energy stored in the crust through the relative displacement of tectonic plates. The energy propagates outward from the focus as seismic waves: body waves (P- and S-waves) travel through the interior of the Earth, while surface

waves (Rayleigh and Love waves) propagate along the ground surface and carry the largest amplitudes at low frequencies [10].

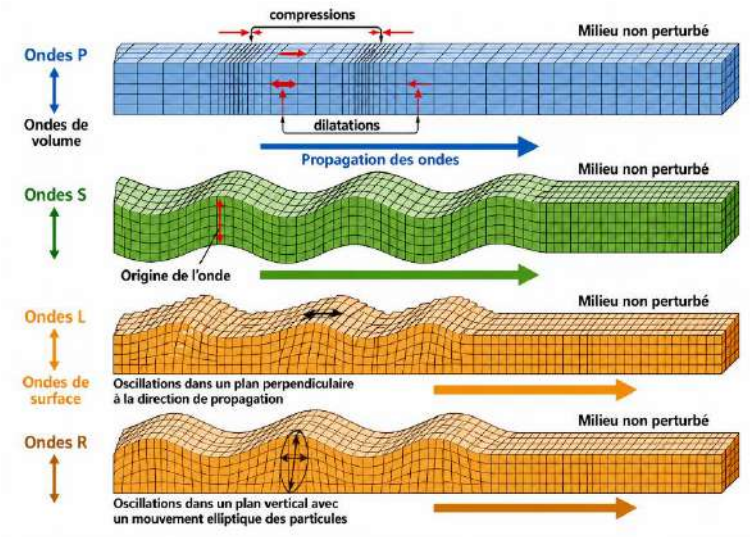


Figure I.*10: Types of seismic waves and associated particle motions [10]*.

I.5.2 Factors Affecting Bearing Capacity Under Seismic Loading

The principal effects of earthquake loading on bearing capacity are [11]:

- Rapid loading rate — may increase undrained shear strength by 30–60% in clays (strain-rate effect).
- Cyclic degradation — repeated loading reduces soil stiffness and strength in sensitive clays and loose sands.
- Excess pore pressure generation — in saturated granular soils, cyclic shear strains generate positive excess pore pressures that reduce effective confining stress and may trigger liquefaction.
- Inertia of the soil mass — horizontal seismic accelerations acting on the soil wedge within the failure mechanism reduce the net passive resistance available.
- Inertia of the structure — the seismic base shear and overturning moment introduce an eccentric and inclined load resultant on the footing.

I.5.3 Literature Review on Seismic Bearing Capacity Methods

The literature on seismic bearing capacity of shallow foundations is extensive and spans more than six decades. Contributions can be classified under three methodological families: pseudo-static, pseudo-dynamic, and time-history (direct dynamic) approaches. Each family is reviewed below, with particular attention to the theoretical basis, assumptions, and key findings of the principal works.

I.5.3.1 Pseudo-Static Methods

The pseudo-static method represents earthquake loading by a set of constant horizontal (and sometimes vertical) force equivalents applied to the soil–foundation system. The seismic acceleration components $kh \cdot g$ and $kv \cdot g$, where kh and kv are the horizontal and vertical seismic coefficients, replace the dynamic loading. This allows the problem to be treated as a modified static bearing capacity calculation.

The main limitation of the pseudo-static approach is that it ignores the transient and cyclic nature of earthquake loading: it neither accounts for the frequency content nor the phase relationship between soil and structural inertia. It is therefore conservative in many situations but may be non-conservative when the loading duration is short relative to the natural period of the system [12].

I.5.3.1.1 Meyerhof (1953) and Richards et al. (1993)

Meyerhof (1953) first extended the static bearing capacity framework to seismic conditions by introducing inclination factors that account for the equivalent horizontal seismic force [6]. He demonstrated that even a moderate horizontal seismic coefficient ($kh = 0.1–0.2$) could reduce bearing capacity by 30–50% in cohesion less soils.

Richards, Elms & Budhu (1993) formalized the seismic bearing capacity equation using Meyerhof's framework with modified seismic inclination factors N^{L} [5]:

$$q_l{}^{L} = c \cdot Nc^{L} + q_0 \cdot Nq^{L} + 0.5\gamma \cdot B' \cdot N\gamma^{L} \quad (I.5)$$

where $Nc^{L}, Nq^{L}, N\gamma^{L}$ are seismic bearing capacity factors that depend on both φ and the seismic inertia angle $\psi E = arctan[kh/(1 - kv)]$. They proposed design charts for N^{L} as a function of φ and kh, and identified a critical seismic acceleration beyond which the foundation undergoes progressive sliding and tilting.

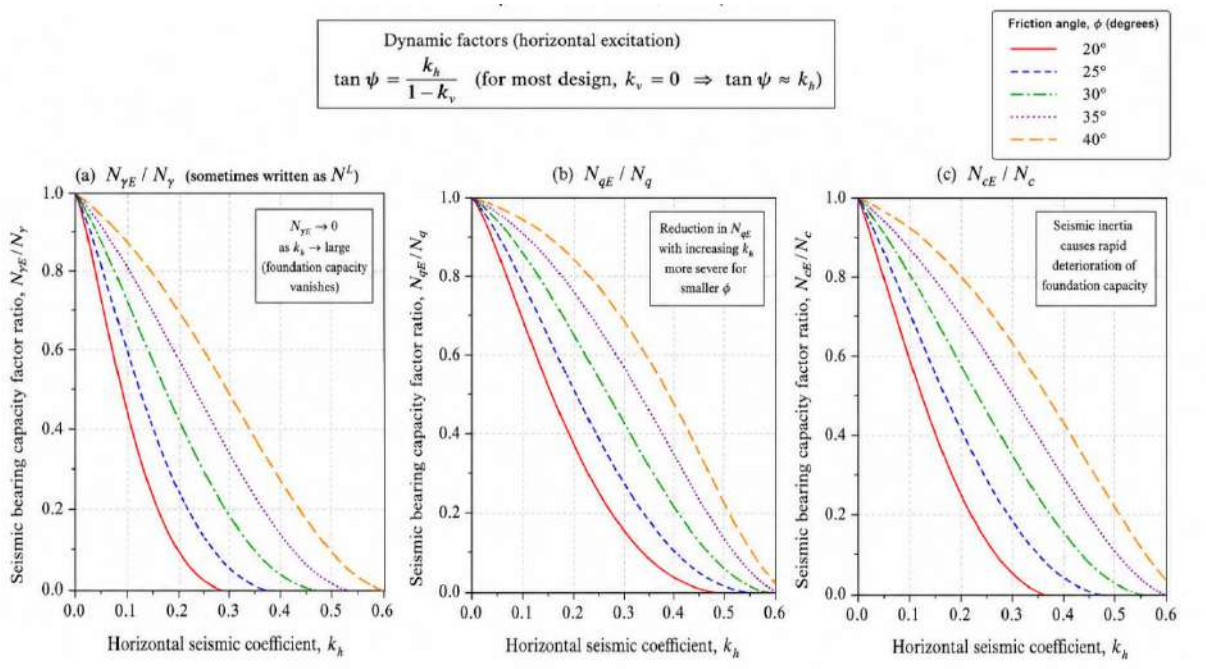


Figure I.*11: Seismic bearing capacity factors N^L as a function of φ and kh (Richards et al., 1993) [5].*

I.5.3.1.2 Paolucci & Pecker (1997)

Paolucci & Pecker (1997) carried out a systematic study of the combined effects of horizontal seismic loading, load eccentricity, and foundation embedment on the bearing capacity of strip footings on cohesive and frictional soils [13]. Using the kinematic approach of limit analysis, they derived closed-form seismic bearing capacity factors and proposed interaction diagrams in the $N-V-M$ (normal force–shear force–moment) space, which remain a reference in performance-based seismic design.

Their key finding was that the combined action of inertia in the structure and inertia in the soil mass must both be included simultaneously to avoid unconservative estimates, particularly in cohesive soils.

I.5.3.1.3 Choudhury & Subba Rao (2005)

Choudhury & Subba Rao (2005) extended the limit equilibrium approach to evaluate seismic bearing capacity factors for shallow foundations on c–φ soils under combined horizontal and vertical seismic loading [14]. They showed that both kh and kv significantly affect N^L and proposed explicit expressions suitable for hand calculation. Their results indicated that vertical seismic acceleration may either increase or decrease bearing capacity depending on its direction relative to the gravitational acceleration.

I.5.3.1.4 Cascone & Casablanca (2016)

Cascone & Casablanca (2016) revisited the pseudo-static problem using the stress characteristics (slip-line) method for strip footings on purely cohesive soils ($\varphi = 0$) under combined vertical load, horizontal seismic force, and moment [15]. They provided new bearing capacity factors and interaction diagrams validated against finite element results, demonstrating that the pseudo-static approach can be made accurate if an appropriate failure mechanism is assumed.

I.5.3.2 Pseudo-Dynamic Methods

The pseudo-dynamic method was introduced to overcome the main shortcoming of the pseudo-static approach: the assumption of a constant acceleration throughout the soil. In reality, seismic waves propagate through the soil with a finite velocity, creating a phase lag between the motion at different depths. The pseudo-dynamic approach captures this spatial variation by modelling the horizontal acceleration as a harmonic wave with a prescribed amplitude, frequency, and phase, while retaining the simplicity of a closed-form failure mechanism.

I.5.3.2.1 Steedman & Zeng (1990) — Original Formulation

Steedman & Zeng (1990) introduced the pseudo-dynamic concept in the context of retaining wall analysis [16]. They modelled the horizontal acceleration as a shear wave propagating vertically through the backfill:

$$ah(z,t) = kh \cdot g \cdot sin[\omega(t - (H-z)/Vs)] \quad (I.6)$$

where $\omega = 2\pi f$ is the circular frequency, Vs is the shear wave velocity, H is the height of the soil mass, and z is the depth below the surface. Integrating this acceleration over the Coulomb failure wedge yields a time-dependent seismic inertia force whose maximum value depends on the ratio $H/\lambda s$ (wavelength ratio), thus introducing a frequency effect absent from the pseudo-static method.

I.5.3.2.2 Choudhury & Nimbalkar (2005) — Application to Bearing Capacity

Choudhury & Nimbalkar (2005) applied the pseudo-dynamic concept to the seismic bearing capacity problem of strip footings on $c-\varphi$ soils [17]. Using the Coulomb failure mechanism with log-spiral transition zone, they computed the time-dependent seismic inertia forces in the soil wedge and derived the time at which the bearing capacity is minimum. Their results showed that the pseudo-dynamic factors $N^{L}(t)$ can be significantly lower than the pseudo-static estimates at certain amplification ratios, particularly for high frequencies.

The seismic bearing capacity factor $N\gamma^{L}$ in their formulation is:

$$N\gamma^{L}(t) = f\left(kh, kv, \varphi, f, \frac{H}{Vs}, \frac{t}{T}\right) \quad (I.7)$$

This expression, evaluated at the critical time $tcr = argmin\, N\gamma^{L}(t)$, constitutes the pseudo-dynamic seismic bearing capacity factor.

I.5.3.2.3 Ghosh (2008)

Ghosh (2008) extended the pseudo-dynamic approach to strip footings resting on the surface of c–φ soil with a log-spiral failure surface [18]. He included both horizontal and vertical seismic accelerations as harmonic waves propagating at velocities Vs (shear) and Vp (compression), respectively. His parametric study showed that the effect of the vertical seismic coefficient kv is more pronounced at higher kh values and at low friction angles.

I.5.3.2.4 Limitations of the Pseudo-Dynamic Method

Bellezza (2014) [19] and Pain et al. (2016) [20] pointed out that the Steedman–Zeng formulation violates the condition of zero stress at the ground surface because the assumed harmonic acceleration does not satisfy free-surface boundary conditions. Modified pseudo-dynamic formulations were proposed using standing wave solutions, which ensure zero stress at the surface and provide more physically consistent acceleration distributions. These modified formulations generally predict slightly lower seismic forces than the original Steedman–Zeng approach.

I.5.3.3 Time-History (Direct Dynamic) Methods

Time-history methods apply recorded or synthetic acceleration time histories as input motions to a nonlinear soil–foundation numerical model. They represent the highest level of rigour and can capture all aspects of dynamic soil behaviour: material nonlinearity, pore pressure generation, radiation damping, soil–structure interaction, and geometric nonlinearity. Their main drawbacks are computational cost and sensitivity to the selection of input motions.

I.5.3.3.1 Theoretical Basis

The equations of motion for the soil–foundation system are integrated step by step in time using an implicit or explicit numerical scheme (Newmark, Wilson-θ, or Hilber–Hughes–Taylor):

$$[M]\ddot{u}g + [C]\dot{u}g + [K(\varepsilon)]ug = -[M] \cdot \ddot{u}base(t) \qquad (I.8)$$

where $[M], [C], [K]$ are the mass, damping, and stiffness matrices; ug is the vector of nodal displacements relative to the base; and $\ddot{u}_{base}(t)$ is the applied base acceleration record. The stiffness $[K(\varepsilon)]$ is updated at each time step to account for material nonlinearity through the constitutive model (Mohr–Coulomb, Hardening Soil, MIT-E3, etc.).

Soil damping is typically modelled using Rayleigh damping:

$$[C] = \alpha R \cdot [M] + \beta R \cdot [K] \qquad (1.9)$$

where α_R and β_R are calibrated to match the target damping ratio ξ at two control frequencies f_1 and f_2 (typically the first and fifth natural modes of the soil column).

I.5.3.3.2 Fishman et al. (2003) — FEM Dynamic Analysis

Fishman, Yegian& Ladd (2003) performed dynamic finite element analyses of strip footings on soft clay subjected to earthquake loading using recorded ground motions from the 1989 Loma Prieta and 1994 Northridge earthquakes [21]. They showed that the peak dynamic bearing capacity factor Nc, dyn can differ from both the static and the pseudo-static estimates by up to 40%, depending on the amplitude, frequency content, and duration of the input motion.

I.5.3.3.3 Gerolymos & Gazetas (2006)

Gerolymos & Gazetas (2006) introduced a Winkler-type nonlinear dynamic macro-element model for shallow foundations subjected to seismic loading [22]. The macro-element represents the soil–foundation interface with coupled spring–dashpot–slider elements in the vertical, horizontal, and rotational degrees of freedom, and captures uplift, sliding, and soil yielding. This model has been widely used as a computationally efficient substitute for full three-dimensional FEM analyses in performance-based earthquake engineering.

I.5.3.3.4 Gazetas et al. (2013) — Foundation Rocking

Gazetas et al. (2013) revisited the role of foundation rocking as a seismic isolation mechanism for structures founded on shallow footings [23]. Using time-history analyses with a range of near-field and far-field records, they demonstrated that allowing controlled rocking — and hence mobilising the ultimate moment capacity of the foundation — can reduce structural ductility demands by a factor of 2–3 compared to the conventional ‘capacity design’ philosophy that prevents foundation yielding. This finding challenged the traditional design assumption that the foundation must remain elastic and contributed to the concept of ‘seismic design through foundation compliance’.

I.5.3.3.5 Conti et al. (2013) — Centrifuge Tests and FEM

Conti, Rovithis, Tamagnini, Anastasopoulos & Gazetas (2013) compared centrifuge model test results with nonlinear FEM time-history analyses for strip footings on dense sand subjected to strong ground motions [24]. The constitutive model used was a multi-surface kinematic hardening plasticity model (Papadimitriou &Bouckovalas, 2002). The comparison showed good agreement for both settlements and rotations, validating the use of advanced constitutive models in seismic foundation analysis.

I.5.3.3.6 Selection of Input Motions

Current seismic design standards (Eurocode 8, Part 5; ASCE 7-22) recommend a minimum of seven ground motion records for time-history analysis when the mean response is used as the design value [25, 26]. Records must be selected to match the target uniform hazard spectrum at the site in terms of: (i) spectral shape, (ii) magnitude and distance, (iii) soil class, and (iv) near-fault directivity effects where applicable. When fewer than seven records are used, the maximum rather than the mean response must be taken as the design value.

1.5.4 Comparative Summary of Seismic Bearing Capacity Methods

Table 1.2 provides a structured comparison of the three methodological families reviewed above.

Table 1.2: Comparative summary of pseudo-static, pseudo-dynamic, and time-history methods for seismic bearing capacity assessment.

Method	**Input Parameters**	**Frequency Effect**	**Nonlinearity**	**Typical Application**
Pseudo-Static	kh, kv, φ, c, B, D	None — constant acceleration	Implicit (limit state)	Preliminary design; low-to-moderate seismicity; simple structures
Pseudo-Dynamic	$kh, kv, \varphi, c, B, H, Vs$	Yes — harmonic wave; phase lag with depth	Implicit (limit state)	Intermediate design; sites with dominant frequency; retaining walls, footings
Time-History (FEM/FDM)	Full constitutive model; acceleration record; soil profile	Yes — full frequency content of record	Full material + geometric nonlinearity	Detailed design; critical structures; near-fault sites; performance-based design

I.6 Conclusion

Accurately determining the bearing capacity of foundations is essential for the design of safe and reliable structures under both static and seismic conditions. This chapter has reviewed the principal static bearing capacity methods (Terzaghi, Meyerhof, Brinch Hansen) and in situ test approaches, and has provided a comprehensive literature review of the three main families of seismic bearing capacity methods: pseudo-static, pseudo-dynamic, and time-history.

The pseudo-static method, despite its simplicity, remains widely used for preliminary design in regions of low-to-moderate seismicity; its main limitation is the inability to account for frequency content and duration effects. The pseudo-dynamic method introduces a physically more realistic representation of seismic wave propagation through the soil, but still relies on a prescribed failure mechanism and a single harmonic frequency. Time-history methods using nonlinear finite element analysis represent the state of the art, capturing the full complexity of dynamic soil–structure interaction, but require careful selection of input motions and advanced constitutive modelling.

The selection of the most appropriate method depends on the level of seismic hazard, the importance and complexity of the structure, the quality of available geotechnical data, and the design philosophy adopted. Advanced methods are recommended for high-risk sites or critical structures, while the pseudo-static approach may be adequate for simple structures in regions of low-to-moderate seismicity.

Chapter II: Voids Analysis

II.1. Introduction

The existence of cavities within the soil mass poses a major challenge in geotechnical analysis and foundation design. These voids, whether naturally formed through geological evolution or artificially created by human activities — including tunneling, mining, and buried infrastructure development — significantly affect soil behaviour.

The presence of cavities disturbs the uniform transmission of stresses, modifies deformation patterns, and may weaken the overall strength of the soil mass. As a result, foundations constructed above or near cavities are exposed to risks such as excessive settlement, instability, or sudden ground failure.

Therefore, evaluating the impact of subsurface cavities is a fundamental step in geotechnical studies. Accurate assessment allows engineers to predict potential failure mechanisms and to design appropriate reinforcement or ground-improvement techniques, ensuring structural safety and serviceability.

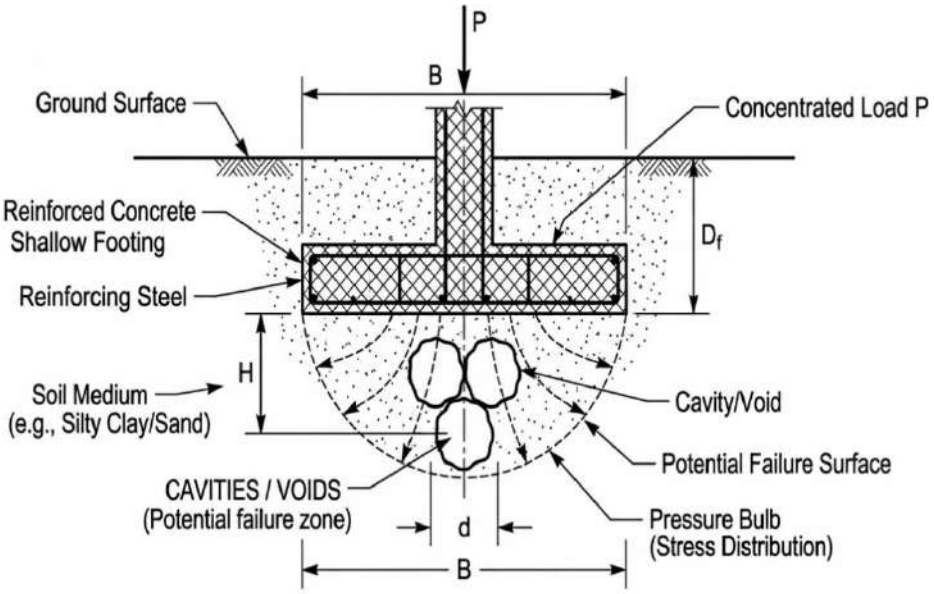


Figure II.1: Schematic representation of a cavity beneath a shallow footing

II.2. Definition

Underground voids are spaces that form within the soil or bedrock, either through natural mechanisms or as a result of human activities. Their configuration, extent, and depth are governed by the geological setting of the area and by external interventions. Such cavities

may develop through natural processes such as chemical dissolution, erosion, volcanic phenomena, or glacial action, or they may be created artificially through excavation, mining, and the construction of underground structures.

This broad definition is commonly recognized in scientific research, particularly in the works of Hoek and Brown (1980), Bell (1992), Waltham et al. (2005), Ford and Williams (2007), Parise and Gunn (2007), Davies et al. (2009), and Zimbelman (2013). These studies highlight that cavity stability is largely controlled by the mechanical characteristics of the surrounding materials, in addition to their geometric configuration and depth.

II.3. Literature Review

A substantial body of research has been conducted on the interaction between underground cavities and surface structures. This review covers experimental techniques, scaled physical models, full-scale tests, and numerical approaches, including finite element analysis and three-dimensional modelling. Key contributions are presented chronologically and thematically below.

Early contributions to this field include the experimental studies of Badie and Wang (1984), Baus and Wang (1983), Wang and Badie (1985), Wang and Hsieh (1987), Wood and Carnach (1985), and Azam, Hsieh and Wang (1991), who examined cavity collapse mechanisms using laboratory and physical model tests. Numerical approaches were subsequently developed by Kiyosumi, Kusakabe and Ohuchi (2007, 2011) using finite element analysis and three-dimensional modelling.

Dyne (1998) conducted a two-dimensional experimental study examining the effects of cavity span, width, and overlying soil cover thickness. Burd et al. (2000) used the OXFEM programme to investigate soil-structure interaction during tunnel excavation beneath masonry buildings. Laefer (2001) performed 1/10 scale model tests to assess structural damage from ground movements due to underground excavations. Mahamma (2002) investigated the progressive collapse of a mine gallery through simulation of failure propagation. Shahin et al. (2004) designed an experimental setup to study soil mechanical response during excavation.

Boumalla (2005) experimentally analysed the effects of cavity span, cover thickness, and sinkhole triggering rate on soil response. Sung et al. (2006) examined surface settlements and stress distributions under controlled laboratory conditions. Castro, Trueman and Halim (2007) investigated soil behaviour during block-caving mining using three-dimensional physical modelling. Lee and Bassett (2007) and Kikumoto et al. (2009) analysed tunnel

deformation relative to diameter to understand adjacent foundation performance. Caudron (2007) combined experimental and numerical methods to evaluate soil-structure interaction in localised ground collapse.

Deck and Anirudh (2010) developed a two-dimensional numerical model using CESAR-LCPC software to study soil-structure interaction under mining subsidence, accounting for structural stiffness, length, soil mechanical properties, and the magnitude of ground movements. Nghiem et al. (2014) designed a 1/40 scale physical model to predict damage to masonry structures from underground subsidence due to tunnel or mining activities. Keawsawasvong (2021) proposed limit-analysis-based solutions for the stability of spherical cavities in sandy soils under surcharge loading, providing a useful tool for evaluating collapse risk. Yongyao et al. (2023) performed numerical simulations examining damage evolution in karst cavities under positive pressure.

II.3.1. Baus and Wang (1983)

This study investigated the behaviour of shallow continuous footings placed above cavities in silty clay soils. As an initial investigation, it was limited to footings centered on regularly shaped, continuous voids loaded by a vertical force applied at the midpoint.

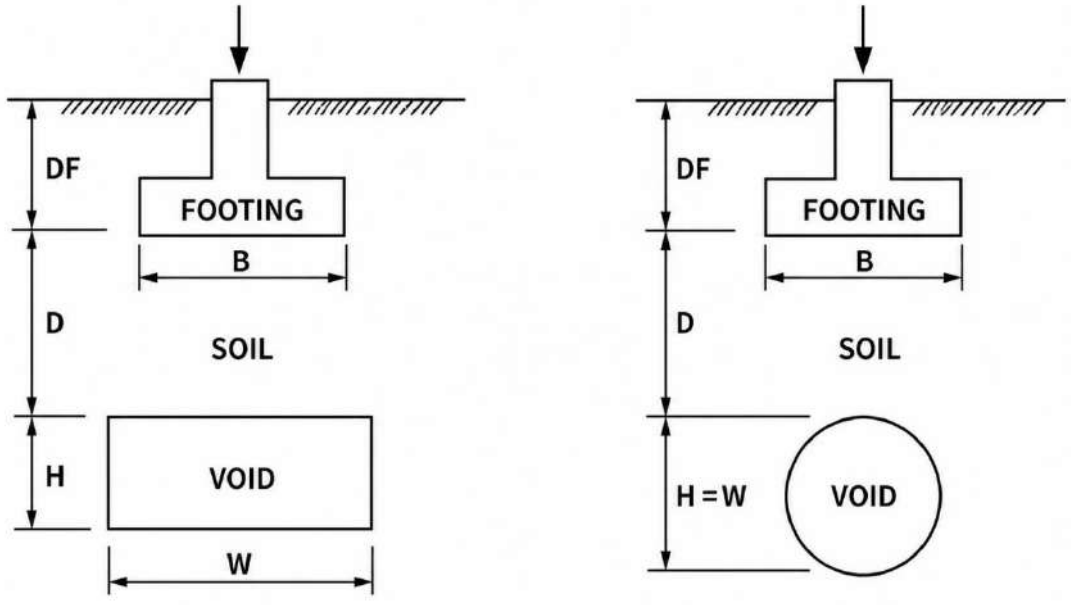


Figure II.2: Centered strip footing above a continuous underground void (Baus & Wang, 1983)

The behaviour of a strip footing resting on a continuous cavity within silty clay soils was examined using both physical model tests and theoretical analysis. The model tests were

conducted in a tank filled with compacted silty clay as the foundation soil. The theoretical analysis was carried out using the finite element method, treating the soil as a perfectly plastic elastic material.

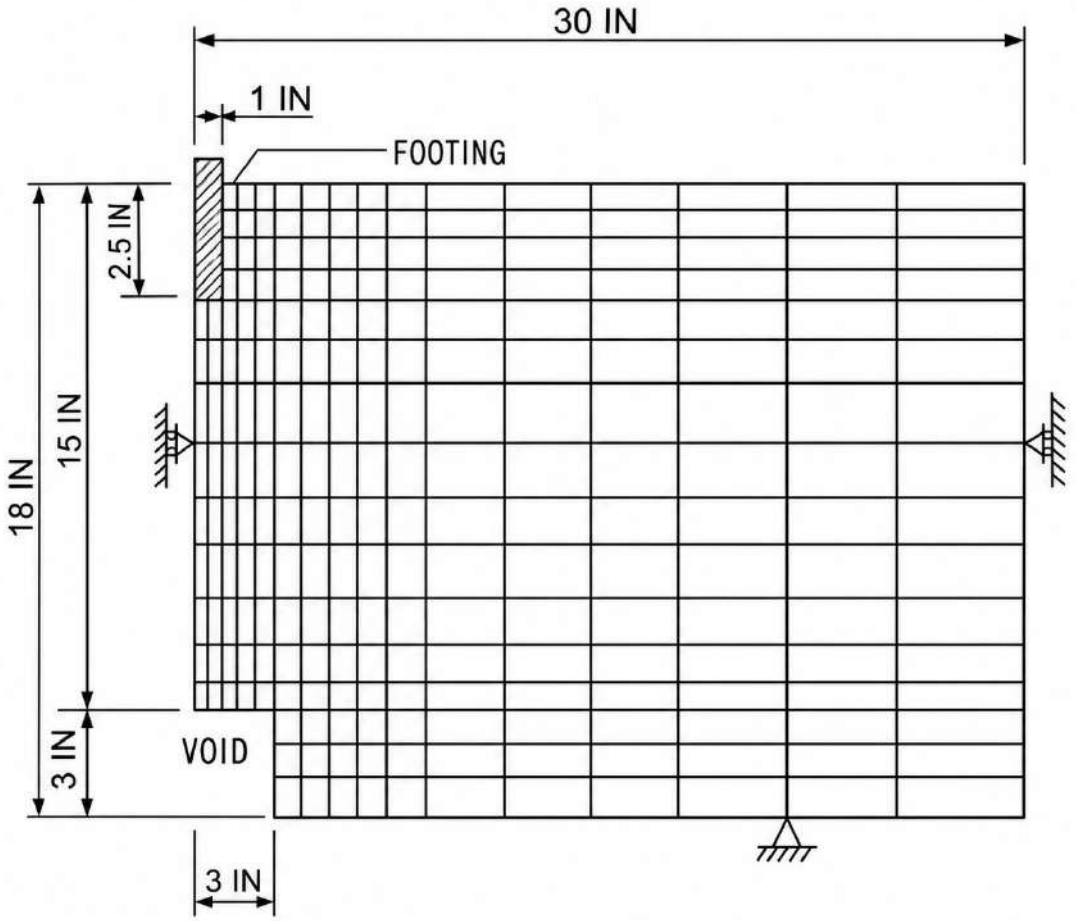


Figure II.3: Numerical model — FEM (Baus & Wang, 1983)

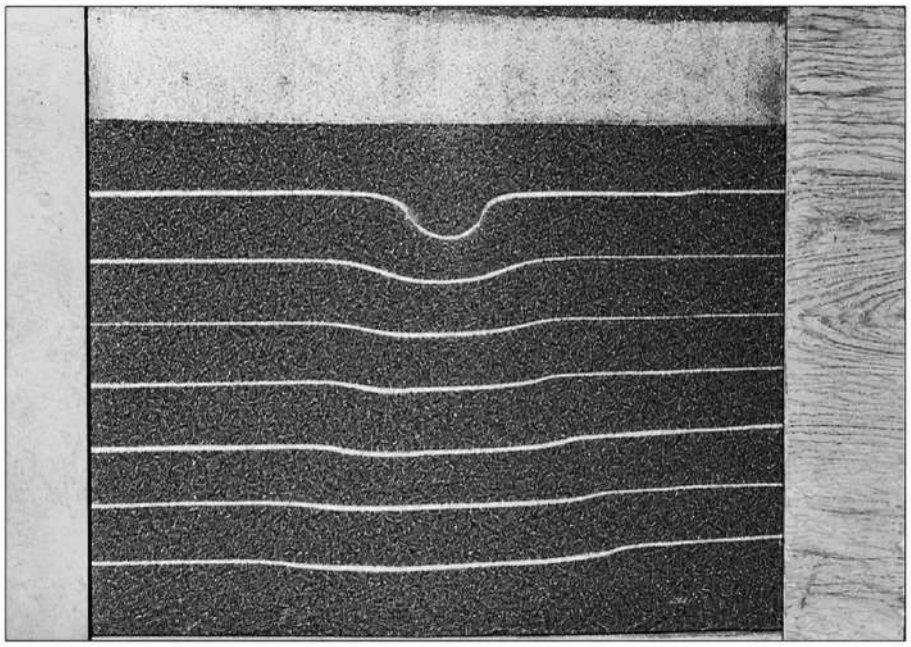
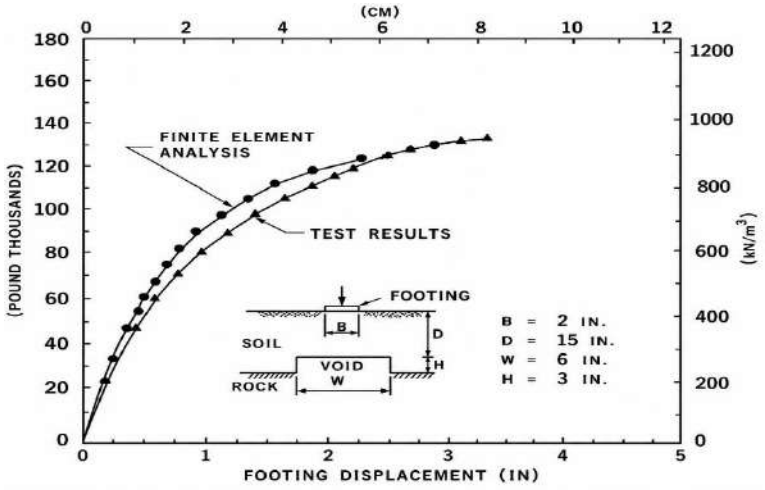


Figure II.4: Experimental model (Baus & Wang, 1983)

The theoretical analysis results correspond closely with the experimental data. A critical depth exists below which the cavity has little effect on footing performance. When the cavity is situated above this depth, the footing's bearing capacity is strongly influenced by foundation depth, cavity size, and cavity position.



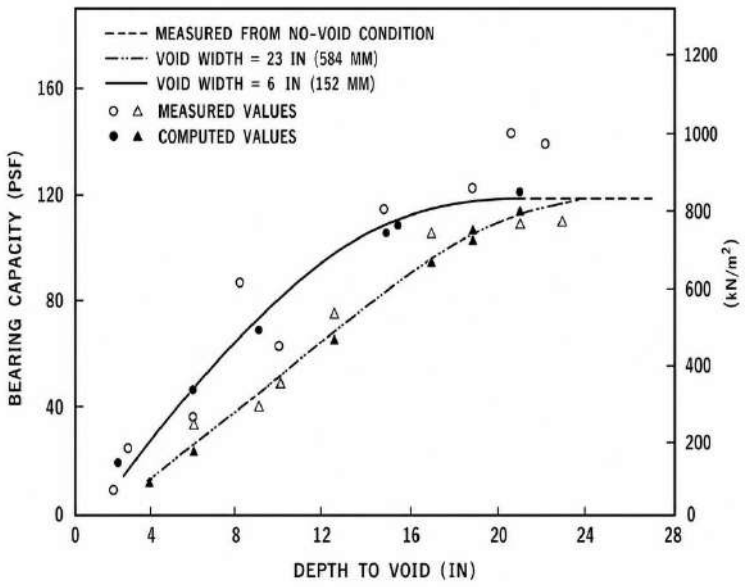


Figure II.5: Comparison between FEM results and physical model test results (Baus & Wang, 1983)

These findings demonstrate that the bearing behaviour of a continuous footing above a void can be effectively analyzed using the finite element method, providing a reliable reference for assessing the bearing capacity of footings over underground voids in silty clay soils.

II.3.2. Kiyosumi et al. (2007, 2011)

These studies examined the influence of single and multiple square voids on the ultimate bearing pressure of a continuous footing. Kiyosumi et al. (2007) carried out numerical analysis using a two-dimensional finite element approach, quantifying results through the bearing pressure reduction factor R = qv / qv', where qv and qv' represent the bearing capacities of a continuous footing on soil with and without a void, respectively.

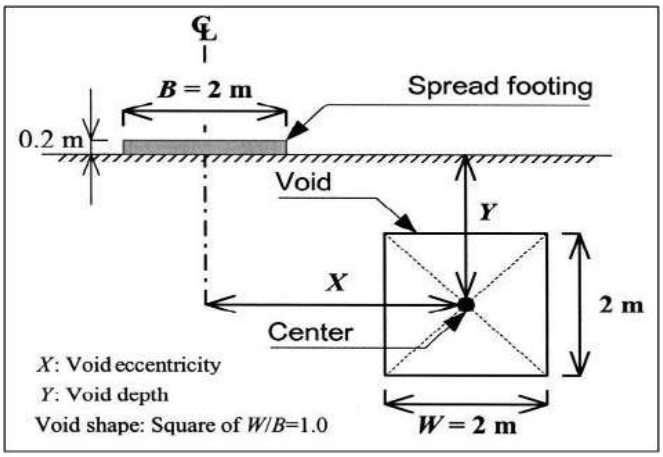


Figure II.6: Representation of a footing system above a square void (Kiyosumi et al., 2007)

When a single void is present, the surface bearing pressure decreases. This reduction is governed by the ratio of void depth to footing width, and the ratio of void eccentricity to footing width. The failure zone propagates from the edge of the footing toward the corners closest to the void, without forming a fully developed active wedge beneath the footing. Beyond a critical parabolic boundary, the effect of a single void on bearing capacity vanishes, corresponding to full development of an active wedge.

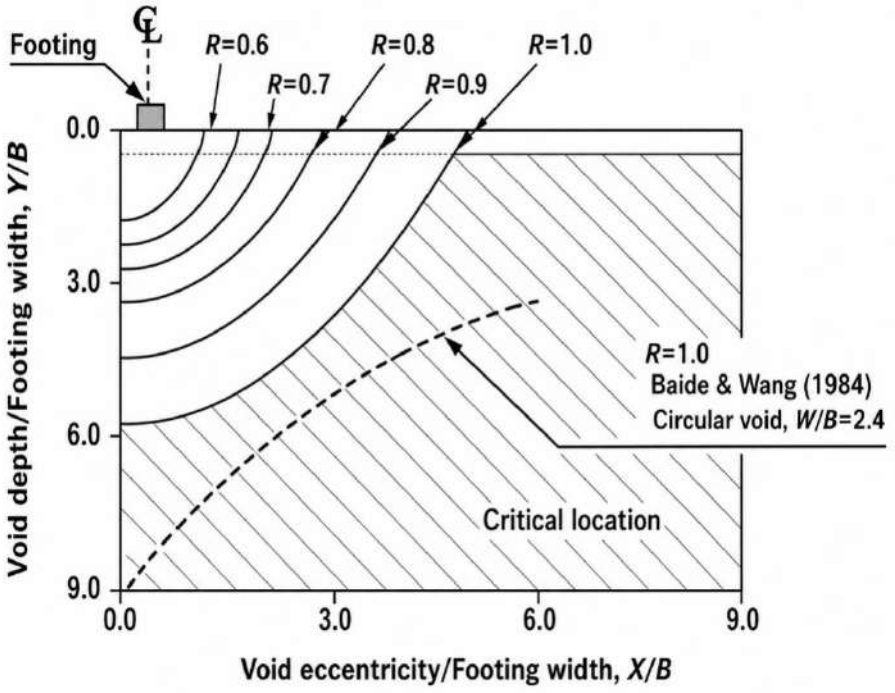


Figure II.7: Variation of R as a function of void depth and eccentricity (Kiyosumi et al., 2007)

When two cavities of the same size are present under different configurations, a failure zone tends to form near the nearest cavity. The reduction in bearing pressure can be estimated by multiplying the reduction factors of the individual cavities. For more than two cavities of the same size, the reduction is estimated by combining the factors of the two nearest cavities with a reduction factor below 0.9.

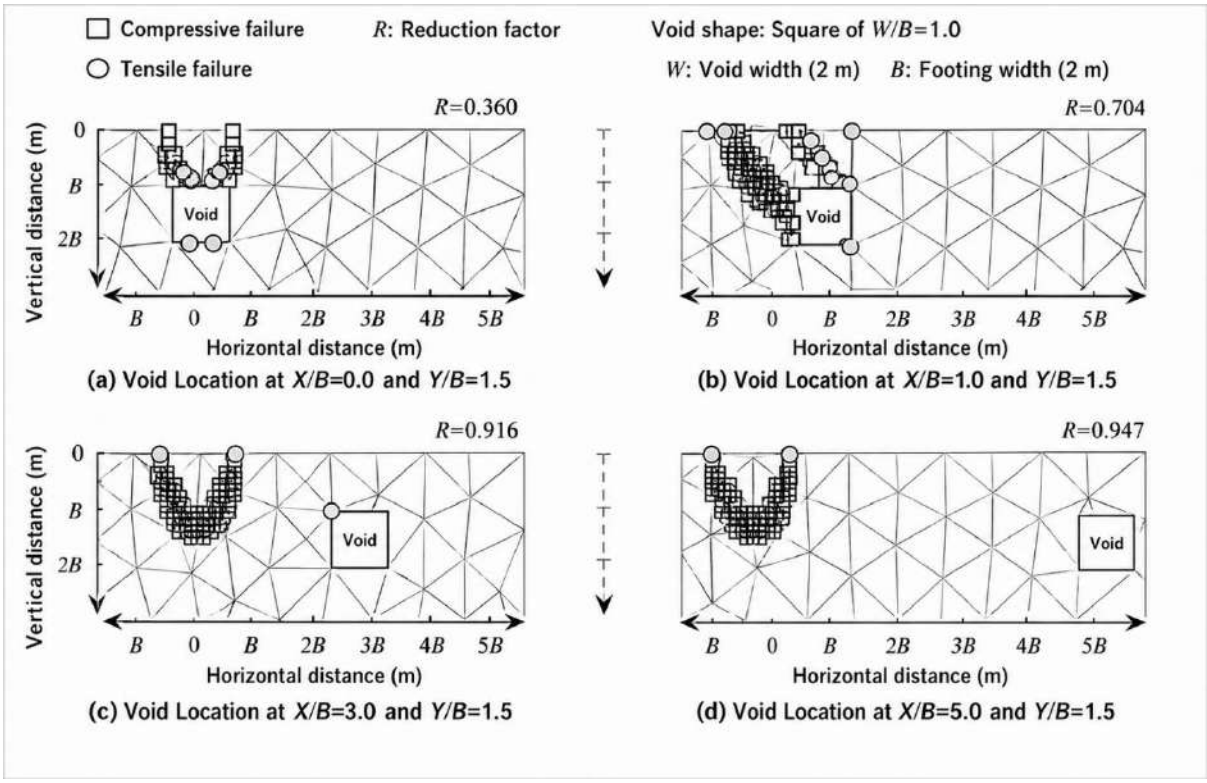


Figure II.8: Soil rupture patterns for different X values at Y/B = 1.5 (Kiyosumi et al., 2007)

Kiyosumi et al. (2I011) presented results of 1G load tests under plane-strain conditions on rigid soil containing continuous square cavities, investigating shallow foundations on sedimentary limestone with cavities smaller than the strip footing width. Three distinct failure modes were identified for a single cavity: bearing failure without cavity collapse, bearing failure with cavity collapse, and cavity collapse without bearing failure. Three patterns of slip-line propagation were also observed, and upper-bound solutions for bearing capacity were derived alongside a parametric study of varying cavity sizes, depths, and positions.

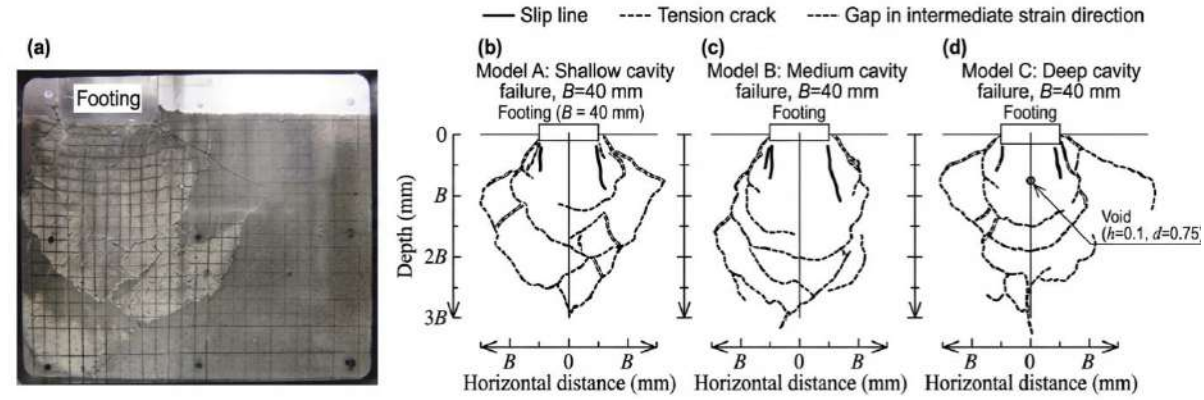


FIGURE 2. Comparison of failure mechanisms in physical model and FEM analysis (based on Baus & Wang, 1983, with permission)

Figure II.9: Failure mechanism (Kiyosumi et al., 2007)

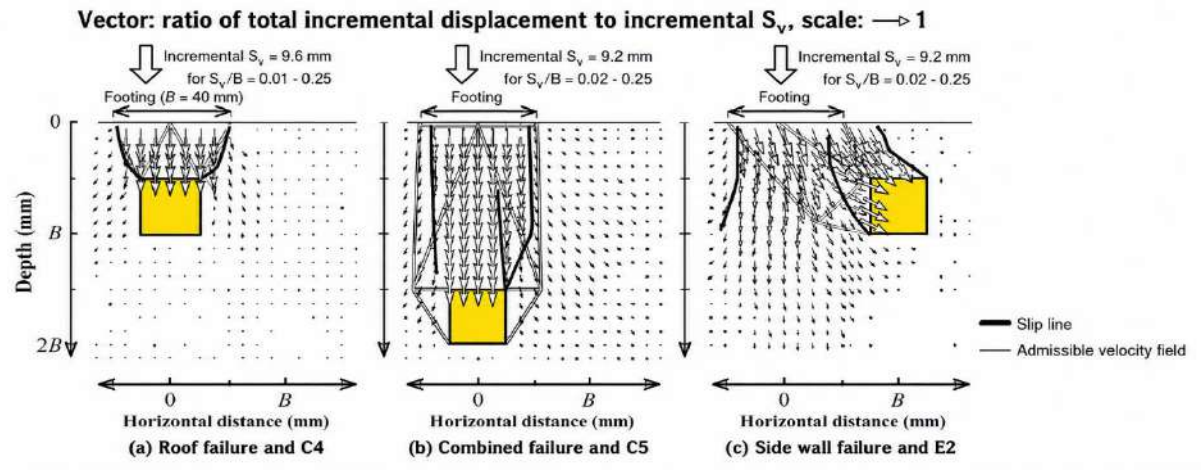


Figure II.10: Comparison of critical failure mechanisms with experimental observations (Kiyosumi et al., 2007)

II.3.3. Lee et al. (2014)

Lee et al. (2014) studied the undrained stability of foundations resting on clayey soil with continuous cavities, using a small-strain finite element method to determine the undrained vertical bearing capacity factor under different geometric and material conditions. Results were validated against established solutions for undrained clay without voids.

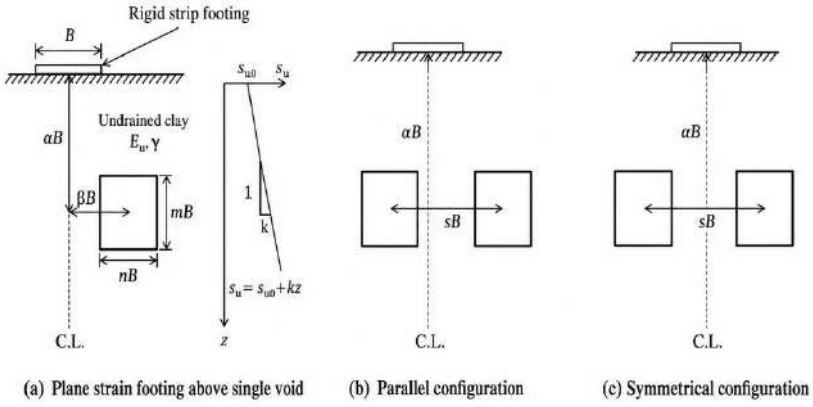


Figure II.11: Problem definition (Lee et al., 2014)

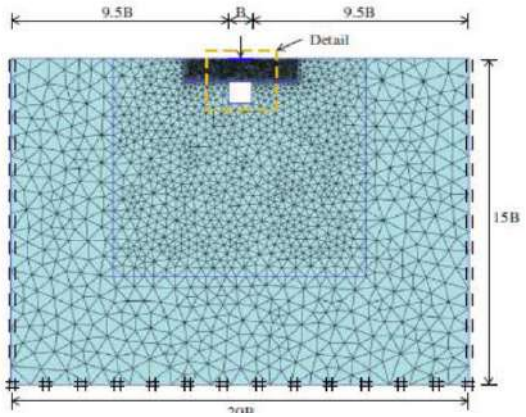


Figure II.12: Typical finite element mesh and boundary conditions (Lee et al., 2014)

For square-shaped cavities, the bearing capacity factor increases almost linearly as the vertical and horizontal void distances (alpha and beta) increase, up to a critical location, beyond which it becomes nearly constant. Lee et al. (2014) also examined how the position, shape, and number of cavities, as well as soil heterogeneity and stiffness, affect foundation behaviour. Design charts were proposed relating the undrained bearing capacity factor to key dimensionless parameters.

For a footing above a centrally positioned rectangular cavity, the bearing capacity factor decreases with increasing cavity width. When two cavities are present, the bearing capacity factor decreases as the spacing between them decreases, with a more pronounced reduction in the symmetric configuration than in the parallel arrangement. Three failure modes were identified from finite element displacement contours: roof failure, wall failure, and a combined mode.

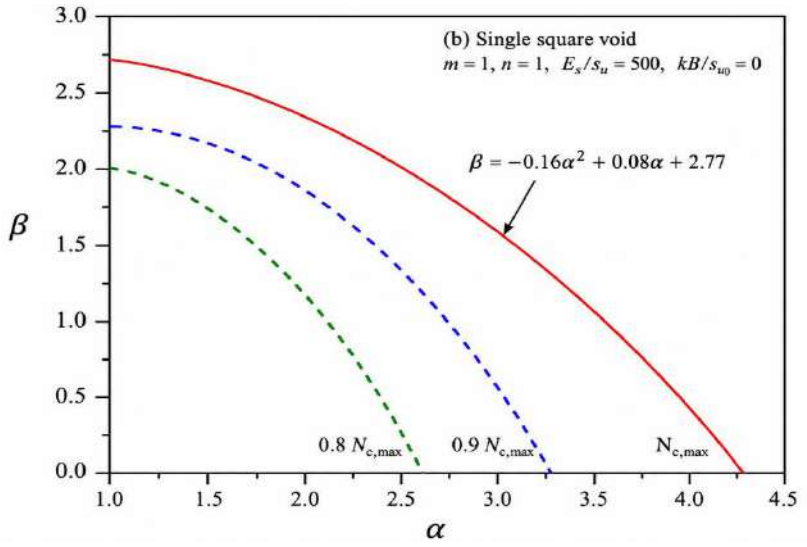


Figure II.13: Critical void location curve under a strip footing (Lee et al., 2014)

II.3.4. Lavasan et al. (2016)

Lavasan et al. (2016) conducted a numerical study on the influence of double underground voids on the ultimate bearing capacity of a strip footing, considering two different cohesive-frictional soil types. After extensive validation against existing experimental and numerical data, a parametric analysis was carried out investigating footing size and void configuration effects on load-settlement behaviour.

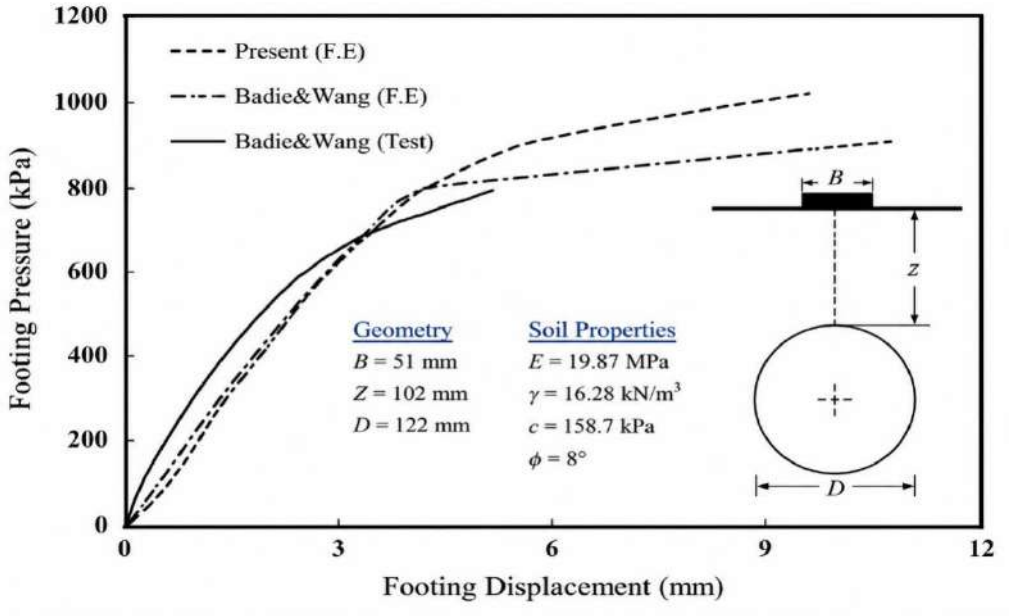


Figure II.14: Load-settlement curve comparison (Lavasan et al., 2016)

The main conclusions of this study are summarised as follows. Double underground voids reduce bearing capacity in a manner dependent on system geometry. For shallow void conditions, bearing capacity decreases with increasing footing width. An increase in cavity diameter causes a significant capacity reduction at constant void-to-footing distance. Beyond a critical depth (Zcr = 4D), void depth has no further effect on bearing capacity. When horizontal void spacing exceeds a critical distance (Lcr ≈ 6D), the bearing capacity is unaffected. The double-void system becomes unstable when edge-to-edge spacing is less than D. Bearing capacity increases with void eccentricity relative to the foundation axis. A void directly beneath the footing induces punching-type failure, while a second nearby void causes block-type failure.

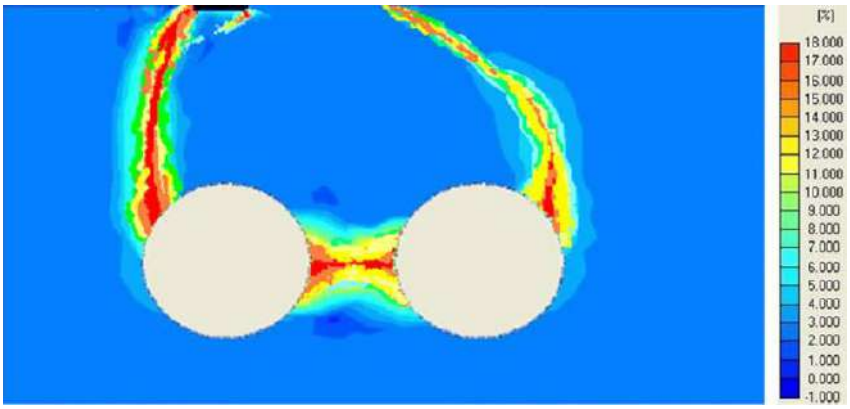


Figure II.15: Failure mechanism with two underground voids beneath the footing (Lavasan et al., 2016)

II.3.5. Zhou et al. (2018)

Zhou et al. (2018) analysed the bearing capacity and failure mechanism of strip footings on cohesive-frictional soils with voids using an optimised discontinuity layout method (DLO). By introducing a reduction factor R, a set of design charts was developed for direct use within the conventional bearing capacity framework.

The critical depth parameter (alpha_0) decreases with increasing void eccentricity (beta_0), while both parameters increase with the soil friction angle, as higher shear strength generates larger failure mechanisms. The undrained bearing capacity depends strongly on soil cohesion and unit weight. Cavities exert a more significant influence on c-phi soils than on purely undrained soils.

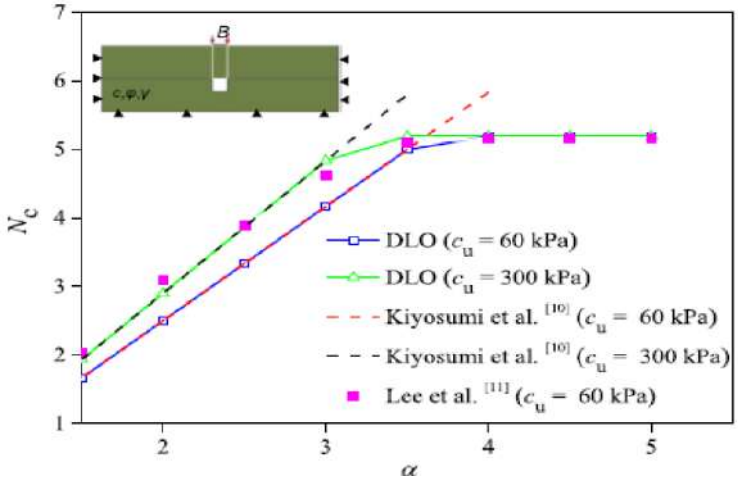


Figure II.16: Comparison of Nc values from the optimised void configuration with results from previous studies (Zhou et al., 2018)

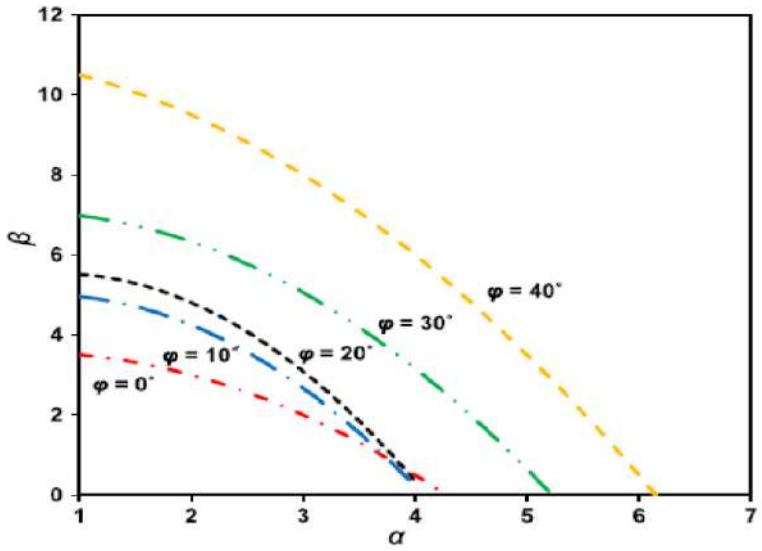


Figure II.17: Critical bearing capacity location (Zhou et al., 2018)

A single cavity within the fan-shaped failure zone reduces bearing capacity; when outside this zone, an increase in ultimate pressure may occur due to mobilisation of passive earth resistance. In the case of double cavities, local minimum values of R arise from instability of the soil mass between the voids. For parallel configurations, R cannot reach 1.0 because the centreline cavity controls the failure mechanism.

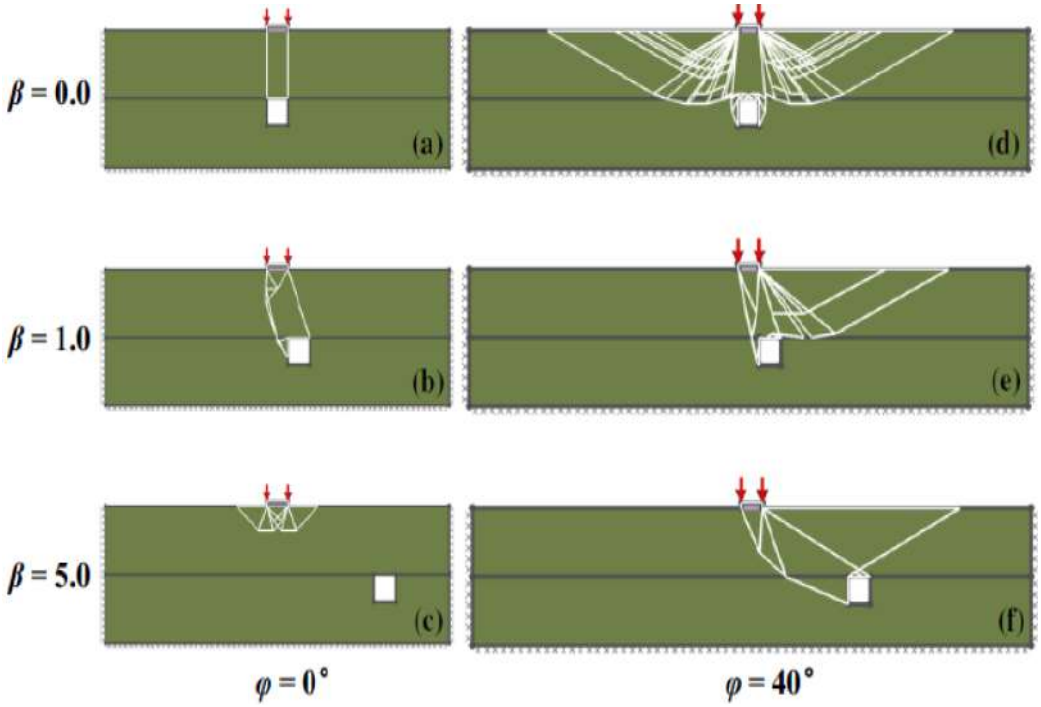


Figure II.18: Failure mechanism for a single underground void (Zhou et al., 2018)

II.3.6. Void Geometry Effects on Foundation Bearing Capacity

A comprehensive body of research demonstrates that underground voids alter the transfer of stresses from foundations to the ground. Void shape, size, depth, and horizontal offset jointly govern the extent of bearing capacity reduction and the nature of failure mechanisms for both shallow and deep foundations.

II.3.6.1. Types of Void Geometries Studied

Research has addressed a wide range of void geometries, which can be grouped by shape and configuration:

Shape: Studies have considered circular and spherical voids and circular tunnels; square and rectangular cavities including continuous square voids; elliptical (horizontal and vertical), rectangular, and square cavities in rock masses; irregular karstic cavities generated with Fourier descriptors; and twin circular voids with multiple (beaded) cavity configurations.

Configuration: Studies have examined single voids versus twin voids beneath strip foundations; voids located beneath slopes or near footing edges; and voids within layered or reinforced profiles, including sand-over-clay systems and geogrid-reinforced fills and slopes.

II.3.6.2. Influence of Void Geometry on Bearing Capacity

The general effects of void geometry on bearing capacity are summarized in Table II.1 below.

Table II.1: Influence of void geometry parameters on foundation bearing capacity

Geometry Parameter	**General Effect on Bearing Capacity**	**Key Studies**
Larger void width / diameter	Stronger reduction in bearing capacity; wider failure zones mobilised	Kiyosumi et al. (2007); Lee et al. (2014); Lavasan et al. (2016)
Circular vs. square / rectangular	Shape modifies the reduction factor and critical depth; captured through design charts	Zhou et al. (2018); Kiyosumi et al. (2011); Lee et al. (2014)
Irregular vs. regular cavities	Irregular shapes produce asymmetric failure and alter the size of the critical influence region	Irregular karst studies (Fourier descriptor models)
Twin voids	Define an unsafe interaction	Lavasan et al. (2016); Zhou

	zone; a critical spacing exists beyond which cavity interaction disappears	et al. (2018)

II.3.6.3. Critical Influence Zone — Depth and Horizontal Offset

Multiple studies consistently identify a critical influence zone beneath the footing, beyond which the presence of a void has negligible effect on bearing capacity:

- Bearing capacity approaches, the intact-ground value when void depth exceeds approximately IIB (twice the footing width) for circular or general voids, or when the horizontal distance from the footing center exceeds approximately II to 3B.
- Within this zone, capacity reductions of up to 70 to 80% are reported depending on void size and position.
- Rigid-plastic finite element analysis and limit analysis show that the shape of the influence zone depends on soil type (cohesive versus c-phi soils) and extends differently in the vertical and horizontal directions.

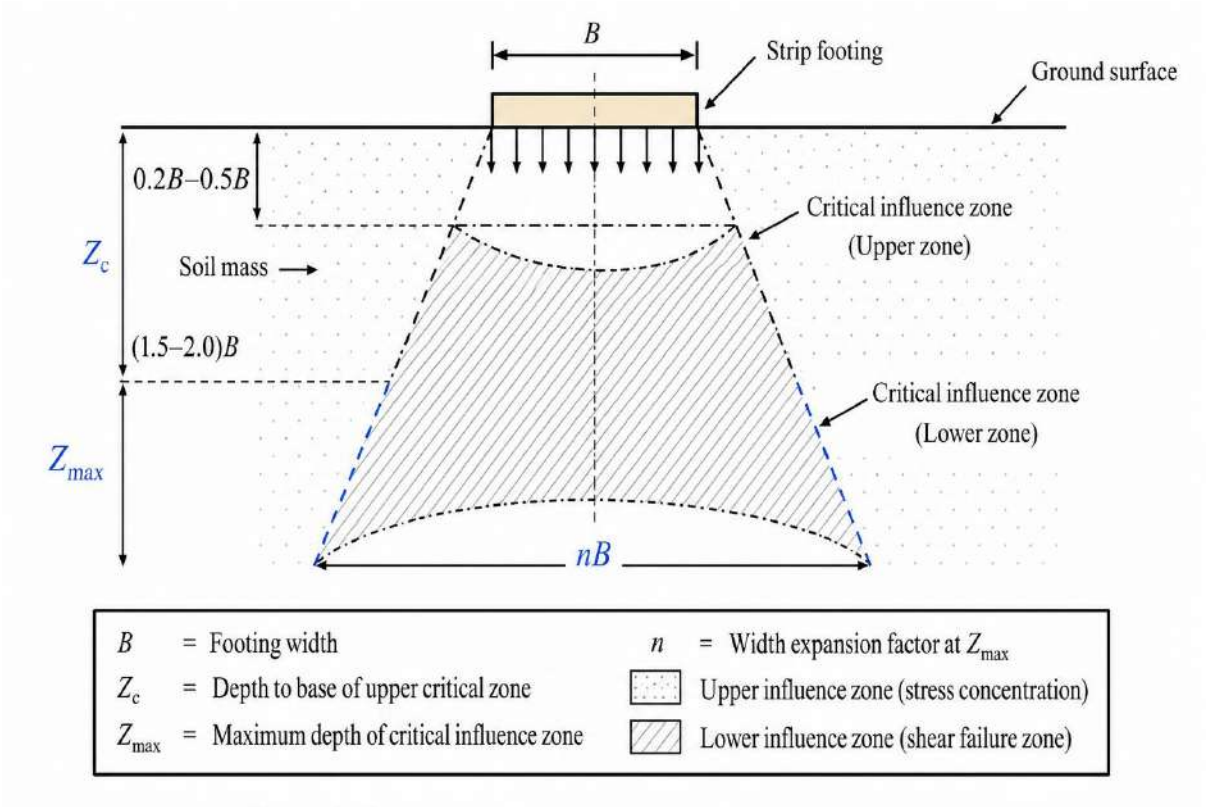


Figure II.19: Critical influence zone concept beneath a strip footing (after Kiyosumi et al., 2007; Zhou et al., 2018)

II.3.7. Factors Controlling Bearing Capacity of Shallow Foundations on Voided Soils

The bearing capacity of shallow foundations above voided ground is governed by both classical bearing capacity factors and void-related geometry and location effects. Under seismic loading, additional reductions arise from soil and superstructure inertia, pore pressure changes, and soil saturation conditions.

II.3.7.1. Void Geometry, Depth, and Horizontal Offset

- Shape and size: Square, rectangular, and circular cavities all reduce bearing capacity as their size increases. Larger voids mobilise wider failure zones and produce greater capacity loss.
- Depth below the footing: A critical depth exists; beyond it, cavity influence becomes negligible and capacity tends toward the intact-soil value.
- Horizontal offset: Increasing horizontal distance from the footing centreline suppresses adverse effects. Centrally located voids are the most critical configuration.

II.3.7.2. Soil Type and Strength

- In c-phi and intermediate soils, bearing capacity is highly sensitive to cohesion, friction angle, and unit weight. The void influence zone extends differently depending on the friction angle.
- Increasing the undrained shear strength of clay significantly reduces the adverse impact of voids on footing capacity.

II.3.7.3. Reinforcement and Layering Effects

The presence of geogrid reinforcement or a layered soil profile can significantly mitigate void-induced capacity loss. The main findings are summarised in Table II.II.

Table II.2: Mitigation measures for void-induced bearing capacity loss

Ground Condition	**Effect on Bearing Capacity above Voids**	**Key References**
Geogrid in granular fill or at sand-clay interface	Increases ultimate capacity; can recover 2-5% (or more) of capacity lost due to the presence	Kiyosumi et al. (2007); Lee et al. (2014)

	of voids	
Thicker overlying sand layer	Shields the foundation from the deep void; capacity approaches the no-void case	Lee et al. (2014); Lavasan et al. (2016)

II.3.7.4. Static Bearing Capacity

Under static loading, bearing capacity decreases with larger, shallower, and more centrally located cavities. Bearing capacity ratios map closely to a zone of influence defined by cavity location and soil strength. In cohesive-frictional and intermediate soils, capacity with voids is highly sensitive to cohesion, friction angle, and unit weight, while void influence zones extend differently depending on the friction angle.

II.3.7.5. Seismic Bearing Capacity

Under seismic loading, bearing capacity is further reduced through additional mechanisms:

- For homogeneous soils without voids, seismic bearing capacity factors Nc, Nq, and N gamma decline with increasing horizontal and vertical seismic coefficients and with earthquake-induced pore pressures.
- For voided soils, adaptive finite element limit analysis (AFELA) studies in undrained clays and c-phi soils quantify seismic capacity reduction versus void size, depth, and horizontal seismic coefficient kh, providing upper and lower bound design charts.
- In unsaturated soils, matric suction increases seismic bearing capacity and partially offsets seismic-induced reductions.

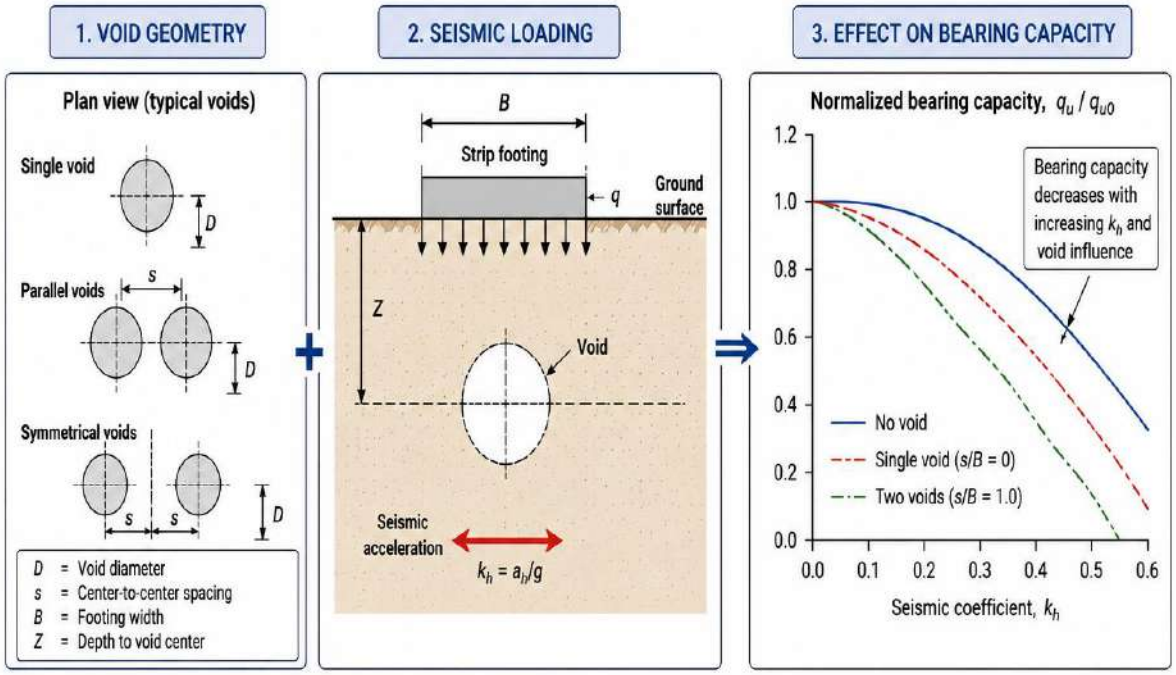


Figure II.20: Schematic showing the combined effects of void geometry and seismic loading on bearing capacity (after AFELA design charts)

II.3.8. Additional Recent Studies and Emerging Approaches

More recent research has extended the analysis of void-foundation interaction in several important directions, including layered and reinforced systems, seismic conditions, and data-driven prediction methods.

II.3.8.1. Single and Twin Voids in Cohesive-Frictional and Clay Soils

- Square voids in c-phi soils: discontinuity layout optimisation (DLO)-based reduction factors and critical void locations were derived for single and dual void cases.
- Circular single and twin cavities in clay: critical distances alpha_cr and beta_cr were identified, beyond which bearing capacity is void-independent. Ceiling, wall, and combined failure modes were classified.
- Twin voids in caves, tunnels, and similar configurations: finite element parametric studies mapped critical depth and spacing at which the influence on ultimate bearing capacity disappears, along with corresponding failure mechanisms.

II.3.8.2. Layered and Reinforced Systems with Voids

- Strip footing on sand over clay with voids: FLAC-based design charts were produced in terms of qu/gammaB, void geometry and location, and geotextile reinforcement at the sand-clay interface.

- Sand-clay profiles with circular void under central and eccentric loading: PLAXIS IID studies investigated eccentricity, sand layer thickness, void depth and size, and geogrid mitigation strategies.
- Circular footing on reinforced granular fill over clay with a continuous square void: three-dimensional FDM-DEM simulations (FLAC3D/PFC3D) investigated the influence of void position, undrained strength, and geogrid stiffness.
- Experimental footings on reinforced slopes with cavities: the influence of H/B and X/B ratios and the number of geogrid layers on ultimate bearing capacity and failure surface evolution were examined.
- Rigid-plastic finite element frameworks providing normalised two-dimensional design charts for cavity shape, size, and location in cohesive and intermediate soils.

II.3.8.3. Seismic Bearing Capacity with Voids

- Pseudo-static AFELA upper and lower bound solutions for strip footings above square voids in c-phi soils provided design tables as functions of c/(gammaB), phi, kh, and void location.
- Machine learning prediction models (MLP, GMDH, ANFIS-PSO) were trained on 38,000 FELA simulations for footings over rectangular voids in heterogeneous soils, varying undrained shear strength, friction angle, seismic coefficient kh, and void geometry.

II.3.8.4. Spatial and Geological Uncertainty

- Bearing capacity of shallow foundations with geological uncertainty was analysed using Markov random fields and random field theory, providing a reduction factor and contribution rates for spatial variability.
- Experimental and PLAXIS 3D studies of square footings on layered sand-clay and clay-sand profiles identified critical layer thickness and non-unique failure patterns.

The studies reviewed above are grouped thematically in Table II.3 for reference.

Table II.3: *Thematic grouping of key studies on foundation-void interaction*

Research Theme	**Methodological Focus**	**Representative References**
Static loading — c-phi / clay with voids	DLO, FEM, rigid-plastic FEM charts; critical void depth and spacing	Baus & Wang (1983); Kiyosumi et al. (2007, 2011); Lee et al. (2014); Lavasan et al. (2016); Zhou et al. (2018)
Layered and reinforced profiles with voids	Sand-clay systems, geogrid mitigation, slopes	Lee et al. (2014); Lavasan et al. (2016)
Seismic loading — homogeneous soils (no voids)	Pseudo-dynamic / MPD methods, heterogeneity, unsaturation	Various FELA / MPD studies
Seismic loading — voided soils	AFELA design charts; machine learning predictors	Recent AFELA and ML studies
Spatial and geological uncertainty	Random fields, Markov random fields	Probabilistic bearing capacity studies

II.4. Classification of Cavities

Cavities are broadly classified into two main types, which are not entirely independent of one another: natural cavities and anthropogenic (human-made) cavities.

II.4.1. Natural Cavities

Natural cavities are underground voids formed primarily through geological processes. Their shapes, dimensions, and origins vary according to the geological structure and climatic conditions of the regions in which they develop. They are commonly associated with chemical dissolution, erosion, volcanic activity, and glacial movement.

II.4.1.1. Karst Cavities

Karst cavities originate in soluble rocks, particularly limestone, through chemical weathering. This process, known as karstification, occurs when rainwater reacts with atmospheric and soil carbon dioxide (COII), forming a weak carbonic acid (HIICO3). Over time, this weak acid

dissolves carbonate minerals, progressively widening fractures and creating underground voids and cave systems (Ford & Williams, II007).



Figure II.21: Karst cavity (cave system)

II.4.1.2. Volcanic Cavities

Volcanic cavities form during volcanic eruptions as a result of lava solidification. When molten lava flows and creates tunnels or channels, these spaces may become cavities once the lava cools. Volcanic craters also represent natural cavities created by explosive eruptions or by the collapse of a volcano's summit (Mangan& Sisson, II000).



Figure II. 22: Volcanic lava tube cavity

II.4.1.3. Erosional Cavities

Erosional cavities develop as a result of surface processes driven by flowing water, wind, and glacial movement. These forces progressively remove and transport rock and soil materials. Fluvial processes play a significant role in carving such cavities, especially in weak or unconsolidated materials such as sand and sandstone (Summerfield, 1991).



Figure II.23: Erosional cavity (canyon formation)

II.4.1.4. Glacial Cavities

Glacial cavities are generated through the dynamic interaction between glacier movement and the underlying geological formations. The immense weight and motion of the ice mass cause erosion, fracturing, and the formation of voids such as crevasses and subglacial hollows. The melting of ice beneath the glacier surface can also create additional voids (Sharp, II005).



Figure II.24: Glacial cavity (subglacial hollow)

II.4.2. Anthropogenic Cavities

Anthropogenic cavities are underground spaces that are excavated, constructed, or substantially modified through human intervention. Unlike natural voids, these cavities are intentionally created to fulfil practical functions, including mining and quarrying, underground storage, military defence, or cultural and religious practices.

II.4.2.1. Underground Quarries

Underground quarries are artificial excavations created to extract building materials such as stone, sand, or clay. They can be extensive and typically develop in linear formations or as interconnected gallery networks.



Figure II.25: Underground quarry

II.4.2.2. Underground Mines

Underground mines are created for the extraction of ores or fossil fuels. Their shapes and dimensions depend on the type of resource and the mining techniques applied. These mines typically consist of networks of shafts, tunnels, and chambers enabling safe and efficient extraction.



Figure II.26: Underground mine tunnel

II.4.2.3. Caves and Troglodyte Dwellings

Anthropogenic cavities are sometimes converted into habitable spaces. Troglodyte dwellings are instances where natural or artificial cavities have been adapted to create shelters and functional residential areas within rock or underground environments.



Figure II.27: Troglodyte dwellings

II.4.2.4. Underground Shelters and Religious Sites

Underground cavities have been used for protective and religious purposes, serving as locations for spiritual ceremonies, burial sites, or places of refuge during conflict or persecution.



Figure II.28: Underground shelter and religious site (catacombs)

In terms of internal structure, cavities may further be classified as single or double:

- Single Cavities: Isolated underground spaces that do not communicate with other cavities. They generally have a single access point and one main chamber. Their simple and linear layout makes them easier to survey and exploit.
- Double Cavities: Two linked chambers forming a more complex underground system. They may have multiple entrances or connecting passages. This type of cavity often develops through the expansion of an existing cavity or the joining of two separate cavities.

II.5. Geotechnical Risks Associated with Cavities

The presence of cavities in the soil alters the equilibrium of the surrounding soil elements. In all types of cavities, deterioration is expected as the mechanical properties of the surrounding material gradually decrease. Cavities can therefore constitute a major risk for construction projects and, in some cases, for human life.

II.5.1. Collapse

Collapse is the sudden and localized failure of the ground, caused by the weakening or rupture of an underground cavity, tunnel, or soil layer. It leads to a rapid downward movement of the surface, often forming a sinkhole or crater with steep and unstable edges. This phenomenon differs from gradual subsidence in that it occurs abruptly and without warning.

Collapses occur when underground materials can no longer support the weight of overlying soil, rock, buildings, or other loads. Triggering factors include water infiltration, erosion, mining activities, and natural cavities. Due to its sudden nature, collapse represents a serious hazard to infrastructure, property, and human safety.

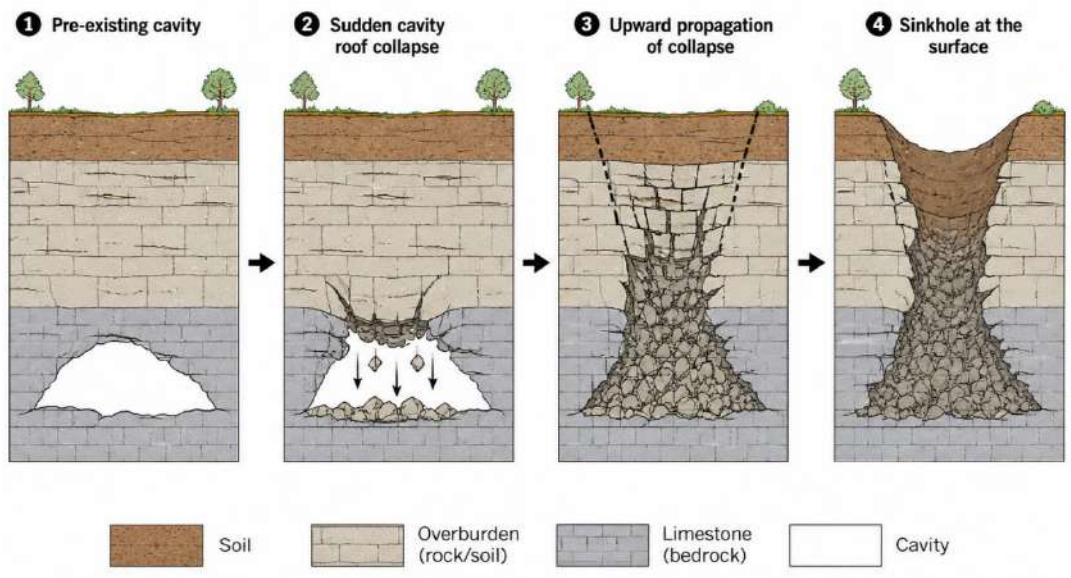


Figure II.29: Progressive collapse mechanism of an underground cavity

II.5.2. Subsidence

Subsidence is a gradual, ductile deformation of the ground surface without rupture, resulting in a basin-shaped depression generally with a flat bottom. It typically occurs in relatively elastic soils capable of deforming without fracturing, and may affect several hectares, particularly above large quarries or mines.



Figure II.30: Ground subsidence above an underground cavity

II.5.3. Pollution and Contamination

Underground voids can pose a serious environmental risk. When used for waste disposal — whether industrial or domestic — they can compromise soil integrity, contaminate groundwater reserves, and degrade air quality. Toxic substances and chemical pollutants may migrate from these sites into the surrounding environment and enter food chains, posing long-term threats to human health.

II.6. Cavity Identification Methods

The identification of underground cavities is a crucial phase in geotechnical investigations and construction planning. Various exploration methods are employed, including geophysical surveys, drilling techniques, and in-situ inspections. The selection of the appropriate method depends on ground conditions, the expected depth of the cavities, and the required level of precision.

II.6.1. Geophysical Methods

Geophysical methods are the most widely used techniques for cavity detection, based on measuring the physical properties of subsurface materials to identify ground anomalies.

II.6.1.1. Gravimetric Methods

Gravimetry measures gravitational acceleration using a gravimeter to evaluate variations in the Earth's gravitational field. Although very small, these variations can indicate the presence of dense underground structures or empty cavities. The unit of measurement is the microgal (microGal).

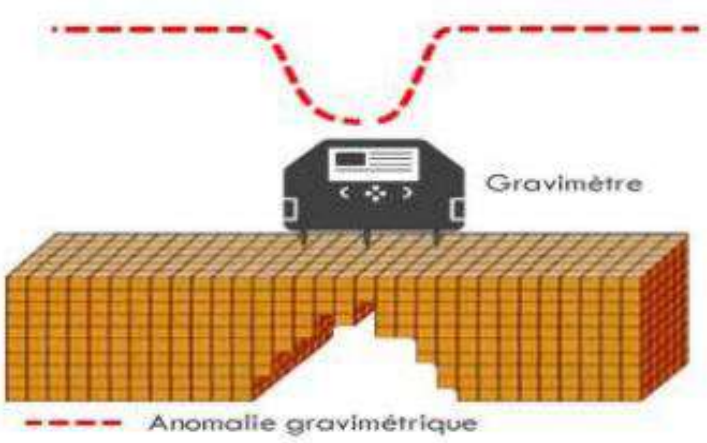
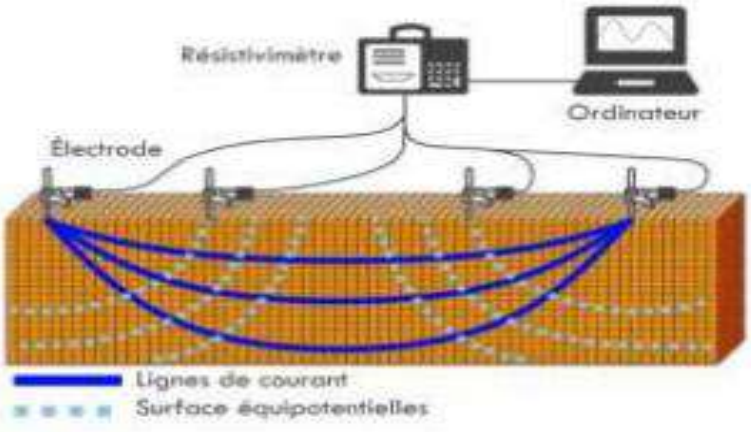


Figure II.31: Principle of gravimetric measurement for cavity detection

II.6.1.2. Electrical Resistivity Method

Resistivity measures a material's ability to resist the flow of electric current, expressed in ohm-metres (Ohm.m). It varies significantly with rock type and soil water content. Conductive formations such as water-saturated or clayey soils exhibit low resistivity, whereas dry materials or compact rocks exhibit higher resistivity.



***

Figure II.32: Principle of electrical resistivity measurement

II.6.1.3. Electromagnetic Method

The electromagnetic method is based on Maxwell's equations describing interactions between electric and magnetic fields. When an electromagnetic wave passes through a material, it interacts with physical properties such as electrical conductivity, magnetic permeability, and permittivity. Cavities create anomalies in the electromagnetic field that can be detected using inductive probes (Palacky, 1987).

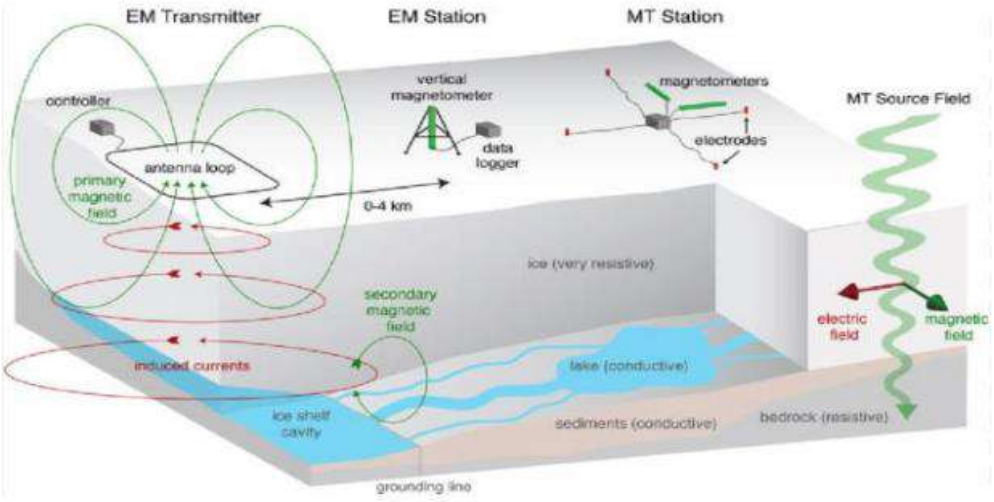


Figure II.33: Electromagnetic survey configuration

II.6.2. Geotechnical Methods

Geotechnical methods involve the direct study of the mechanical and physical properties of the soil through boreholes, drilling, or in-situ testing, allowing both localisation of cavities and assessment of ground conditions and associated risks.

II.6.II.1. Boreholes and Coring

Boreholes involve penetrating the ground using an auger or mechanical tool to collect samples or measure soil properties. Coring extracts intact soil or rock cylinders, providing a detailed view of the subsurface structure and composition. These techniques confirm the presence of cavities and help assess the condition of the surrounding material.

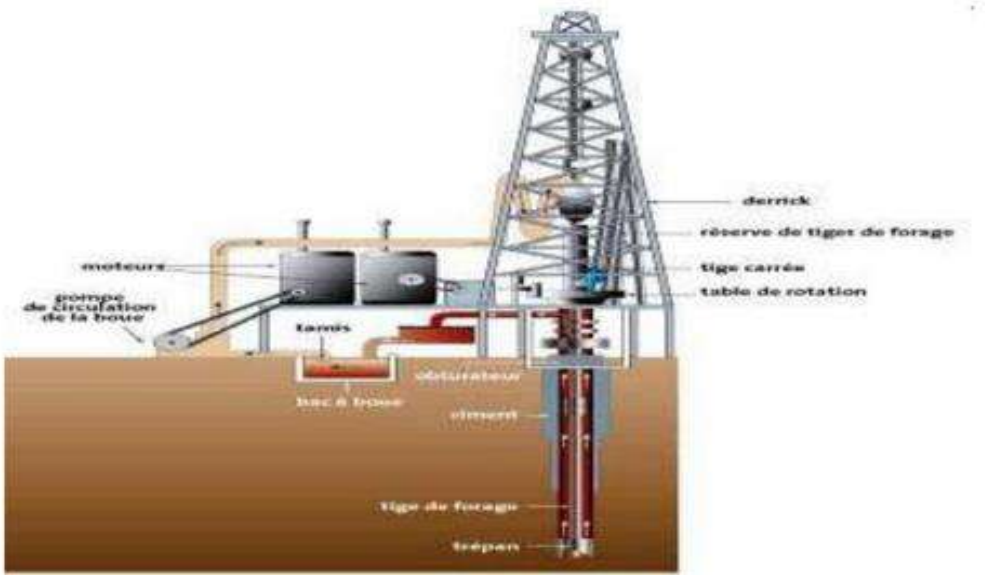


Figure II.34: Illustration of the coring method

II.6.2.2. Cone Penetration Test (CPT)

The Cone Penetration Test (CPT) involves pushing a cone into the ground at a constant rate while measuring tip resistance and sleeve friction. These measurements identify variations in the soil's mechanical properties that may indicate the presence of cavities or low-density zones, providing a fast and accurate means of locating subsurface anomalies without extensive drilling.

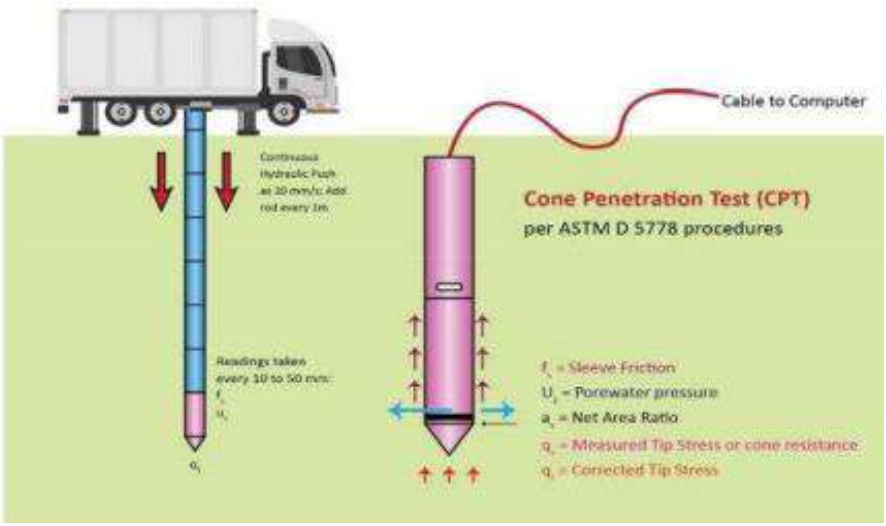


Figure II.35: The Cone Penetration Test (CPT)

II.6.3. Optical and Radar Methods

II.6.3.1. Ground Penetrating Radar (GPR)

Ground Penetrating Radar (GPR) transmits electromagnetic waves into the ground and records signals reflected back from subsurface layers. By analysing these reflections, anomalies indicating the presence of cavities can be identified. This technique is particularly effective for detecting shallow subsurface voids.

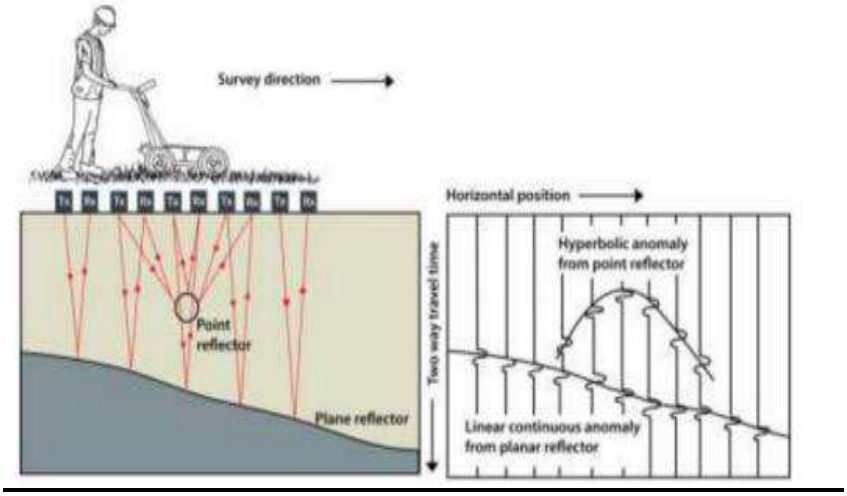


Figure II.36: Procedure for Ground Penetrating Radar (GPR) surveying

II.6.3.2. Cameras and Drones

The use of cameras and drones is increasingly common for detecting cavities, especially in mines and tunnels. Drones equipped with optical sensors or LiDAR (Light Detection and Ranging) can detect visual or topographic anomalies (Laouar et al., II018). Cavity detection ultimately relies on geophysical, geotechnical, and optical methods selected according to depth, ground conditions, and available equipment.

II.7. Conclusion

Underground cavities constitute a critical factor in the geotechnical behaviour of soils and the stability of shallow foundations. Their presence significantly alters failure mechanisms and bearing capacity through complex interactions between voids, soil properties, and applied loads.

Research has consistently shown that void geometry — encompassing shape, size, depth, and horizontal offset — jointly defines a critical influence zone beneath the footing where bearing capacity is most sensitive to cavity presence. Within this zone, capacity reductions of up to 70 to 80% have been reported, while effects become negligible beyond approximately II to 3 footing widths in depth or plan. Under seismic loading, additional capacity reductions arise

from soil inertia, pore pressure effects, and saturation conditions, with reinforcement and unsaturation acting as key mitigating factors.

Despite progress achieved through experimental studies, numerical modelling, and field investigations, knowledge gaps remain, particularly for granular soils, interfering footing configurations, and seismic scenarios involving combined void-inertia effects. Improving the understanding of these phenomena requires the development of more reliable investigation techniques and more accurate analytical and numerical models. This will help optimise foundation design and enhance the safety and performance of structures built on soils that may contain underground cavities.

Chapter III: Numerical Analysis

Chapter III:

III.1. Introduction

In this chapter, numerical modeling using PLAXIS 2D is employed to analyze soil-foundation interaction in the presence of underground voids in cohesive-frictional soils. The adapted modeling approach for evaluating the bearing capacity and failure mechanisms is described in detail, covering the constitutive model, boundary conditions, meshing strategy, and calculation parameters. Particular attention is given to model validation in order to ensure reliable and accurate results.

III.2. Geometry

The numerical model used in this study consists of a rectangular soil domain measuring 60 m in length and 40 m in depth.

Figure III.1 presents the geometry and parameters considered in the model. The studied configurations include a single void, two symmetrical voids, and two parallel voids. In Figure III.1, α denotes the void depth coefficient, while β and s represent the eccentricity of a single void from the footing centerline and the horizontal distance between the centers of two voids, respectively.

In this study, a square-shaped void was adopted, as the influence of void shape on bearing capacity can be considered negligible [13]. Based on field observations, Kiyosumi et al. reported that the size of voids in Japanese calcareous sediments ranges from less than 1 m to approximately 10 m, with continuous horizontal extension. Therefore, a void width W = 2 m was assumed, resulting in a void-width-to-footing-width ratio of W/B = 1.0, which is consistent with the assumptions of Lee et al. [14, 15]. In addition, symmetrical and parallel void configurations were considered to investigate interaction effects between multiple voids.

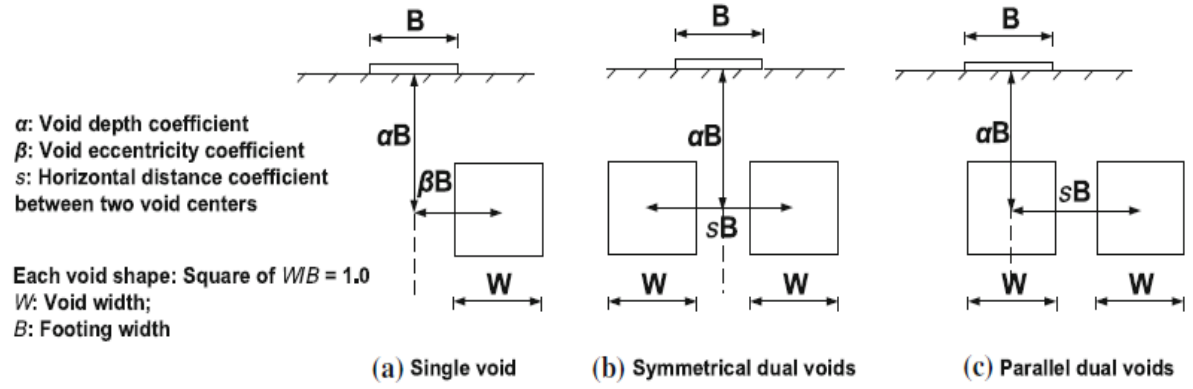
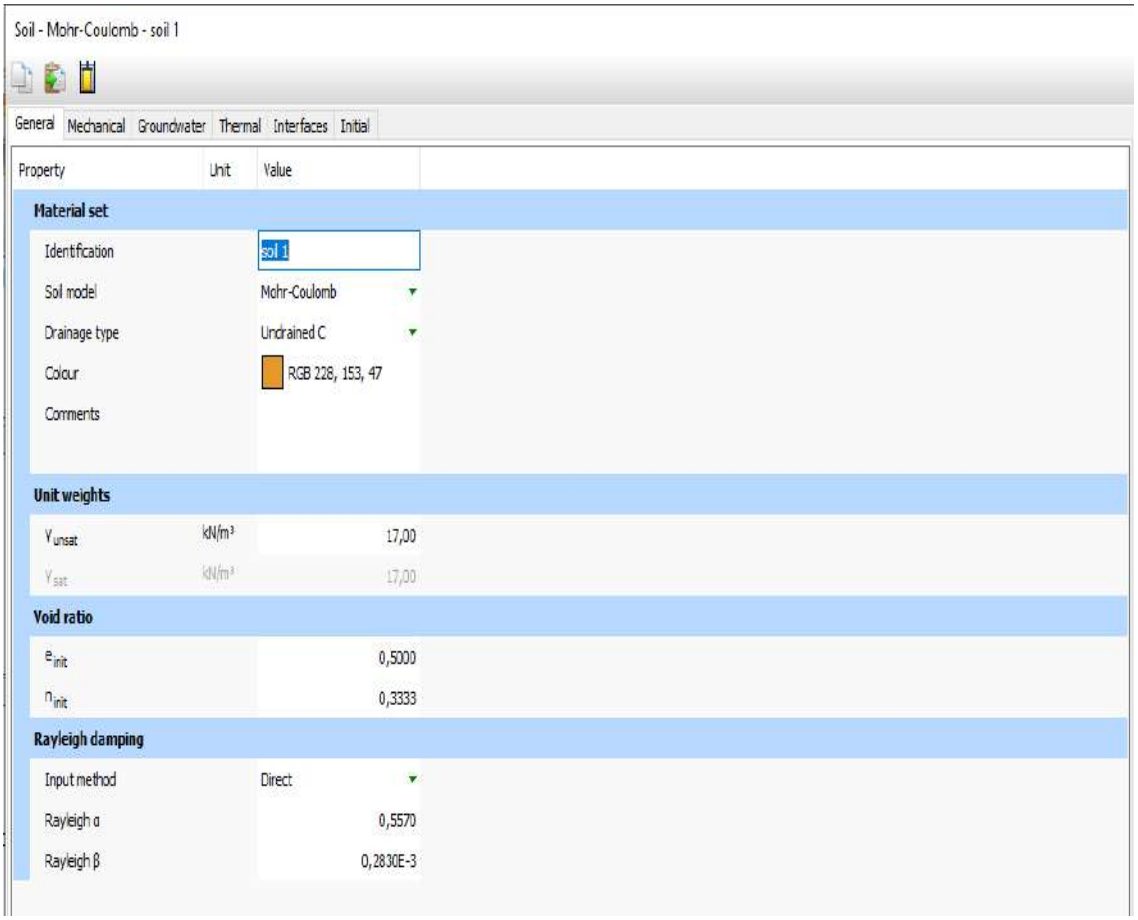


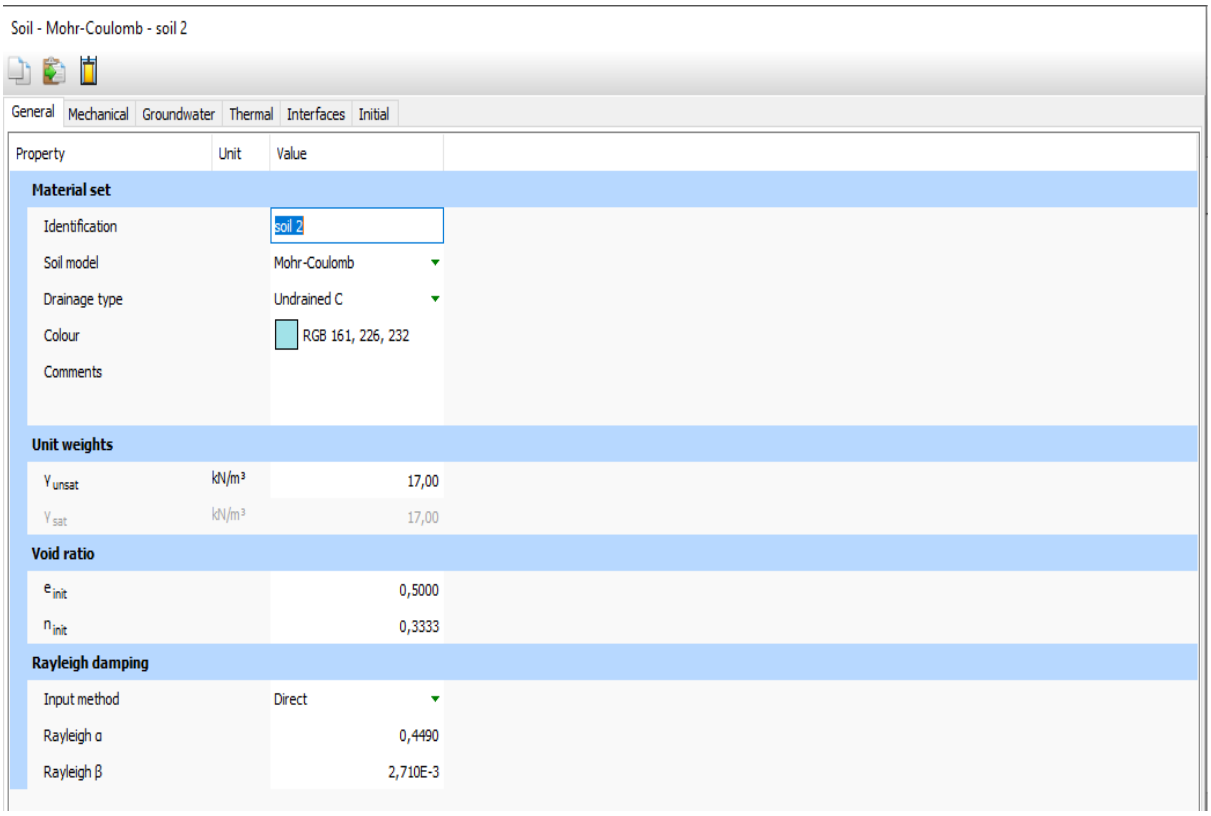
Figure III.1: Problem definition -- (a) single void, (b) symmetrical dual voids, (c) parallel dual voids

III.3. Material Properties and Constitutive Model

Small-strain finite element analyses of surface strip footings resting above voids were carried out using the commercially available software PLAXIS 2D Version 2024. The soil was modeled with fifteen-node triangular elements, while the footing was represented by six-node triangular plate elements compatible with the triangular faces of the degenerated soil elements.

The soil was modeled as an elastic-perfectly plastic material governed by the Mohr-Coulomb failure criterion. In order to simulate undrained clay behavior, both the friction angle and the dilation angle were set to zero (phi = psi = 0 degrees), and a Poisson's ratio of v = 0.495 was adopted. The undrained Young's modulus, cohesion, and unit weight were set to Eu = 30 MPa, cu = 60 kPa,100KPa,300KPa and gamma = 20 kN/m3, respectively.




Soil - Mohr-Coulomb - soil 2
General
Mechanical
Groundwater
Thermal
Interfaces
Initial
Property
Unit
Value
Material set
Identification
soil 2
Soil model
Mohr-Coulomb
Drainage type
Undrained C
Colour
RGB 161, 226, 232
Comments
Unit weights
Y unsat
kN/m³
17,00
Y sat
kN/m³
17,00
Void ratio
e init
0,5000
n init
0,3333
Rayleigh damping
Input method
Direct
Rayleigh α
0,4490
Rayleigh β
2,710E-3

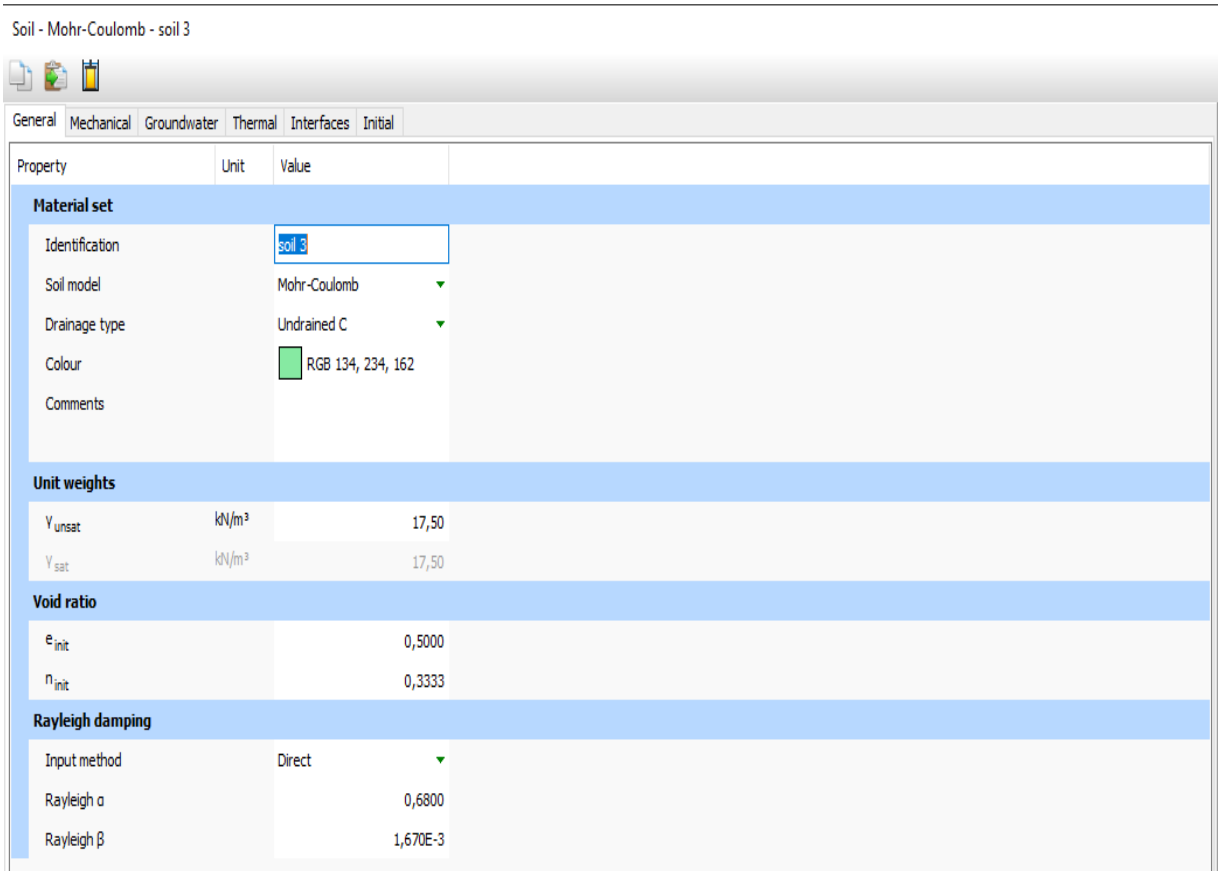
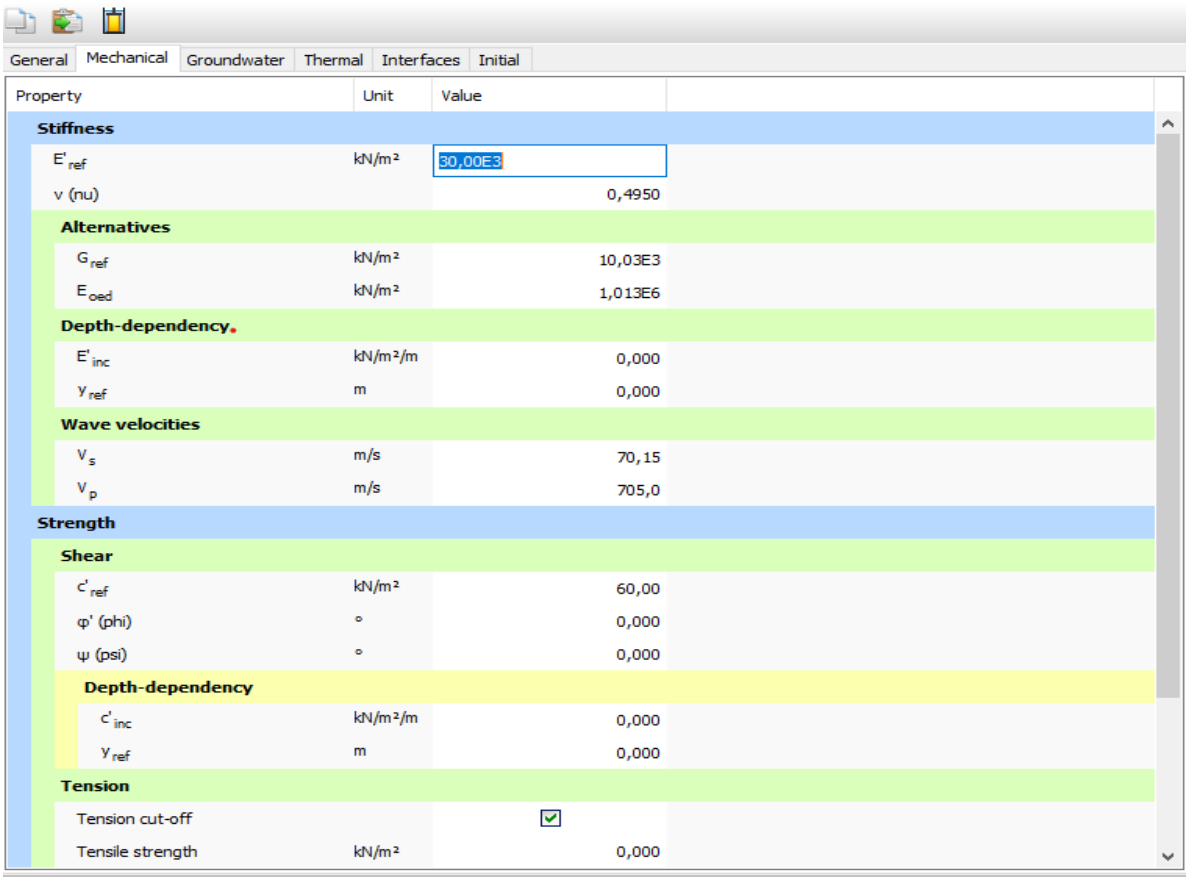
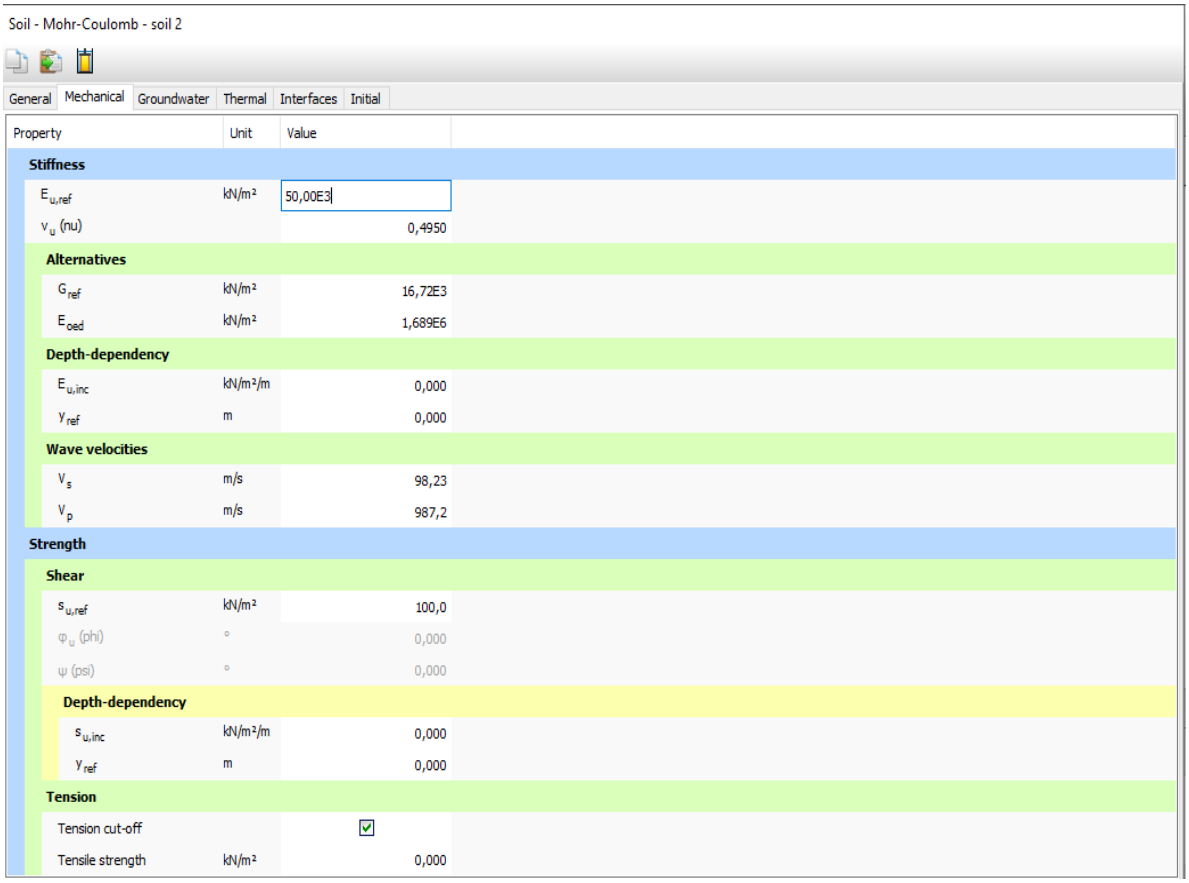


Figure III.III: Input window for general material data in PLAXIS 2D


General
Mechanical
Groundwater
Thermal
Interfaces
Initial
Property
Unit
Value
Stiffness
E'ref
kN/m²
30,00E3
ν (nu)
0,4950
Alternatives
Gref
kN/m²
10,03E3
Eoed
kN/m²
1,013E6
Depth-dependency
E'inc
kN/m²/m
0,000
yref
m
0,000
Wave velocities
Vs
m/s
70,15
Vp
m/s
705,0
Strength
Shear
c'ref
kN/m²
60,00
φ' (phi)
°
0,000
ψ (psi)
°
0,000
Depth-dependency
c'inc
kN/m²/m
0,000
yref
m
0,000
Tension
Tension cut-off
Tensile strength
kN/m²
0,000


Soil - Mohr-Coulomb - soil 2
General
Mechanical
Groundwater
Thermal
Interfaces
Initial
Property
Unit
Value
Stiffness
$E_{u,ref}$ kN/m² 50,00E3
ν_u (nu) 0,4950
Alternatives
G_{ref} kN/m² 16,72E3
E_{oed} kN/m² 1,689E6
Depth-dependency
$E_{u,inc}$ kN/m²/m 0,000
y_{ref} m 0,000
Wave velocities
V_s m/s 98,23
V_p m/s 987,2
Strength
Shear
$s_{u,ref}$ kN/m² 100,0
φ_u (phi) ° 0,000
ψ (psi) ° 0,000
Depth-dependency
$s_{u,inc}$ kN/m²/m 0,000
y_{ref} m 0,000
Tension
Tension cut-off
Tensile strength kN/m² 0,000

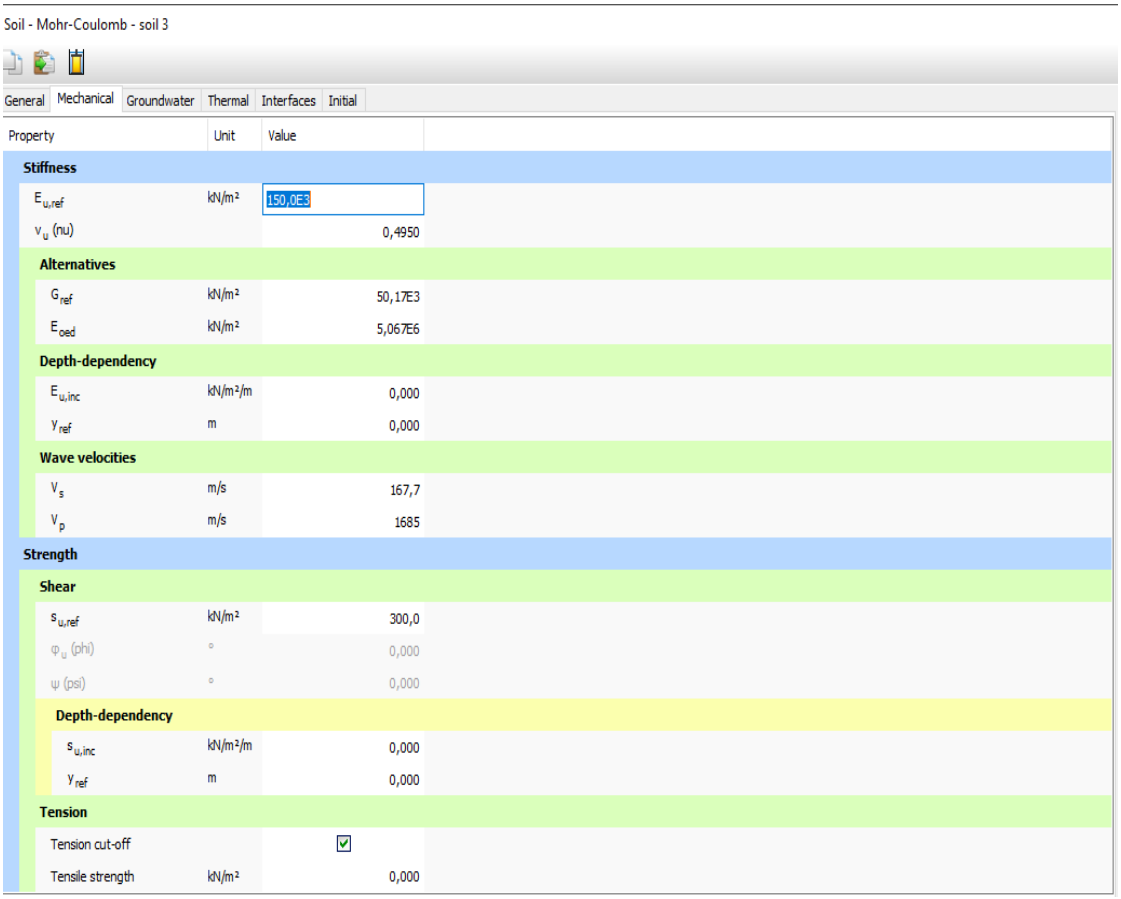


Figure III.4: Input window for mechanical properties in PLAXIS 2D

III.4. Dynamic Damping Parameters (Rayleigh Coefficients)

To determine the dynamic damping parameters of the soil model -- namely, the Rayleigh coefficients alpha and beta -- in PLAXIS 2D, the following procedure was adopted.

The governing equation of motion for a deformable volume element subjected to a dynamic load is:

$$M\,u'' + C\,u' + K\,u = F \qquad \text{(III.1)}$$

where M is the mass matrix, u is the displacement vector, C is the damping matrix, K is the stiffness matrix, and F is the applied load vector. The displacement u, velocity u', and acceleration u" may all vary with time. The last two terms (K u = F) correspond to the static deformation component.

In PLAXIS 2D, the mass matrix M accounts for the mass of all materials -- including soil, water, and structural elements -- and is implemented as a lumped matrix. The damping matrix C represents the material damping arising from friction and irreversible deformations

(plasticity or viscosity). In finite element formulations, C is commonly expressed as a linear combination of the mass and stiffness matrices following the Rayleigh damping formulation:

$C = \alpha\ [M] + \beta\ [K]$ (III.2)

where alpha and beta are the Rayleigh damping coefficients, calibrated from two target natural frequencies and the desired damping ratio.

The n-th natural frequency of vibration of a homogeneous soil deposit of thickness H is given by:

$fn = (Vs / 4H) \times (1 + 2n), \quad n = 0, 1, 2, \ldots$ (III.3)

where fn is expressed in Hz and Vs is the shear wave velocity of the soil. For n = 0, Equation (III.III) reduces to the fundamental frequency of the deposit:

$f1 = Vs / (4H)$ (III.4)

The shear wave velocity Vs is obtained from:

$Vs = \sqrt{(G / \rho)}$ (III.5)

where G is the shear modulus and rho is the mass density of the soil. The shear modulus G is related to the Young's modulus E and Poisson's ratio v by:

$G = E / [2 (1 + v)]$ (III.6)

Applying Equations (III.5) and (III.6) with the adopted soil parameters (E = 30 MPa, v = 0.495, gamma = 20 kN/m3):

- $G = 30\,000 / [2\ x\ (1 + 0.495)] = 10\,033\ kPa = 10.03\ MPa$
- $\rho = \gamma / g = 20 / 9.81 = 2.038\ t/m3$
- $Vs = \sqrt{(10\,033 / 2.038)} = 70.17\ m/s$

Applying Equation (III.4) with H = III0 m, and taking $f2 = 5 \times f1$ as the second target frequency:

- $f1 = 70.17 / (4\ x\ 30) = 0.585\ Hz$
- $f2 = 5\ x\ f1 = 5\ x\ 0.585 = 2.925\ Hz$

For a target damping ratio epsilon = 5%, the Rayleigh coefficients are determined from the following two-frequency calibration expressions:

$\alpha\ \varepsilon \times [4\ \pi\ f1\ f2 \div (f1 + f2)]$ $(III.7)$

$\beta = \varepsilon \times [1 / (\pi\ f1\ f2)]$ (III.8)

Substituting the computed frequencies into Equations (III.7) and (III.8):

$\alpha = 0.05\ x\ [4\ x\ \pi\ x\ 0.585\ x\ 2.925 / (0.585 + 2.925)] = 0.305$

$\beta = 0.05\ x\ [1\ /\ (\pi\ x\ 0.585\ x\ 2.925)] = 2.83\ x\ 10^{-3}$

The values entered in PLAXIS 2D for the model presented in this study are $\alpha = 0.557$ and $\beta = 0.01080$, as specified by the authors based on their original parameter set.

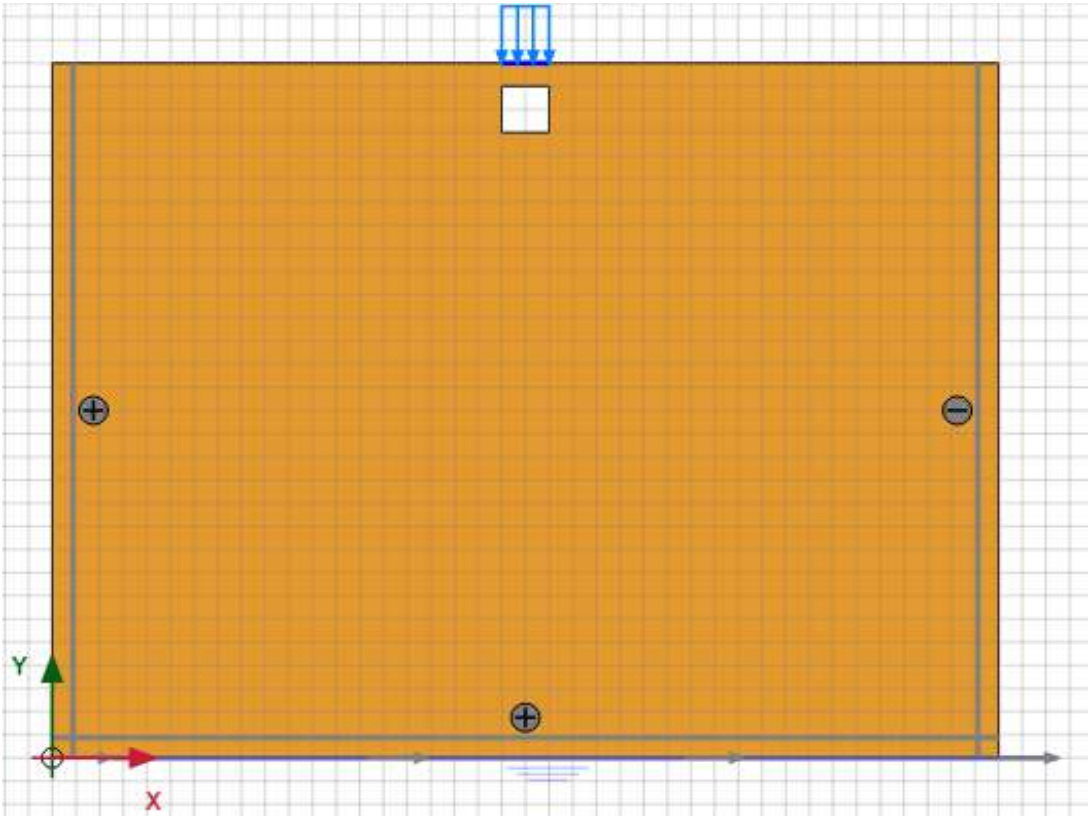


Figure III.5: Model geometry in PLAXIS 2D

III.5. Boundary Conditions

The definition of boundary conditions is crucial for maintaining numerical stability and for realistically representing soil behavior. In this model, the following assumptions are adopted:

Bottom boundary: The lower boundary is fully fixed in both the horizontal and vertical directions, simulating a rigid base layer at depth. This constraint prevents any displacement at the base of the model and ensures a stable computational response.

Side boundaries: The vertical boundaries are constrained against horizontal movement while remaining free in the vertical direction. This configuration allows the soil to settle freely while limiting lateral displacements, which is consistent with typical field conditions for a semi-infinite soil medium.

III.6. Hydraulic Conditions

The numerical analysis was carried out under the assumption of dry or unsaturated conditions. The soil was considered free of groundwater, meaning that pore water pressures

were neglected and assumed to have no effect on the mechanical response during loading. Consequently, no seepage analysis or permeability parameters were included in PLAXIS 2D.

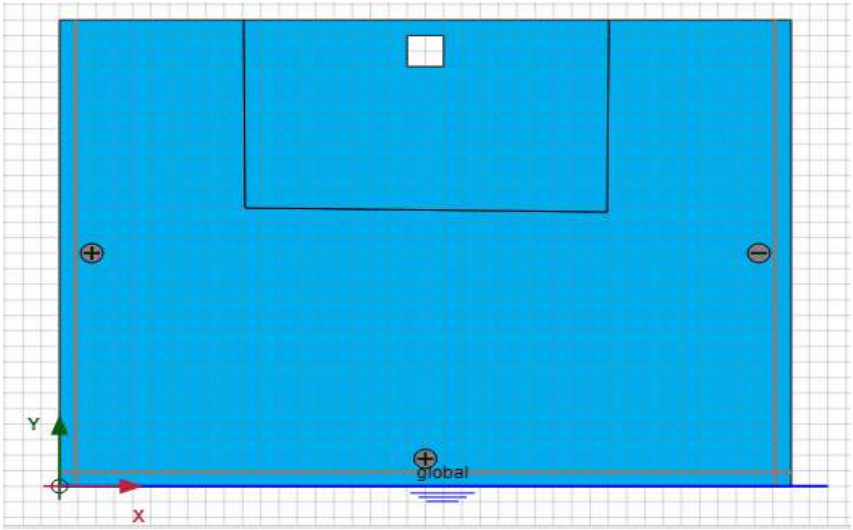


Figure III.6: Hydraulic conditions as defined in PLAXIS 2D

III.7. Applied Load

In this model, a uniform vertical load is applied to the foundation over a strip of width B,with an intensity of 100 kN/m. The load is positioned directly above the cavity to simulate the presence of a superstructure. This uniform loading condition enables a systematic evaluation of the influence of the applied load on the behavior and stability of the soil mass, as well as on the cavities located beneath the foundation.

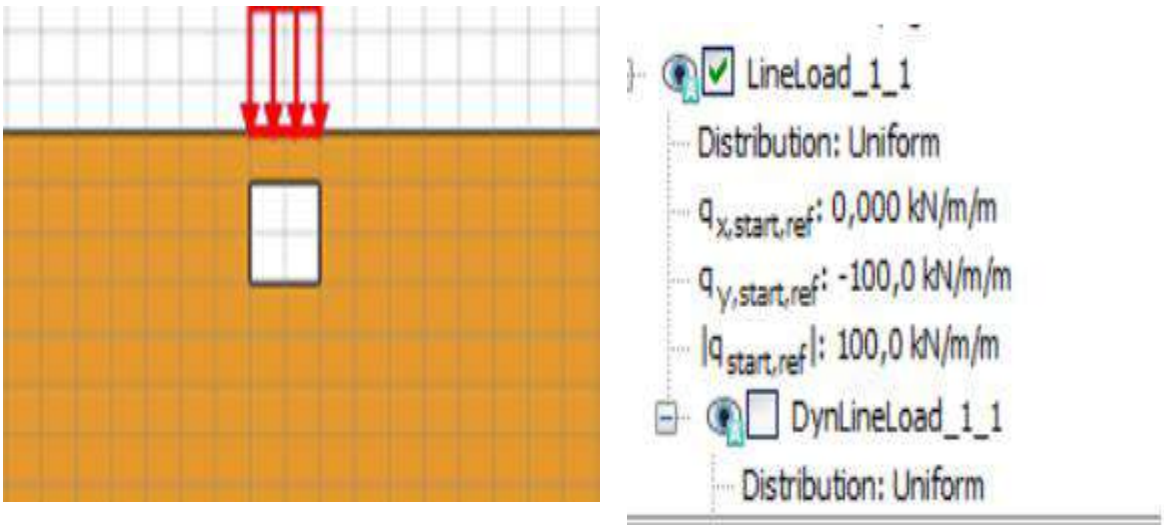


Figure III.7: Load configuration in PLAXIS 2D

III.8. Meshing

In PLAXIS 2D, soil layers can be discretized using triangular elements with either 6 or 15 nodes. In this study, 15-node triangular elements were selected because they allow fourth-order interpolation of displacements, thereby providing a more accurate representation of soil behavior. Additionally, twelve Gauss integration points are used per element, which enhances the precision of stress and strain calculations within each element.

An appropriate and refined mesh is essential for obtaining accurate simulation results. The mesh density was adapted to the problem geometry: a finer mesh was applied in the vicinity of the cavities and beneath the loaded zone, where stress gradients are highest, while a coarser mesh was used in regions of lower gradient in order to reduce computation time without sacrificing accuracy.

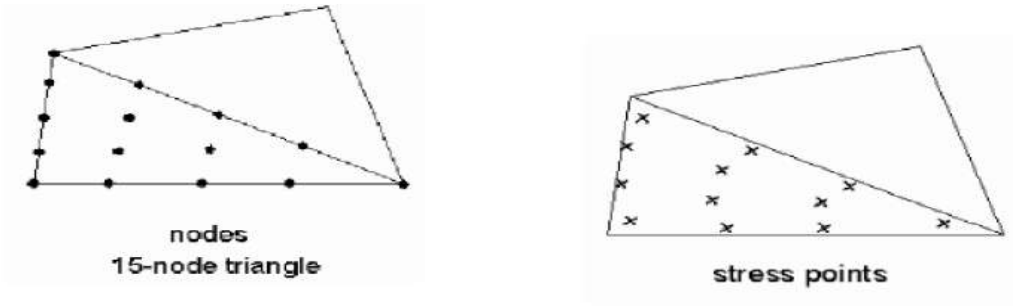


Figure III.8: Node and stress point positions within a 15-node triangular soil element [12]

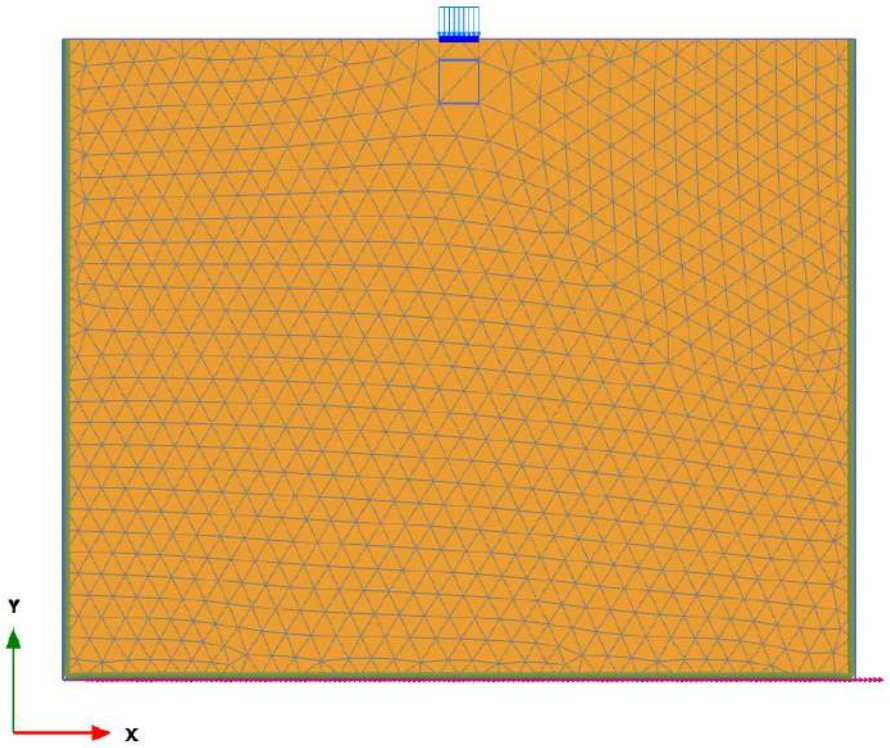


Figure III.9: Generated finite element mesh in PLAXIS 2D

III.9. Calculation Phases

III.9.1. Initial Phase

In the initial phase, the model geometry and the mechanical properties of all materials are defined -- in particular, the Young's modulus and cohesion. These parameters govern the elasto-plastic response of the soil under applied loading and establish the initial in-situ stress state prior to any external load application.

III.9.2. First Phase -- Application of Foundation Load

In this phase, the footing is activated and a uniform vertical load of 100 kPa is imposed on the foundation area. This load is maintained constant throughout the analysis in order to evaluate the influence of the cavities on the foundation's stability and on the distribution of stresses within the soil mass.

III.9.III. Second Phase -- Introduction of Cavities

The cavities are introduced within the soil layer at varying normalized depths alpha. Their sizes and positions are systematically varied in order to analyze the influence of cavity geometry on the mechanical response of the soil.

III.9.4. Third Phase -- Plastic Failure Analysis

In this phase, a plastic analysis is performed using PLAXIS 2D to assess the bearing capacity and failure behavior of the soil supporting a strip footing. This type of analysis is particularly suited to simulating yielding and irreversible deformations in the soil, which are necessary for determining the ultimate load capacity of the foundation.

All simulations were performed under drained conditions, assuming a sufficiently slow rate of load application such that excess pore water pressures could fully dissipate. The soil behavior was described using the Mohr-Coulomb constitutive model, which offers a reasonable compromise between computational simplicity and a realistic representation of soil response.

The plastic calculation procedure allows the model to capture both the initial elastic response of the soil and its subsequent plastic behavior as failure is approached. The analysis is continued until either failure occurs or the load-displacement response stabilizes, indicating that the ultimate bearing capacity has been reached.

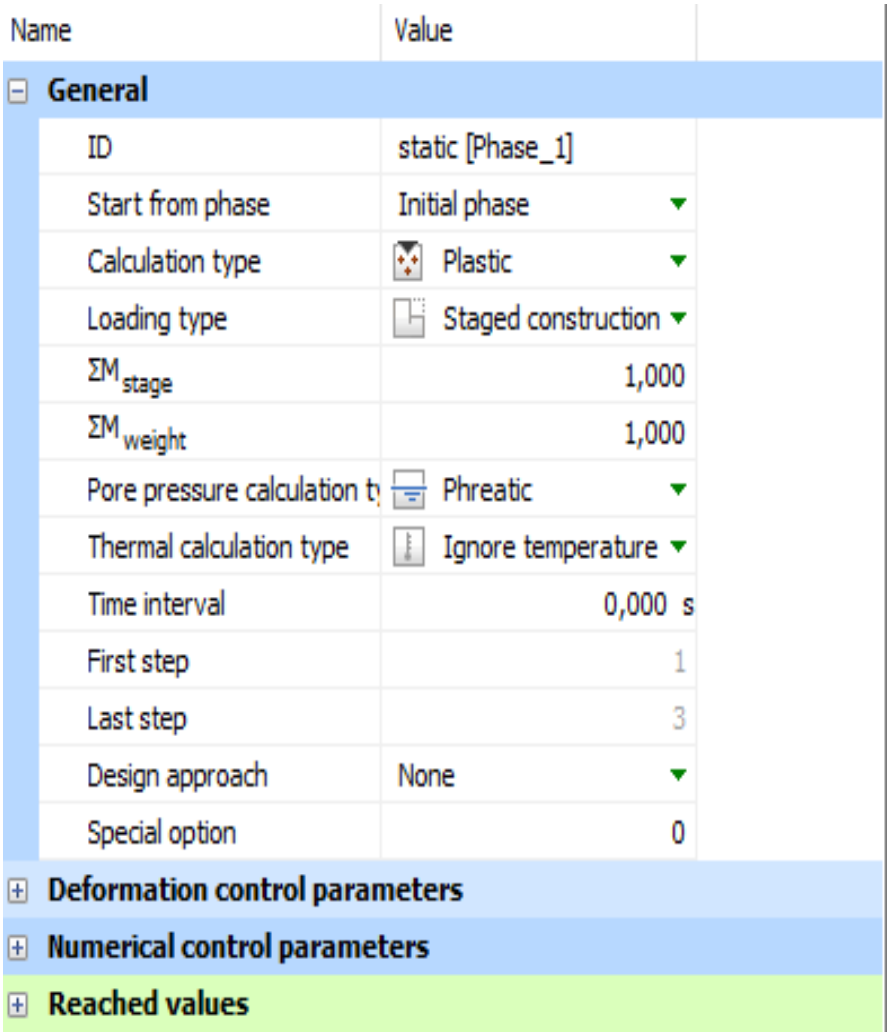


Figure III.10: Calculation phase settings in PLAXIS 2D

III.10. Analysis of Mesh Deformation and Displacements

III.10.1. Mesh Deformation

The deformed mesh represents the overall response of the soil domain under loading conditions. It enables the identification of localized zones of significant deformation, which are indicative of the development of potential failure surfaces within the soil mass.

III.10.2. Total Horizontal Displacement

The horizontal displacement results depict the lateral response of the soil mass subjected to vertical loading. They are useful for assessing the overall stiffness of the soil system and for identifying zones where notable lateral deformation develops.

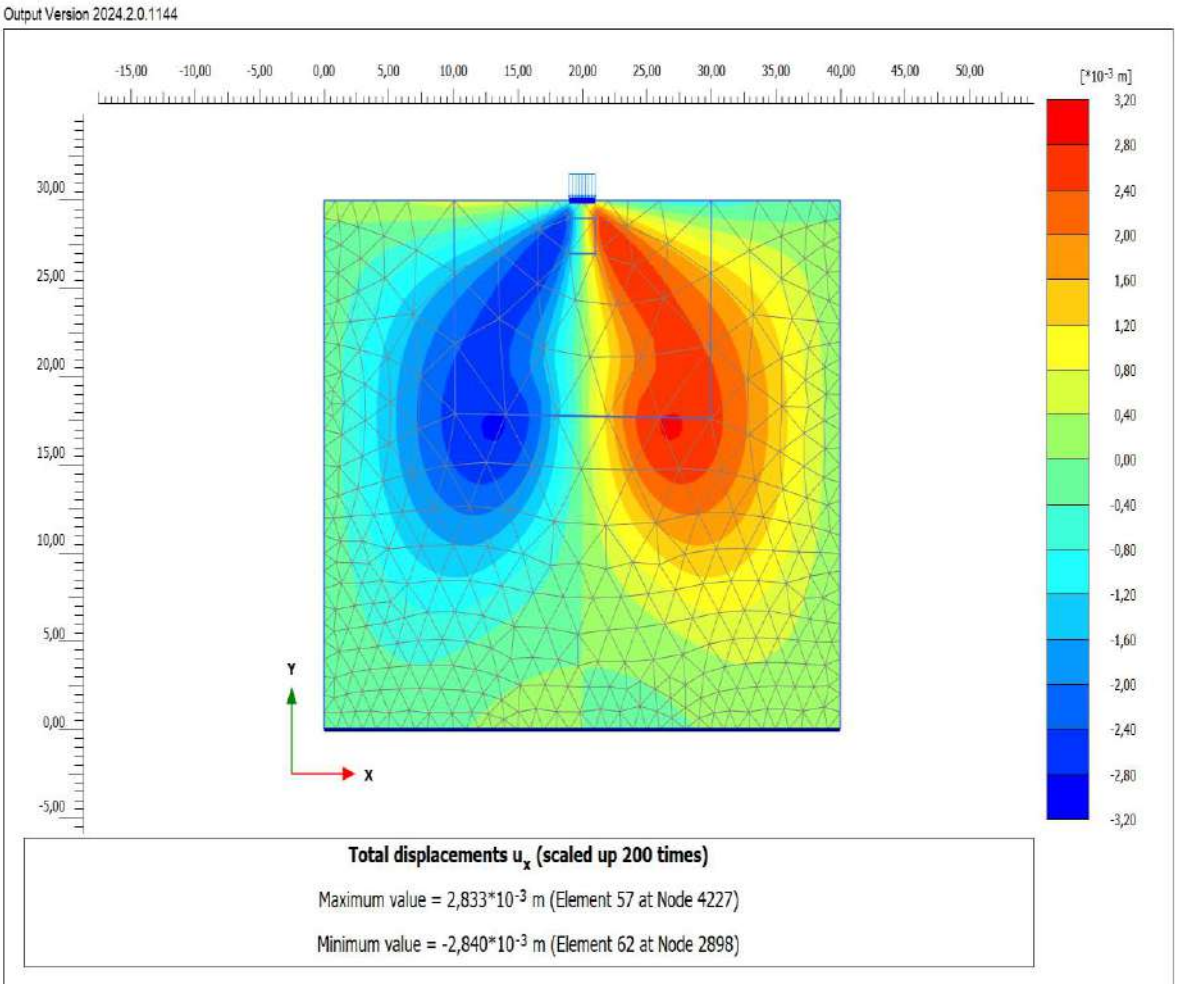


Figure III.11: Total horizontal displacement contours obtained from PLAXIS 2D analysis

III.10.III. Total Vertical Displacement

The vertical displacement results illustrate the soil mass's settlement behaviour. They indicate the extent of compression beneath the foundation and may also reveal slight upward displacement in adjacent zones, suggesting edge-heave effects at the ground surface.

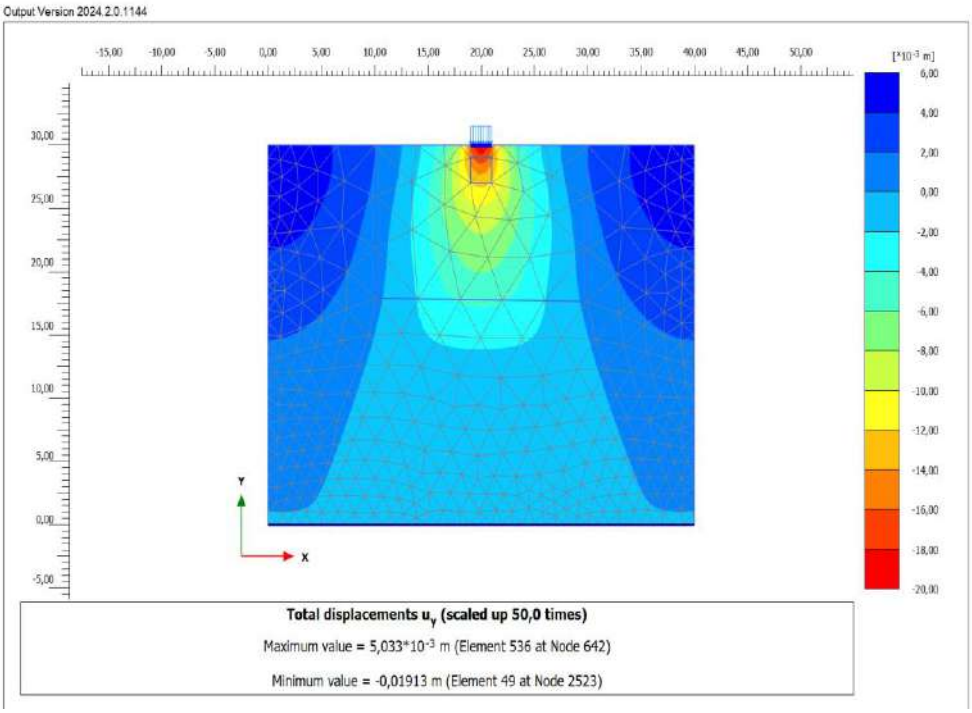


Figure III.12: Total vertical displacement contours obtained from PLAXIS 2D analysis

III.11. Bearing Capacity

A plastic analysis was carried out in PLAXIS 2D to determine the ultimate bearing capacity of the shallow foundation using the finite element method. Based on the Terzaghi bearing capacity framework for a strip footing on a purely cohesive soil (phi = 0), the dimensionless bearing capacity factor Nc is back-calculated from the numerical results as:

$$Nc = q / cu \quad \text{(III.9)}$$

where q is the applied reference load intensity (kN/m2), m) and cu is the undrained shear strength (kPa). The computed values of Nc for the different void depth coefficients alpha are summarized in Table III.1.

Table III.1: Bearing capacity factor Nc for varying void depth coefficients alpha

alpha (m)	M stage	qu (kN/m2)	Nc
1	0.6208	100	2.06
2	0.9III00	100	III.11
III	0.9470	150	4.75
4	0.9III9III	150	4.69

alpha (m)	M stage	qu (kN/m2)	Nc
5	0.9662	150	4.66

The results indicate that the bearing capacity factor Nc increases with depth alpha, reaching a near-constant value for alpha >= III. This trend suggests that the influence of the void on the failure mechanism diminishes as the void is located further below the foundation level.

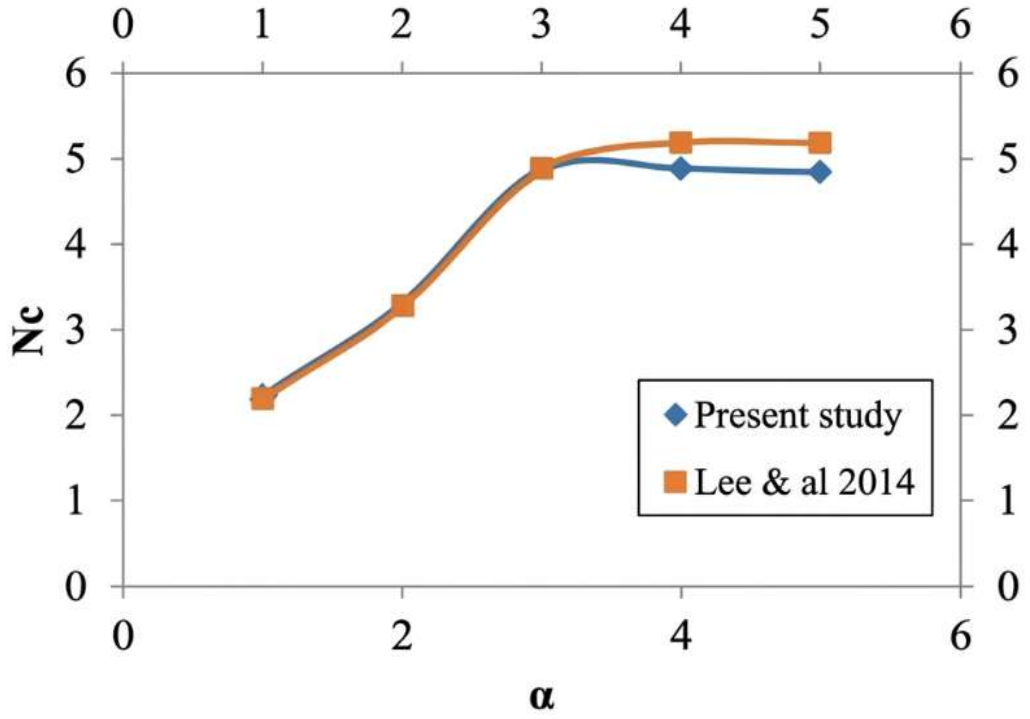


Figure III.1III: *Variation of the bearing capacity factor Nc with the normalized void depth coefficient α — comparison between the present PLAXIS 2D results and those of Lee et al. (2014)*

Figure III.1III compares the bearing capacity factor Nc obtained in the present numerical study using PLAXIS 2D with the values reported by Lee et al. (2014) using the Discontinuity Layout Optimization (DLO) method.

It can be observed that Nc increases progressively with increasing normalized void depth α. For shallow void positions (low values of α), the bearing capacity factor remains significantly reduced, reflecting the strong interaction between the failure mechanism beneath the footing and the void. A pronounced increase in Nc is observed as α increases from 2 to III, indicating

a transition from a void-influenced failure mode to a deeper, less-affected mechanism. Beyond $\alpha \geq$ III, the factor Nc approaches a near-constant value of approximately 5.14, which is consistent with the classical Prandtl solution for an undrained strip footing on a homogeneous cohesive half-space ($Nc = \pi + 2 \approx 5.14$). This convergence confirms that, at sufficient depth, the void no longer intersects the critical failure surface and ceases to influence the ultimate bearing capacity.

The results obtained in the present study show good agreement with those of Lee et al. (2014), with only minor discrepancies observed for high values of Nc.

This close agreement confirms the reliability of the present numerical model and validates the use of PLAXIS 2D for bearing capacity analysis in the presence of underground cavities.

The minor differences observed between the two sets of results can be attributed to the distinct numerical approaches adopted in each study. The present analysis was carried out using PLAXIS 2D, which is based on the finite element method (FEM) with an elasto-plastic Mohr–Coulomb constitutive model. In contrast, Lee et al. (2014) employed the Discontinuity Layout Optimization (DLO) method, which is a limit analysis technique based on the upper-bound theorem of plasticity. These differences in formulation — including mesh discretization, element type, and boundary conditions — inherently lead to slight deviations in the predicted Nc values. Despite this methodological difference, the agreement between the two approaches is considered satisfactory and lends confidence to both methods for this class of problem.

III.12. Conclusion

This numerical study, conducted using PLAXIS 2D, has demonstrated the significant influence of underground cavities on the bearing capacity of shallow foundations. The results show that the presence of voids in the soil leads to a reduction in bearing capacity, which is most pronounced when the cavity is located close to the failure zone beneath the foundation. This reduction is primarily attributed to the disruption of stress transmission and the consequent weakening of the soil mass.

It was also observed that the position and size of the cavities play a key role in governing the soil response and may substantially alter the failure mechanism, in some cases leading to premature foundation instability. A comprehensive parametric study will be conducted in the following chapter to further investigate the influence of these parameters on the bearing capacity and the overall behavior of the soil.

CHAPTER IV

Parametric Study of the Seismic Bearing Capacity of a Strip Footing on Cohesive Soil in the Presence of Underground Cavities

IV.1. Introduction

This chapter presents a parametric investigation of the seismic bearing capacity of a strip footing founded on cohesive soil. The numerical simulations are performed using PLAXIS 2D, which is based on the finite element method.

The main objective of this study is to compare the behavior of the soil–foundation system under three different cavity configurations:

- Single cavity
- Two symmetrical cavities
- Two parallel cavities

Several parameters are considered throughout this analysis, including the soil type, the cavity depth, the eccentricity relative to the footing axis, and the spacing between cavities in the case of double-cavity configurations.

The variation of these parameters makes it possible to evaluate the interaction between the geometry of an underground cavity and the surrounding soil mass.

All analyses were performed considering the seismic excitation of the Great Hanshin Earthquake. The details of this seismic event are presented in Section IV.2 below.

IV.2. Record of Earthquake

The seismic loading adopted in this study is based on the accelerogram recorded during the Great Hanshin Earthquake, one of the most destructive seismic events in modern Japanese history. The main characteristics of this earthquake are summarized as follows:

- Date: January 17, 1995
- Location: Kobe city, Hyogo Prefecture, Japan
- Magnitude: approximately 6.9 to 7.3 (depending on the scale used)
- Duration: approximately 20 seconds of strong motion
- Focal depth: approximately 16 km

The earthquake caused severe damage to the urban infrastructure of Kobe, including widespread collapse of elevated expressways, port facilities, and residential buildings. Its proximity to a densely populated area, combined with the shallow focal depth, generated high peak ground accelerations and significant soil–structure interaction effects.

From a geotechnical standpoint, the Great Hanshin Earthquake is particularly relevant for the study of foundation behavior under seismic loading. The event was associated with extensive

ground deformation, soil liquefaction in reclaimed land areas, and failure of shallow foundations, making it a reference case for dynamic soil–foundation analyses.

The seismic input used in PLAXIS 2D is introduced as a dynamic multiplier applied to the model boundary conditions. The acceleration time history is discretized and imported as a tabular signal, as illustrated in Figure IV.1. The signal shows a peak dynamic multiplier of approximately ±3.0 during the first 10 seconds, followed by a progressive attenuation of amplitude toward the end of the record.

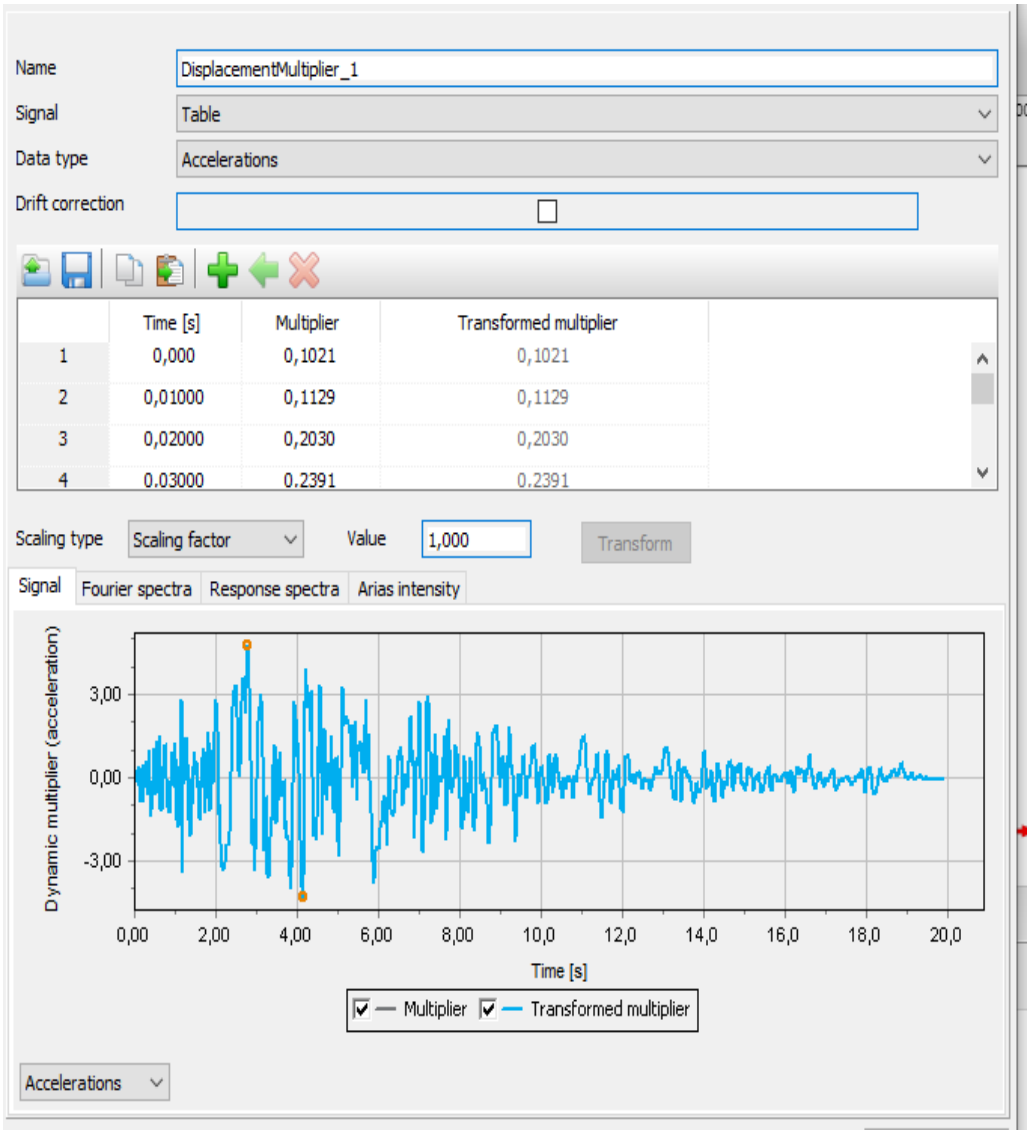


Figure IV.1: Time history of the seismic accelerogram of the Great Hanshin Earthquake (Kobe, 1995), as implemented in PLAXIS 2D

During the seismic analysis, large deformations were observed due to the strong dynamic loading. To control these excessive deformations and ensure numerical stability, the model was analyzed using an imposed settlement equal to 10% of the footing width.

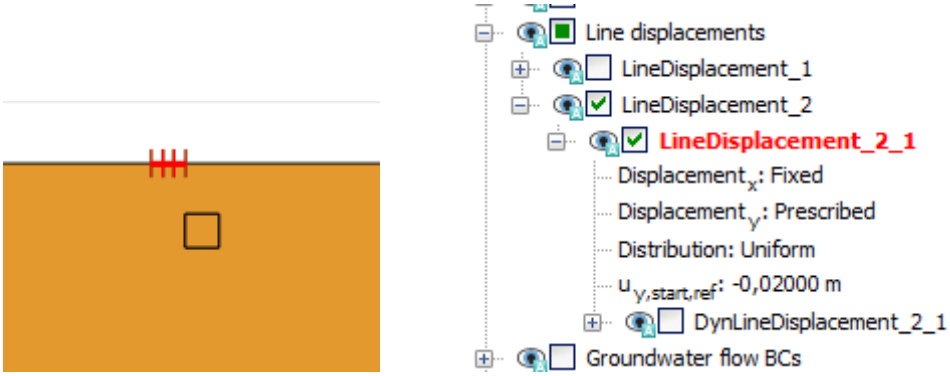


Figure IV.2: Aplication of the imposed settelement in the PLAXIS 2D

IV.3. Result Analysis

IV.3.1. Effect of Soil Cohesion on Seismic Bearing Capacity

To study the influence of soil cohesion on the seismic bearing capacity, the following observations can be made:

Figure IV.3 illustrates the effect of soil cohesion on seismic bearing capacity — single cavity, $\beta = 0$ ($\alpha = 1, 2, 3, 4$), It is observed that the seismic bearing capacity increases with increasing soil cohesion in all cases studied. This trend is physically consistent, since higher cohesion enhances the shear strength of the soil, making it stiffer and more capable of sustaining applied loads — including those transmitted by foundations and structures — even under seismic excitation.In the case without a cavity, the values of F_y remain the highest, confirming that the absence of an underground void ensures a better distribution of stresses within the soil mass. Conversely, the presence of a cavity leads to a significant reduction in seismic bearing capacity due to the disturbance of the stress field and the decrease in soil stiffness beneath the foundation.

For $\beta = 0$ (cavity located directly beneath the foundation axis), the values of Fy are generally the lowest when a cavity is present, particularly for $\alpha = 1$. This indicates that when the cavity is shallow and aligned with the applied load, it significantly disturbs the stress distribution, resulting in a substantial reduction in bearing capacity.As the cavity depth increases ($\alpha = 2, 3$), the curves progressively approach the reference curve corresponding to soil without a cavity, indicating that the detrimental effect of the cavity diminishes with increasing depth.

For α = 4, the curve closely approaches the no-cavity case, demonstrating that a deeply embedded cavity has a negligible influence on the seismic bearing capacity.

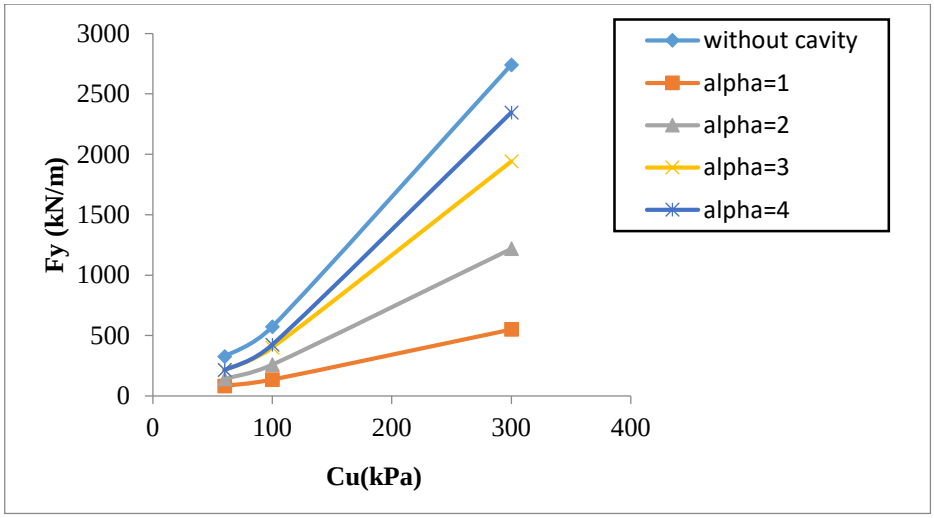


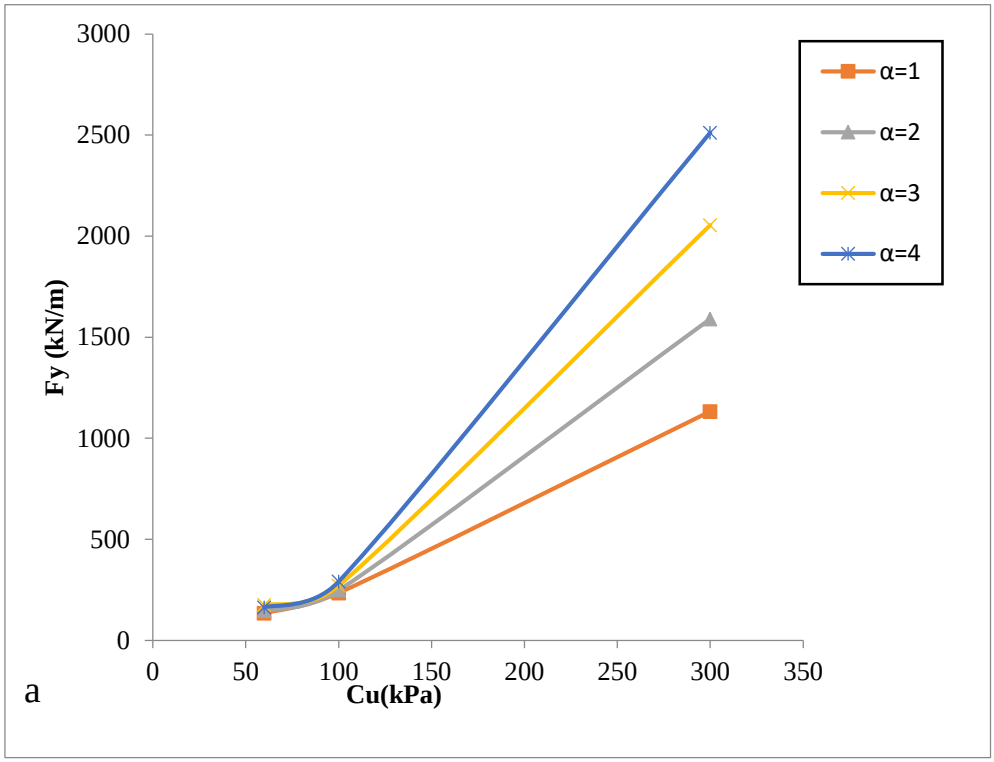
Figure IV.3: Effect of soil cohesion on seismic bearing capacity — single cavity, β = 0 (α = 1, 2, 3, 4)

Figure IV.4 and Figure IV.5 shows the effect of cavity eccentricity for β=1 and 2. The results indicate that varying the eccentricity and modifies the seismic bearing capacity. For β = 1 and β = 2, the curves maintain the same increasing trend, with differences in the magnitude of Fy. An increase in eccentricity displaces the cavity further from the foundation loading axis, thereby reducing its influence on the failure mechanism. Consequently, the seismic bearing capacity tends to increase as the cavity eccentricity increases.

For β = 3 and β = 4, both curves display the same increasing trend but with different values of Fy: the seismic bearing capacity consistently increases with increasing soil cohesion. This confirms that cohesion remains the dominant parameter governing the resistance of the soil mass under seismic loading.

For β = 4, the values of Fy are generally slightly higher than those obtained for β = 3. This difference is explained by the fact that a larger eccentricity moves the cavity further from the foundation loading axis, reducing its influence on the failure zone and improving the load transmission through the soil.

It is also noted that the differences between the curves remain relatively small for large values of β, indicating that the effect of eccentricity becomes less significant when the cavity is sufficiently remote from the foundation.



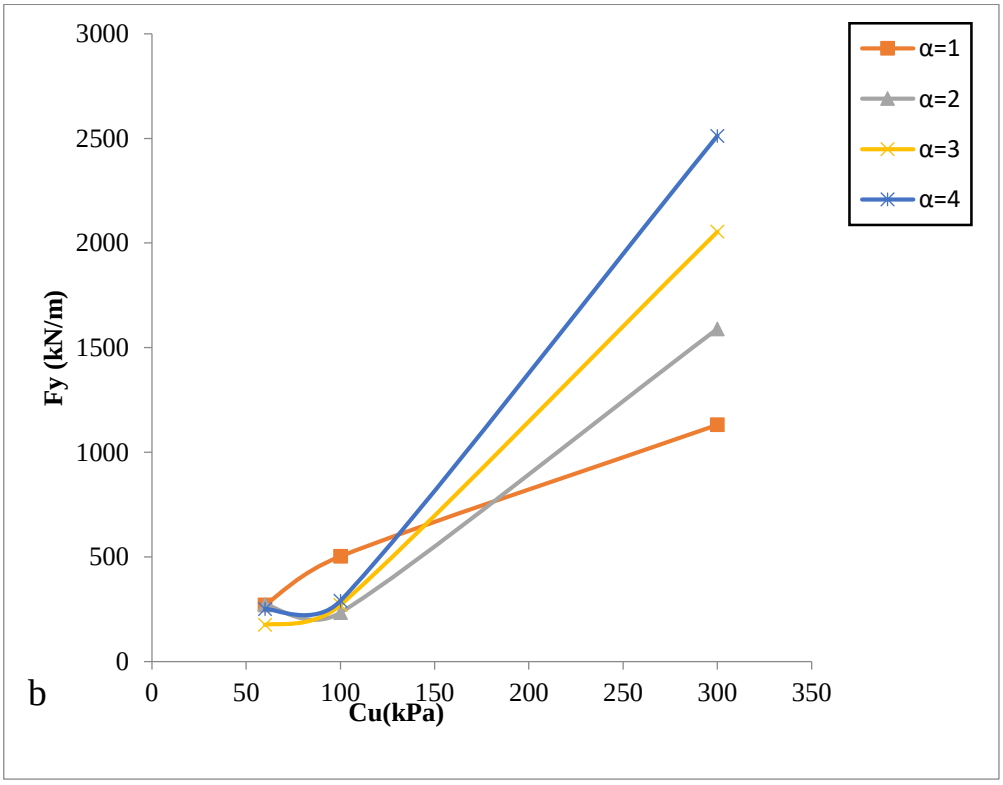
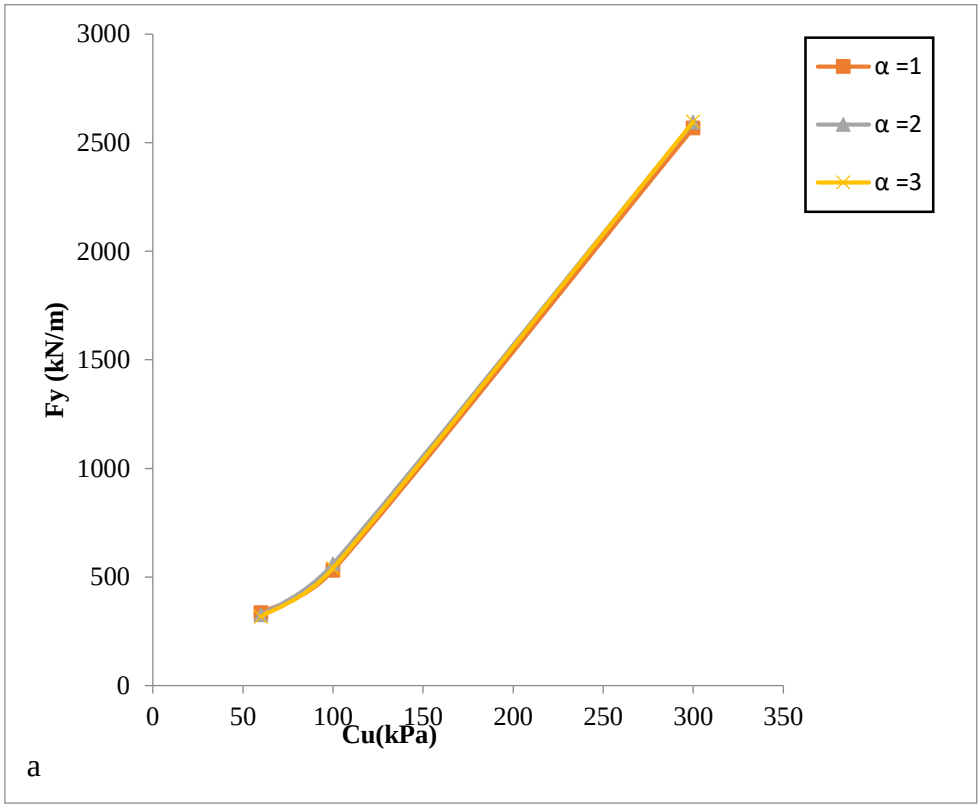


Figure IV.4: Effect of soil cohesion on seismic bearing capacity — single cavity with eccentricity β = 1 (a) and β = 2 (b)



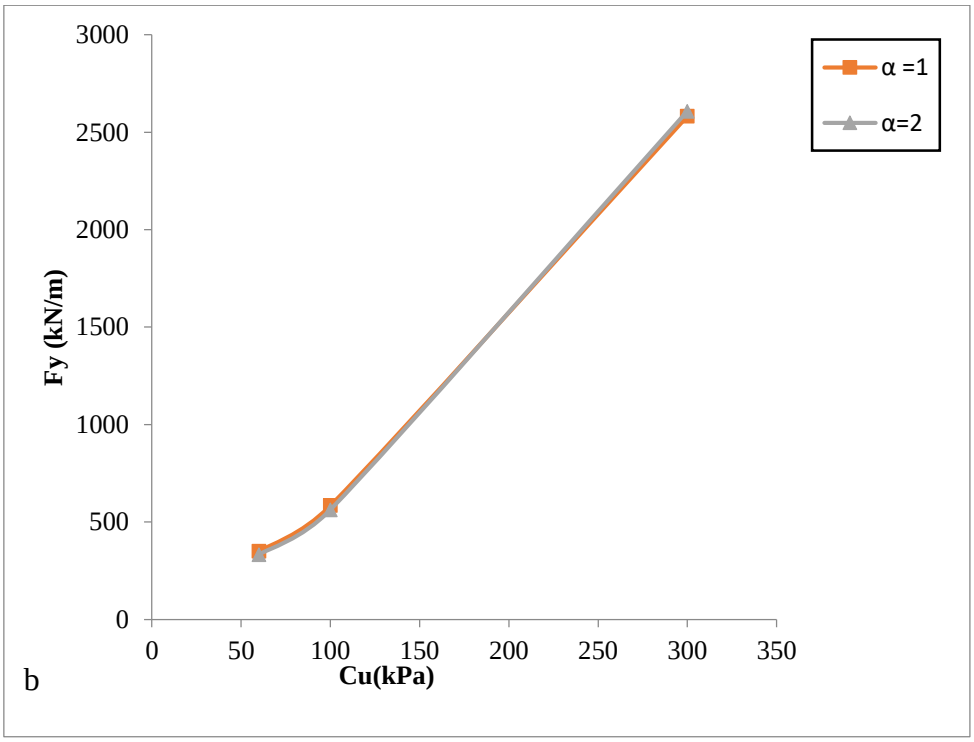


Figure IV.5: Effect of soil cohesion on seismic bearing capacity — single cavity with eccentricity β = 3 (a) and β = 4 (b)

Figure IV.6 shows the effect of soil cohesion on seismic bearing capacity with two symmetrical cavities, S = 1 m, for various cavity depths α. In the case of two symmetrical cavities centered beneath the foundation with a constant spacing of S = 1 m, the 'without cavity' curve yields the highest values of Fy, confirming that the absence of cavities ensures better foundation stability. The presence of two symmetrical cavities reduces the bearing capacity due to the disturbance of the stress distribution and the decrease in soil stiffness beneath the foundation.

Although two symmetrical cavities represent a significant weakness in the soil mass, their adverse effect becomes less critical in more cohesive soils. Higher cohesion improves the shear strength and stiffness of the soil, enabling it to better resist deformation and stress concentration, thereby limiting the influence of the cavities on the seismic bearing capacity.

Regarding the effect of cavity depth α, the bearing capacity increases as α increases. For shallow depths (α = 1), the cavities are located close to the foundation and strongly influence the soil failure zone, resulting in a significant reduction in Fy. In this configuration, the two cavities behave almost as a single large cavity, causing an expansion of the failure zone beneath the foundation and a reduction in the seismic bearing capacity.

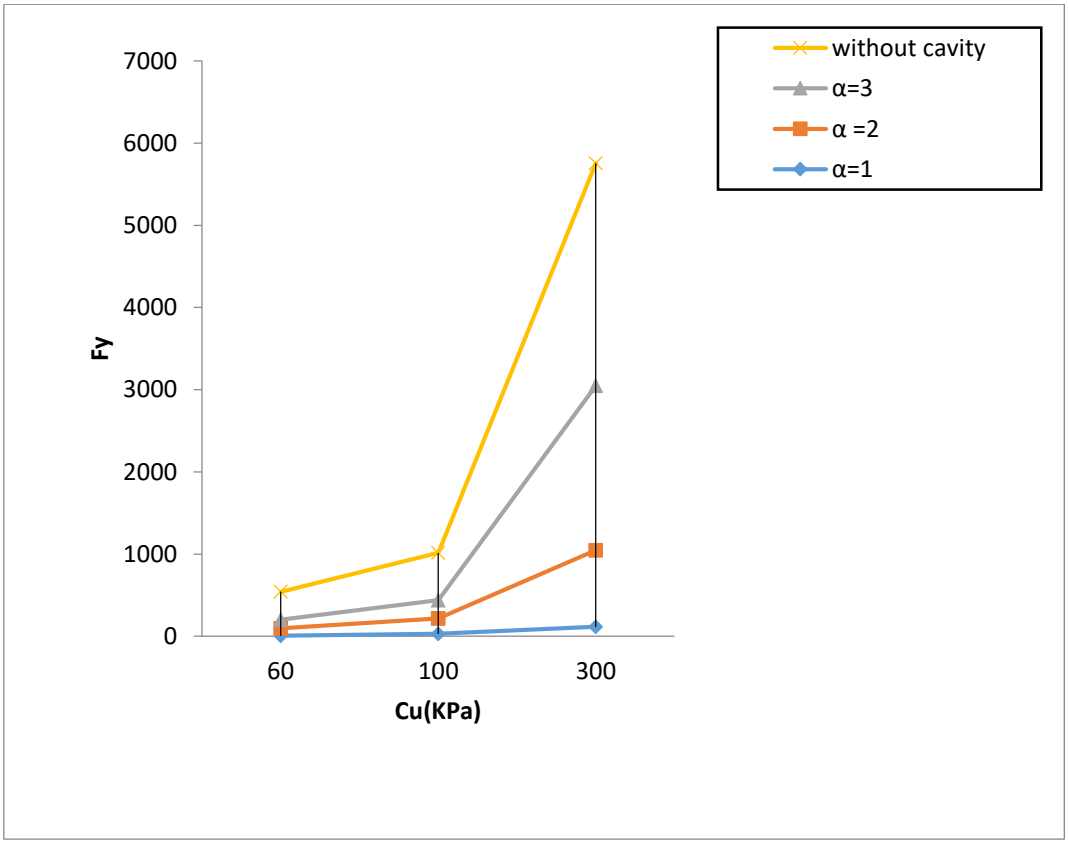
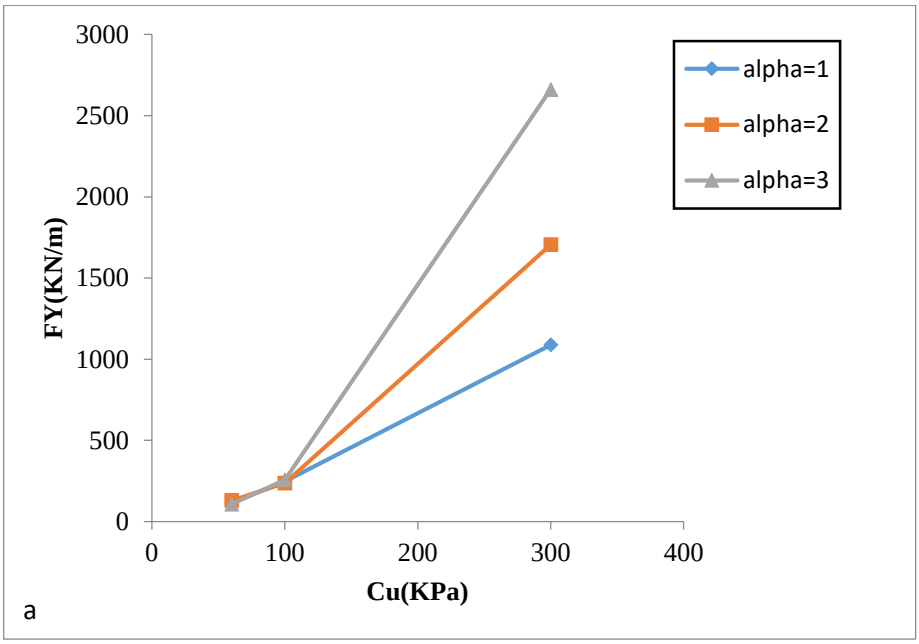


Figure IV.6: Effect of soil cohesion on seismic bearing capacity — two symmetrical cavities, S = 1 m, for various cavity depths α

Figure IV.7 shows theeffect of soil cohesion on seismic bearing capacity with two symmetrical cavities, S = 2 m and S = 3 m. For S = 2 m, the interaction between the two cavities becomes less significant compared to the S = 1 m case. The cavities no longer behave as a single large void, which reduces the extent of the failure zone and improves the seismic bearing capacity.

For S = 3 m, the curves show further improvement in the seismic bearing capacity with increasing soil cohesion. The values of Fy are higher compared to the S = 1 m and S = 2 m cases. As the spacing increases, each cavity behaves almost independently, limiting the stress disturbance beneath the foundation and decreasing the extent of the failure zone within the soil mass.

The reduced interaction between the cavities and the foundation system can explain the convergence of the curves for S = 3 m. As the spacing increases, the influence of the cavities on the failure mechanism becomes less significant, resulting in smaller differences between responses for the various cavity depths.



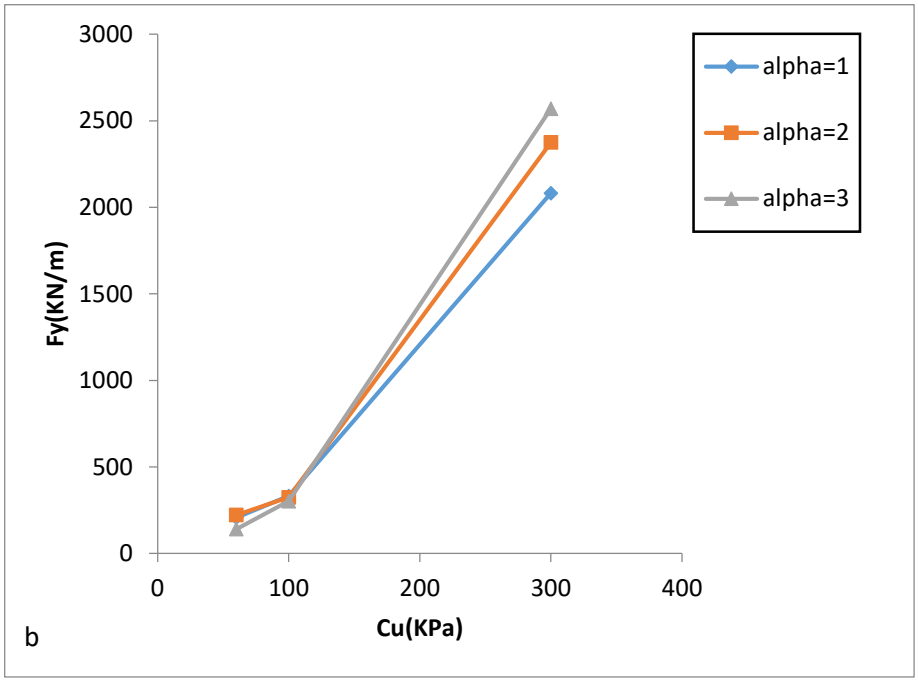


Figure IV.7: Effect of soil cohesion on seismic bearing capacity — two symmetrical cavities, S = 2 m (a) and S = 3 m (b)

Figure IV.8 shows theeffect of soil cohesion on seismic bearing capacity with two parallel cavities, S = 1 m, for various cavity depths α. In the case of two parallel cavities with S = 1 m, their proximity leads to strong mutual interaction. This interaction significantly disturbs the failure zone beneath the foundation and leads to a substantial decrease in bearing capacity, especially for shallow cavity depths (α = 1 and α = 2). Conversely, as the depth increases (α = 3), the effect of the cavities becomes less critical, and the bearing capacity increases significantly.

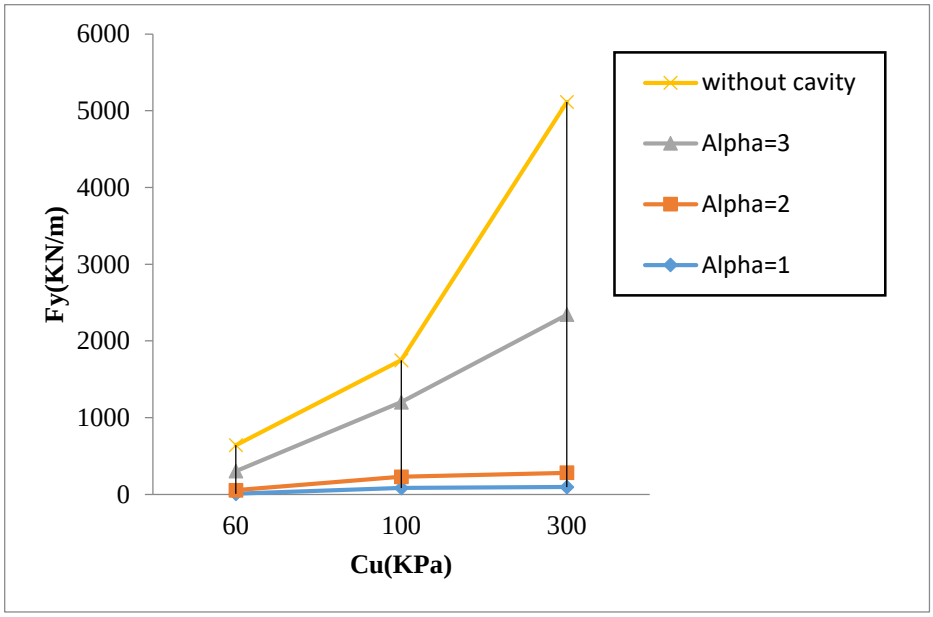
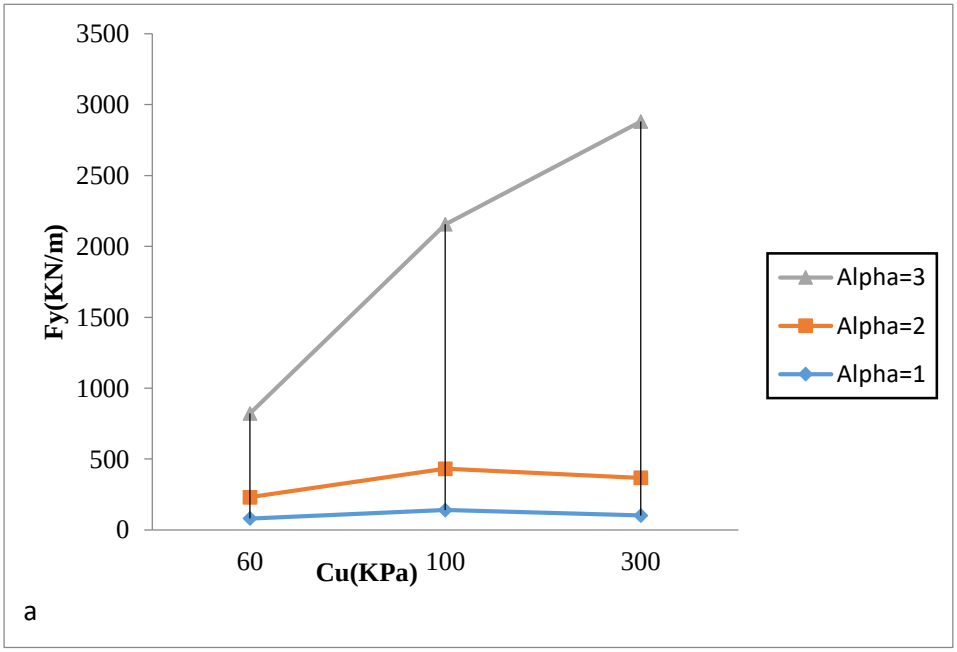


Figure IV.8: Effect of soil cohesion on seismic bearing capacity — two parallel cavities, S = 1 m, for various cavity depths α

Figure IV.9 shows the effect of soil cohesion on seismic bearing capacity with two parallel cavities, S = 2 m (b) and S = 3 m (b). For S = 2 m and S = 3 m, increasing the spacing reduces the interaction between the two parallel cavities. The failure zones become less disturbed, improving the stability of the soil–foundation system. The curves then show a more gradual increase in Fy with Cu, particularly for deeper cavity depths. The differences between the curves become less pronounced as the spacing increases, indicating that the influence of the cavities gradually decreases.



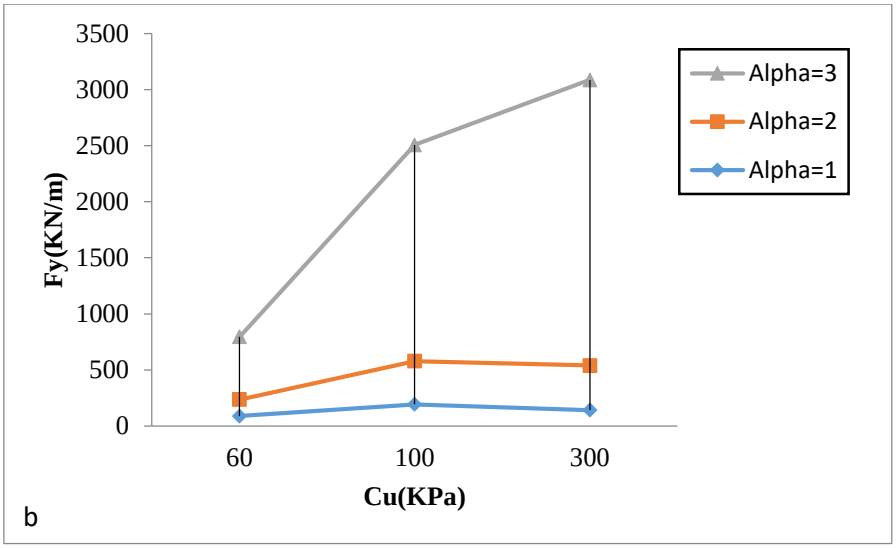


Figure IV.9: Effect of soil cohesion on seismic bearing capacity — two parallel cavities, S = 2 m (b) and S = 3 m (b)

IV.3.2. Influence of Cavity Depth

To study the effect of cavity depth on the seismic bearing capacity, the following observations are made.

Figure IV.10 shows the effect of cavity depth on seismic bearing capacity with single cavity, β = 0. For Cu = 60, 100, and 300 kPa. The curves illustrate the variation of Fy with the normalized depth α for different values of soil cohesion Cu, for zero eccentricity (β = 0), meaning the cavity is positioned directly beneath the foundation axis.

Overall, the seismic bearing capacity increases with increasing cavity depth for all cohesion values studied. This trend is explained by the fact that a deeper cavity has less influence on the failure zone that develops beneath the foundation. As α increases, the interaction between the cavity and the failure mechanism weakens, thereby improving the stability of the soil–foundation system.

The effect of depth is particularly pronounced for Cu = 300 kPa, where the bearing capacity increases sharply with depth. This demonstrates that in highly cohesive and rigid soils, increasing the distance from the cavity enables the soil mass to mobilize its shear strength more effectively under seismic loading.

For Cu = 100 kPa, the increase in bearing capacity with depth remains visible but is less pronounced. For Cu = 60 kPa, the variations in bearing capacity are relatively small,

indicating that in poorly cohesive soils, the overall shear resistance of the soil mass remains limited regardless of the cavity depth.

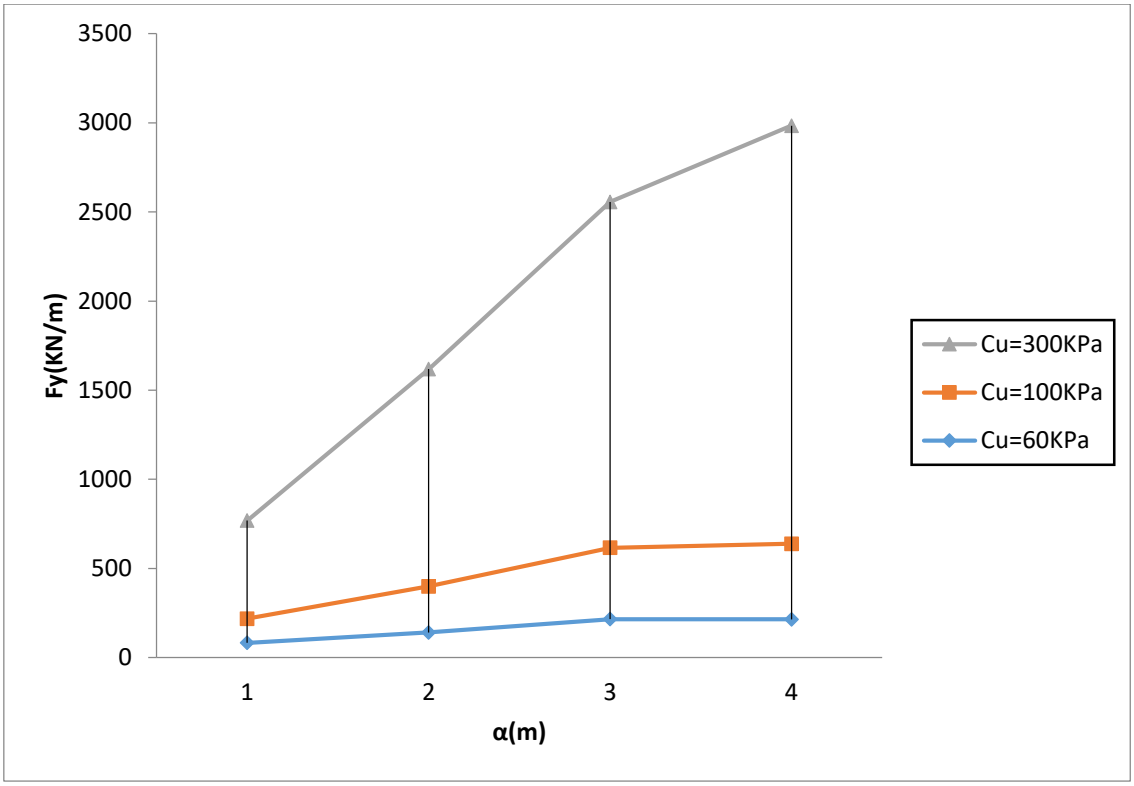
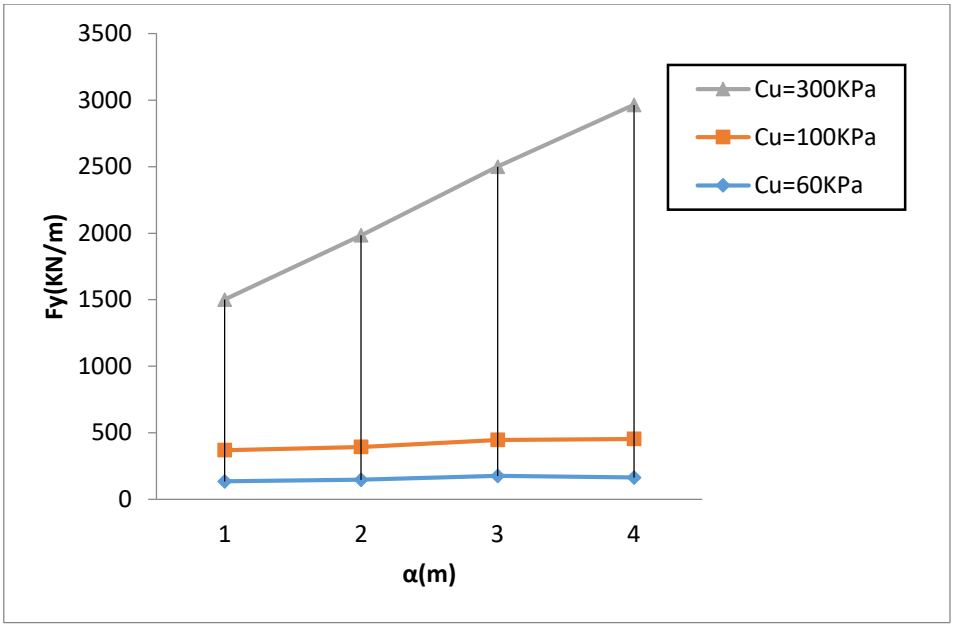


Figure IV.10: Effect of cavity depth on seismic bearing capacity — single cavity, β = 0, for Cu = 60, 100, and 300 kPa

For the effect of cavity depth for non-zero eccentricity values, the graphs generally show that increasing depth leads to an increase in seismic bearing capacity. As the cavity deepens, its influence on the foundation decreases, thereby improving the stability of the soil–foundation system. This trend is particularly visible for Cu = 300 kPa, where Fy increases almost linearly with α. For low cohesion values (Cu = 60 and 100 kPa), the increase remains limited, as the soil is generally weaker.

Figure IV.11 shows the effect of cavity depth on seismic bearing capacity with single cavity, β = 1 and β = 2. For Cu = 60, 100, and 300 kPa. The effect of cavity eccentricity is apparent when comparing the graphs for β = 1 and β = 2. As eccentricity increases, the cavity moves further from the loading axis, altering the stress distribution within the soil. For high cohesion (Cu = 300 kPa), the bearing capacity remains high and continues to increase with depth. For low-cohesion soils (Cu = 60 and 100 kPa), the variations become less regular and

occasionally slightly non-monotonic, indicating greater sensitivity of weak soils to the horizontal position of the cavity.



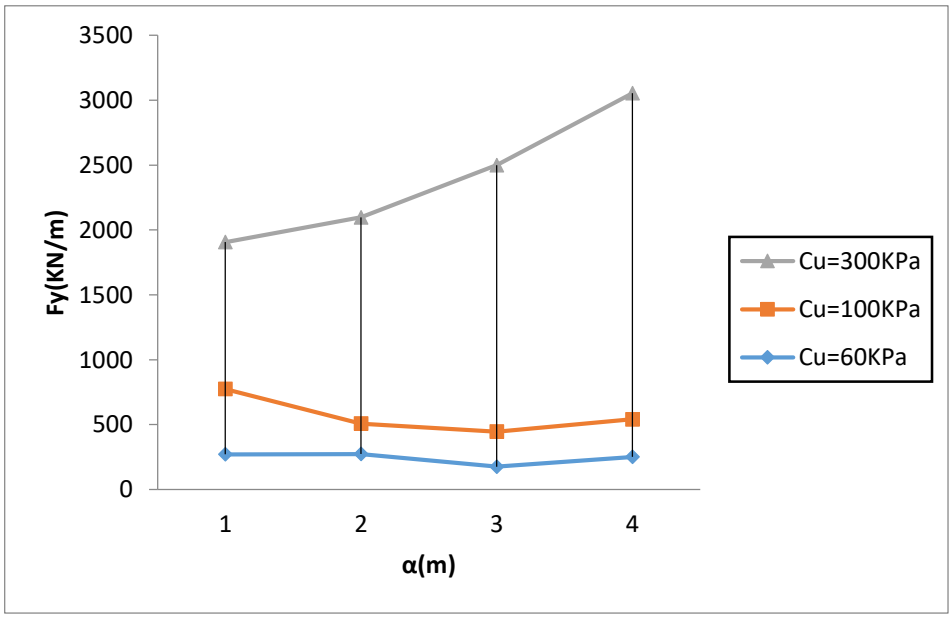


Figure IV.11: Effect of cavity depth on seismic bearing capacity — single cavity, β = 1 (b) and β = 2 (b), for Cu = 60, 100, and 300 kPa

Figure IV.12 shows the effect of cavity depth on seismic bearing capacity with single cavity, β = 3 and β = 4, for Cu = 60, 100, and 300 kPa. For high eccentricity values (β = 3 and β = 4), the results show that the seismic bearing capacity increases significantly with increasing cavity depth for all cohesion values. This increase becomes particularly important at α = 3, where all curves exhibit a sharp rise in Fy. This indicates that a deeply embedded cavity

substantially reduces its negative influence on the foundation, thereby improving the resistance of the soil–foundation system under seismic loading.

The influence of soil cohesion also remains very significant for all values of α. Soils with Cu = 300 kPa consistently exhibit the highest bearing capacities. By comparing the results forβ = 3 and β = 4 with those for β = 0 and β = 1, it is evident that increasing the eccentricity leads to a significant improvement in the seismic bearing capacity. For small values of β, the cavity is located close to the foundation loading axis, strongly disturbing the stress distribution and reducing bearing capacity. As β increases, the cavity moves away from the most highly stressed zone, and its influence diminishes accordingly.

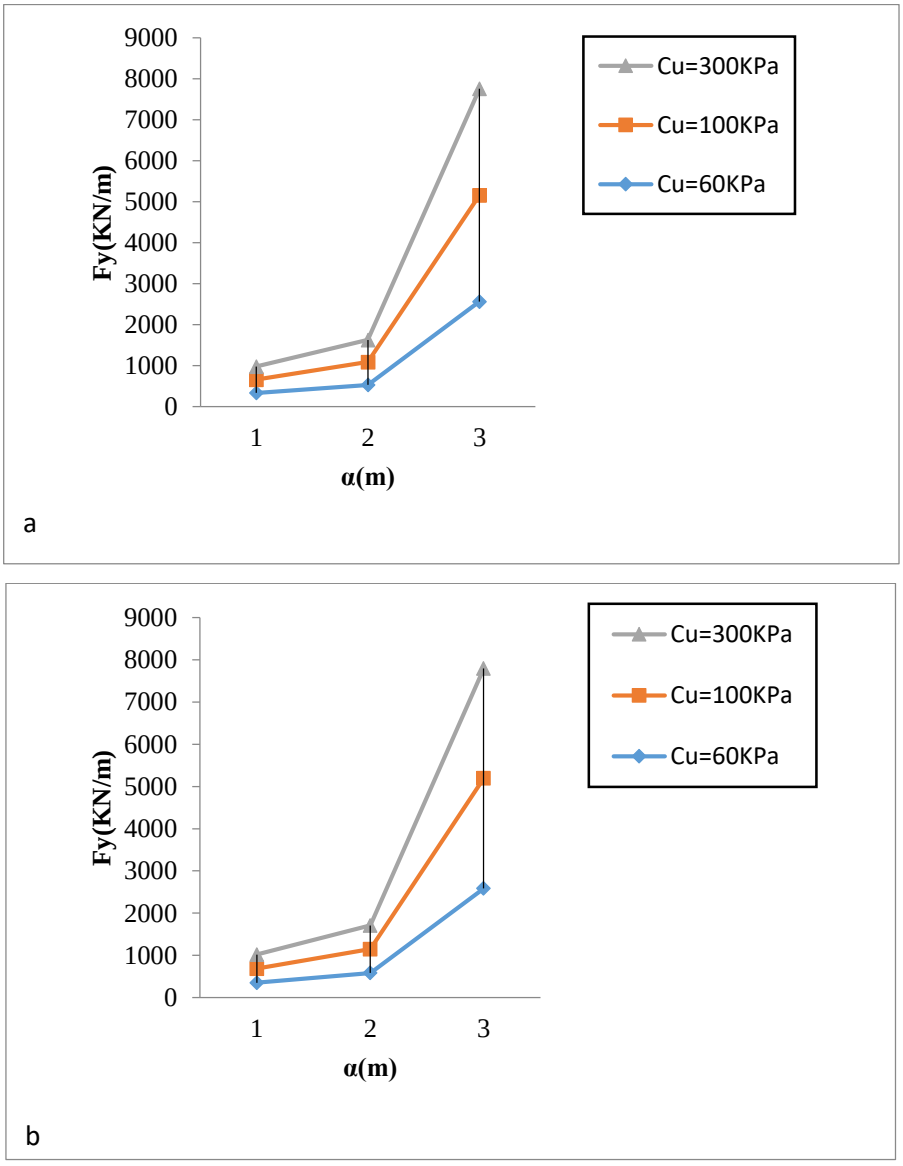


Figure IV.12: Effect of cavity depth on seismic bearing capacity — single cavity, β = 3 (a) and β = 4 (b), for Cu = 60, 100, and 300 kPa

Figure IV.13 shows the effect of cavity depth on seismic bearing capacity with two symmetrical cavities, S = 1 m, for Cu = 60, 100, and 300 kPa. For two symmetrical cavities with a spacing of S = 1 m, the results confirm that the seismic bearing capacity increases with increasing cavity depth. When the cavities are deeper, their influence on the foundation becomes less significant, thereby improving the stability of the soil–foundation system under seismic loading. The effect of soil cohesion is also very pronounced: for all studied depths, soils with Cu = 300 kPa exhibit the highest values of Fy. The bearing capacity increases rapidly with depth, demonstrating that cohesive soils resist more effectively against the combined effects of closely spaced symmetrical cavities and seismic loads.

For low cohesion values (Cu = 60 and 100 kPa), the values of Fy remain relatively low and the increase with depth is limited, indicating that weaker soils are more sensitive to the presence of nearby cavities.

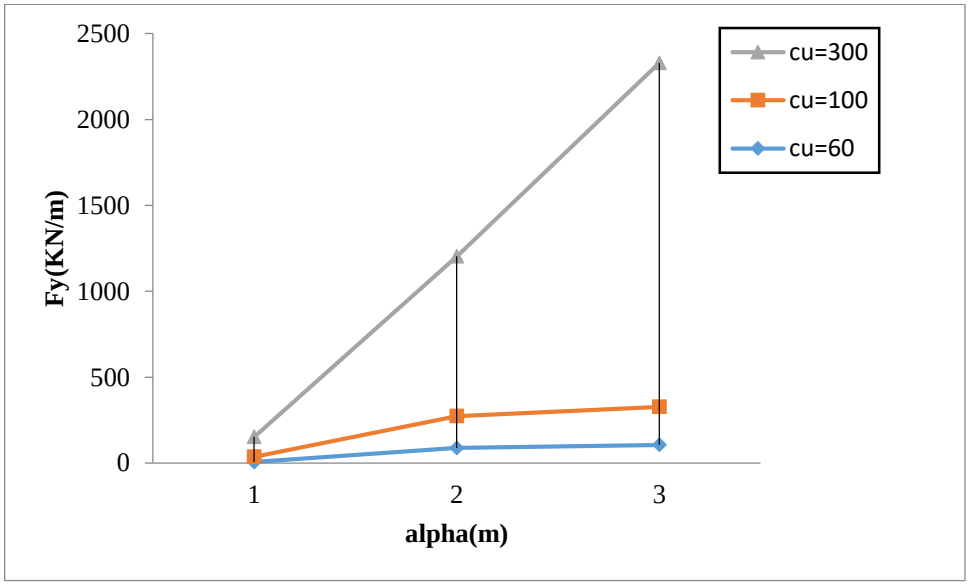
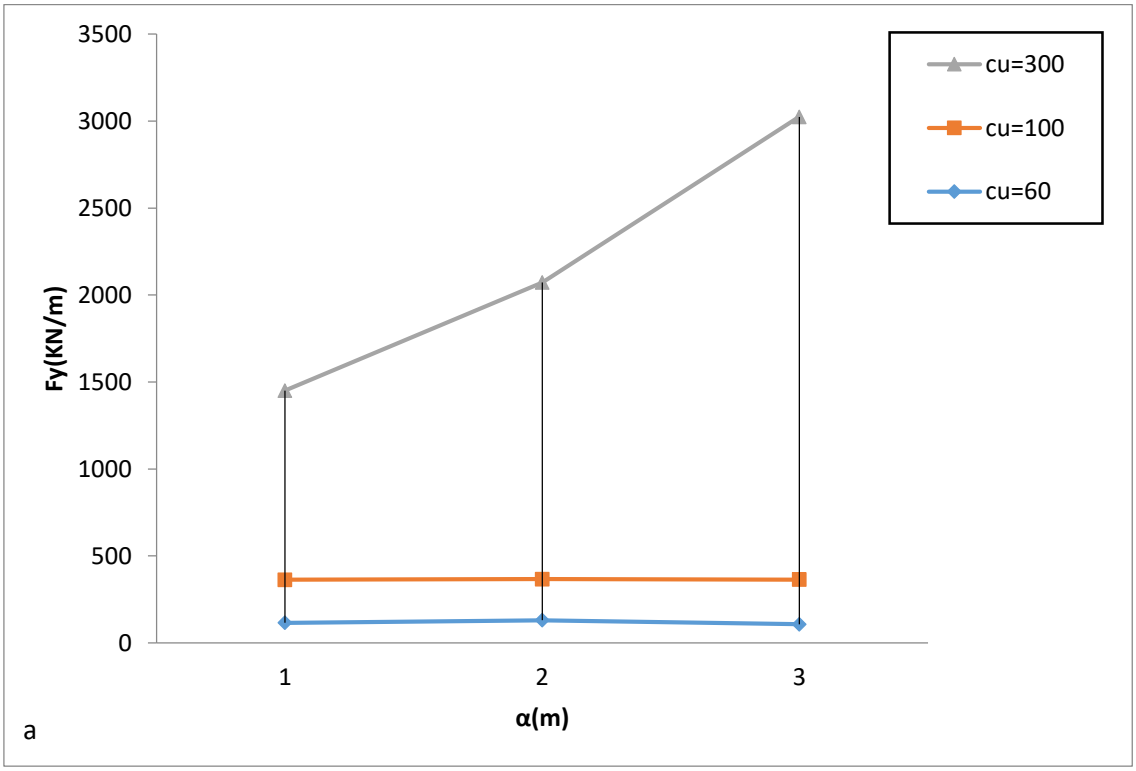


Figure IV.13: Effect of cavity depth on seismic bearing capacity — two symmetrical cavities, S = 1 m, for Cu = 60, 100, and 300 kPa

Figure IV.14 shows the effect of cavity depth on seismic bearing capacity with two symmetrical cavities, S = 2 m (a) and S = 3 m (b), for Cu = 60, 100, and 300 kPa. When the spacing is increased from S = 2 m to S = 3 m, the cavities become farther apart, reducing the interaction between their respective stress zones. As a result, the negative influence of the cavities on the foundation decreases, and the seismic bearing capacity Fy becomes higher and more stable, especially for large values of α.

The curves remain relatively close to each other, particularly for low cohesion values, indicating limited variations in Fy. This shows that when the cavities are sufficiently spaced and located at greater depths, their influence on the soil–foundation system becomes negligible under seismic loading.



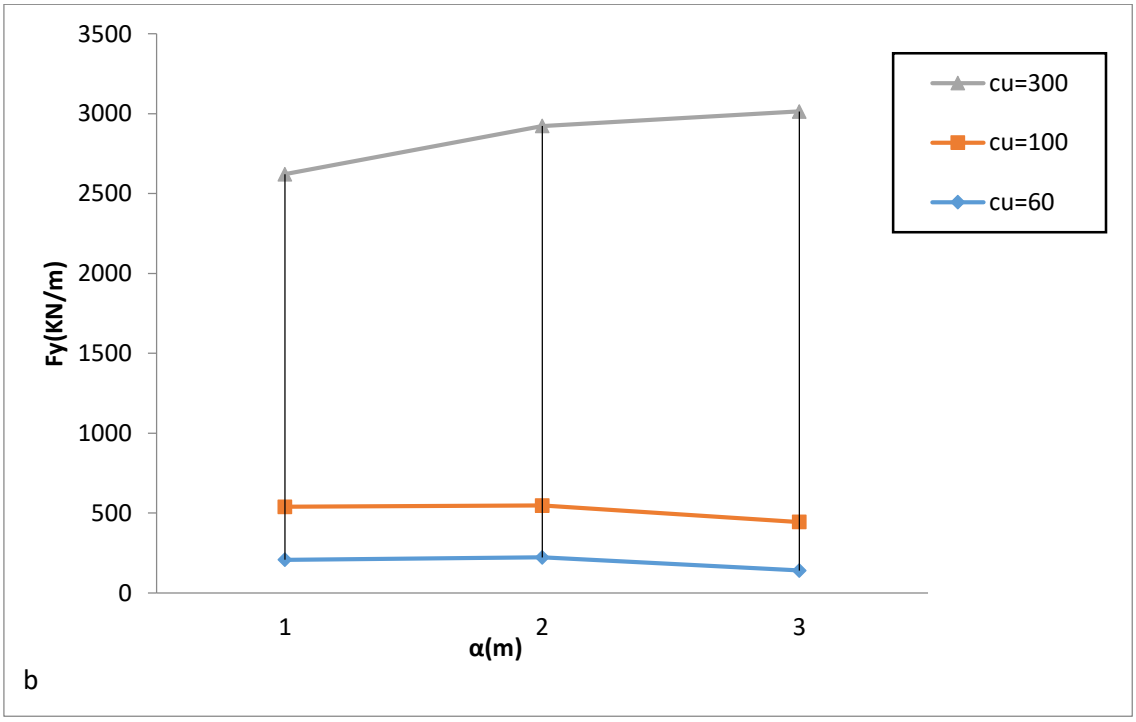
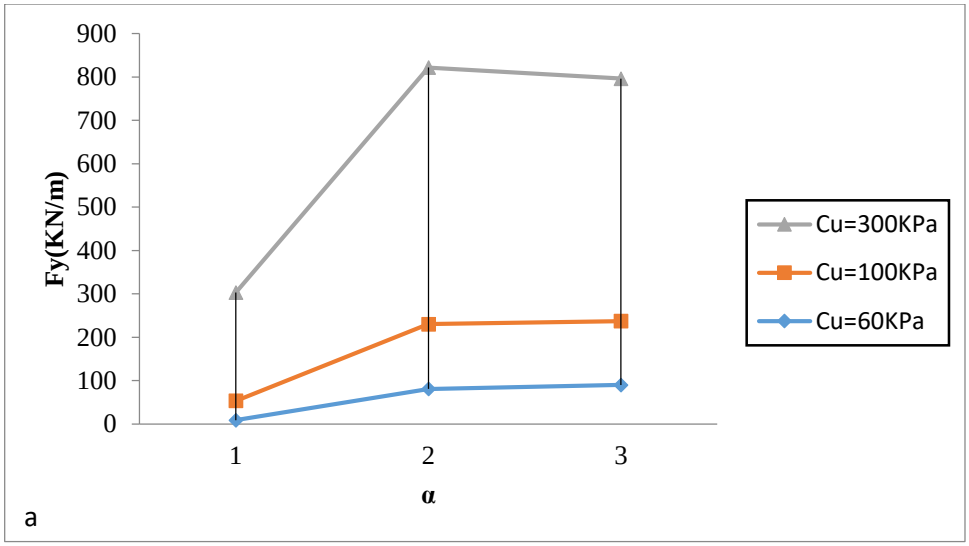
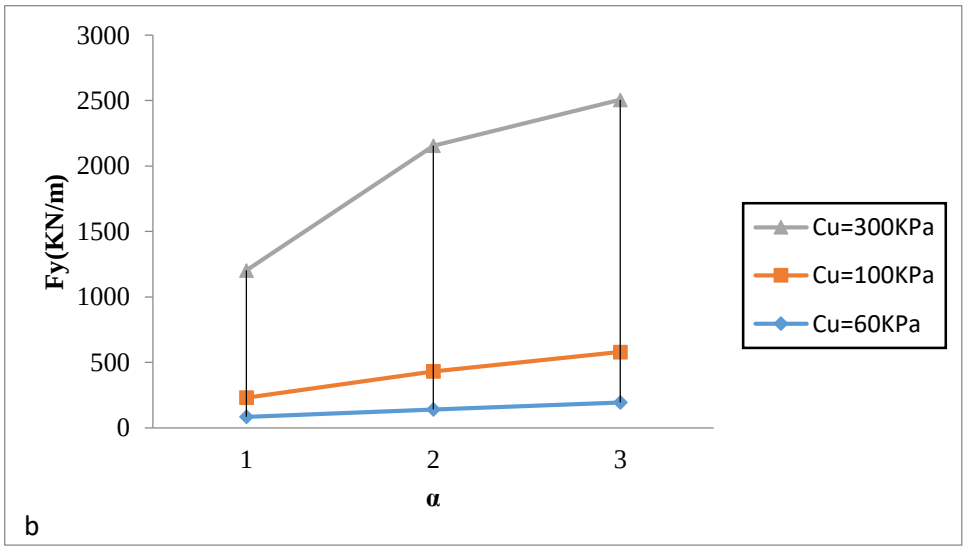


Figure IV.14: Effect of cavity depth on seismic bearing capacity — two symmetrical cavities, S = 2 m (a) and S = 3 m (b), for Cu = 60, 100, and 300 kPa ,

Figure IV.15 shows theeffect of cavity depth on seismic bearing capacity with two parallel cavities: S = 1 m, S = 2 m, and S = 3 m, for Cu = 60, 100, and 300 kPa. In this figure the curves become relatively close and more stable. This demonstrates that when the parallel cavities are sufficiently deep and well separated, their influence on the foundation behavior becomes weak and, in some cases, negligible under seismic loading.





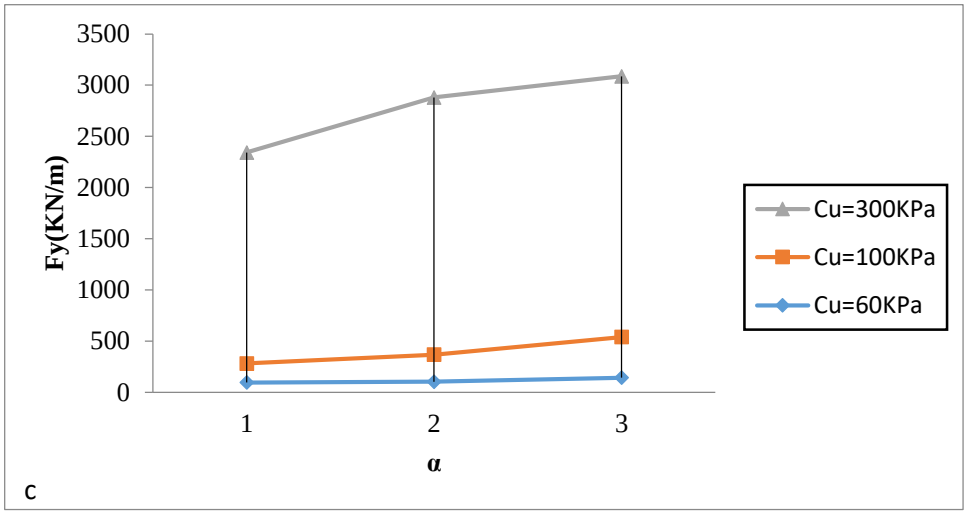


Figure IV.15: Effect of cavity depth on seismic bearing capacity — two parallel cavities: S = 1 m (a), S = 2 m (b), and S = 3 m (c), for Cu = 60, 100, and 300 kPa

IV.3.3. Influence of Cavity Eccentricity

Figure IV.16 shows the effect of cavity eccentricity on seismic bearing capacity with single cavity, α = 1 and α = 2, for Cu = 60, 100, and 300 kPa. The results show that the seismic bearing capacity generally increases with increasing cavity eccentricity β. This increase becomes particularly significant for large values of β, especially between β = 3 and β = 4.

For α = 1 and α = 2, where the cavity is relatively shallow, the influence of the cavity on the foundation remains significant for low eccentricity values. At β = 0 and β = 1, the cavity is located close to the foundation loading axis, which strongly disturbs the stress distribution in the soil and reduces the seismic bearing capacity. However, as β increases, the cavity progressively moves away from the most highly stressed zone beneath the foundation, leading to a noticeable improvement in Fy. This improvement becomes particularly clear between β = 2 and β = 3.

As the cavity moves further from the foundation loading axis, its influence on the stress distribution in the soil decreases, which improves the stability of the soil–foundation system under seismic loading. For large values of β, the curves tend to stabilize, indicating that the influence of the cavity gradually becomes negligible.

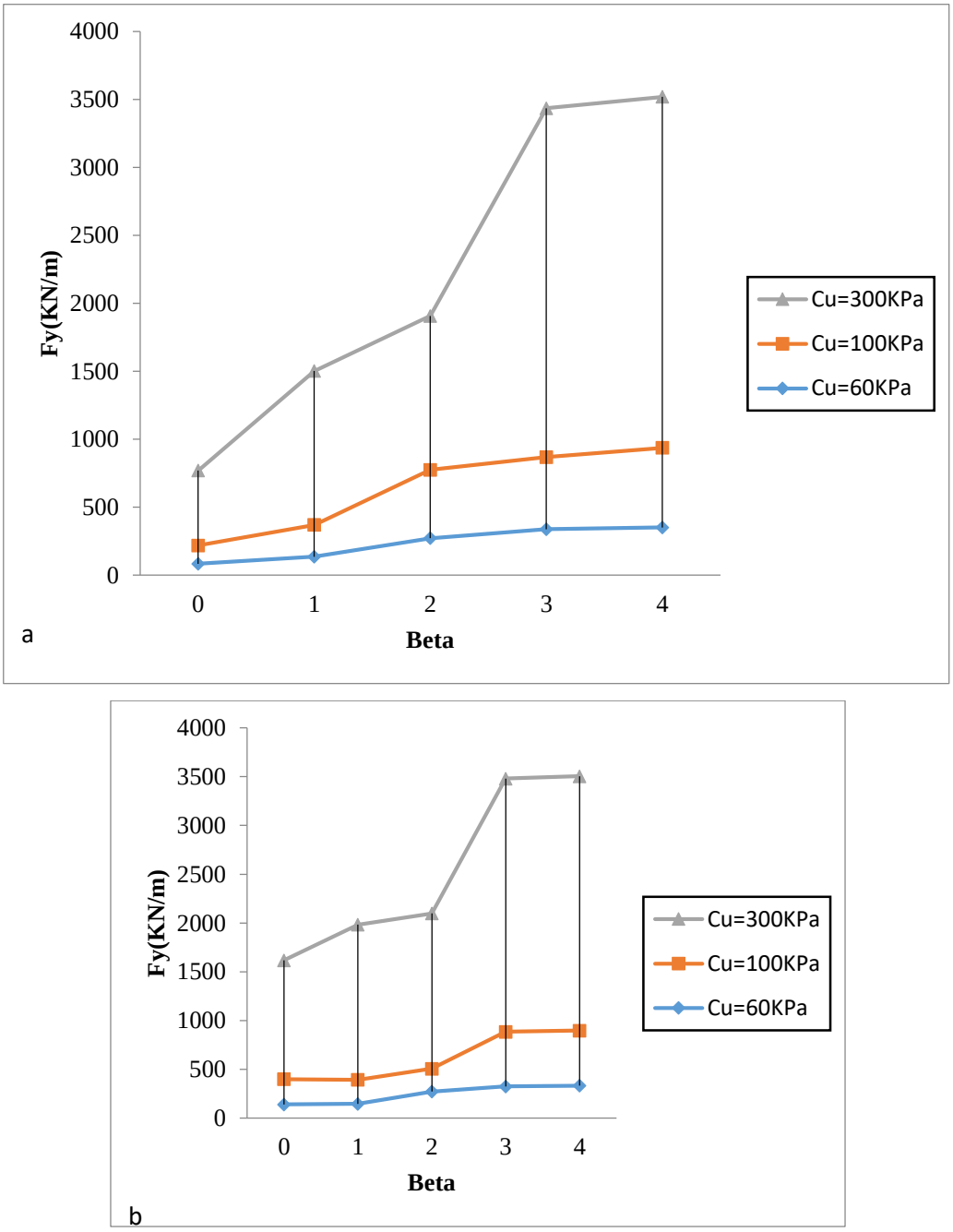


Figure IV.15: Effect of cavity eccentricity on seismic bearing capacity — single cavity, α = 1 (a) and α = 2 (b), for Cu = 60, 100, and 300 kPa

Figure IV.16 shows the effect of cavity eccentricity on seismic bearing capacity with ingle cavity, α = 3 and α = 4, for Cu = 60, 100, and 300 kPa. For α = 3 and α = 4, the results show that the curves remain relatively stable despite the increase in cavity eccentricity β.

This indicates that at a significant depth, the influence of the horizontal position of the cavity on the bearing capacity becomes weak. When the cavity is embedded deeply within the soil, its effect on the highly stressed zone beneath the foundation decreases considerably.

The variations of Fy with β remain limited for all cohesion values.

The curves become nearly horizontal, showing that increasing eccentricity no longer has a significant influence on the behavior of the soil–foundation system when the cavity is deep.

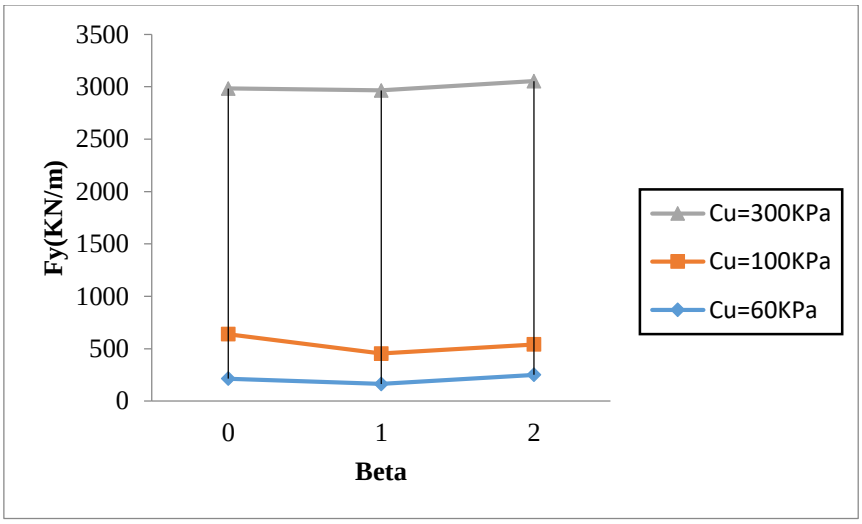


Figure IV.16: Effect of cavity eccentricity on seismic bearing capacity — single cavity, α = 3 and α = 4 (combined), for Cu = 60, 100, and 300 kPa

IV.3.4. Influence of Cavity Spacing

The obtained curves highlight a progressive increase in the seismic bearing capacity Fy with the spacing S between the symmetrical cavities.

Figure IV.17 shows the effect of cavity spacing on seismic bearing capacity with two symmetrical cavities, α = 1, for Cu = 60, 100, and 300 kPa. For α = 1 and Cu = 300 kPa, the increase is very significant: Fy rises from low values to approximately 1500 kN/m as S increases from 1 m to 3 m. This indicates that closely spaced cavities strongly disturb the soil mass, whereas a larger spacing reduces their interaction and considerably improves the soil resistance. For Cu = 100 kPa, the same trend is observed but with lower values of Fy. For Cu = 60 kPa, the values of Fy remain low despite the increase in S, since the beneficial effect of increasing the cavity spacing is limited in poorly cohesive soils. Overall, the effect of spacing is most pronounced in highly cohesive soils and least significant in soils with low cohesion.

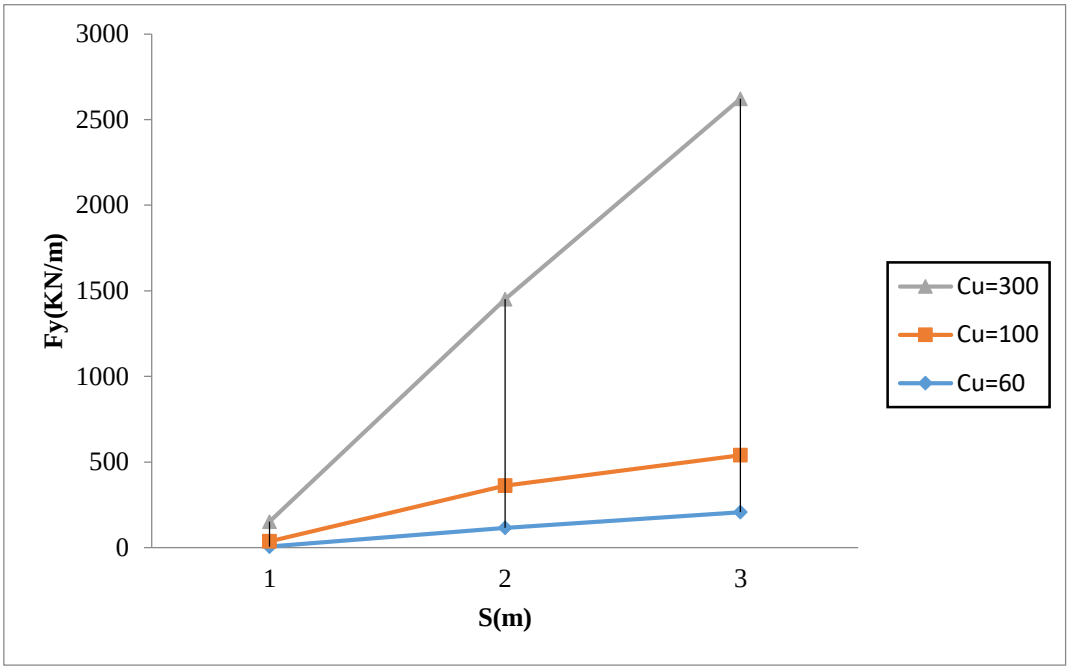


Figure IV.17: Effect of cavity spacing on seismic bearing capacity — two symmetrical cavities, α = 1, for Cu = 60, 100, and 300 kPa

Figure IV.18 shows theeffect of cavity spacing on seismic bearing capacity with two symmetrical cavities, α = 2 and α = 3, for Cu = 60, 100, and 300 kPa. For α = 2, the curves retain the same general trend: the seismic bearing capacity increases with the spacing between the cavities. The values of Fy are even higher than those obtained for α = 1, and the increase is nearly linear with S, indicating that increasing the distance strongly reduces the interaction between the cavities.

For α = 3, the curves show that the increase of Fy with S tends to stabilize, particularly for highly cohesive soils. At high values of α, the beneficial effect of increasing the spacing reaches a limit: once the cavities are sufficiently far apart, their influence on the bearing capacity becomes negligible.

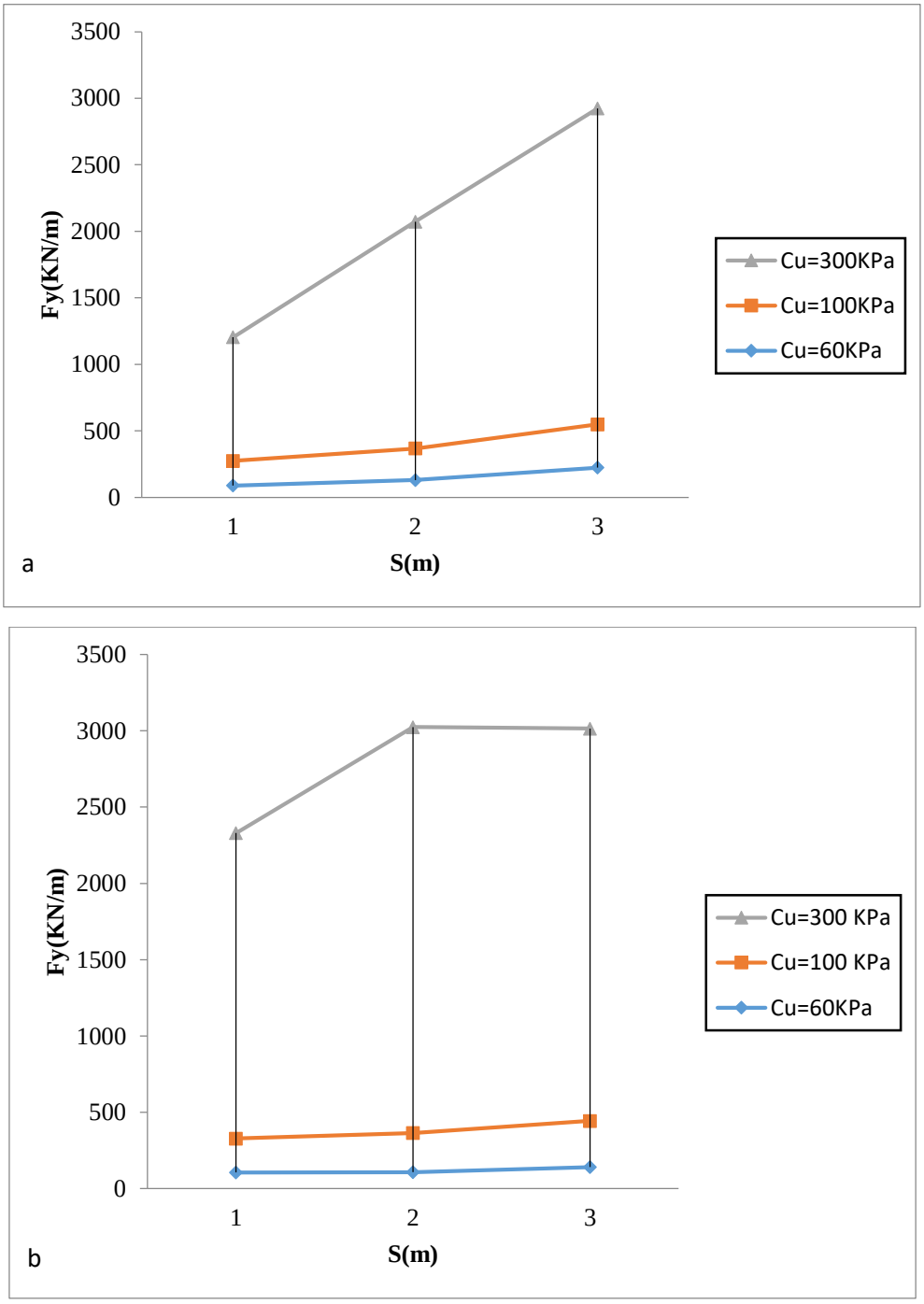


Figure IV.18: Effect of cavity spacing on seismic bearing capacity — two symmetrical cavities, α = 2 (a) and α = 3 (b), for Cu = 60, 100, and 300 kPa

.

Figure IV.19 show the effect of cavity spacing on seismic bearing capacity with two parallel cavities, α = 1, for Cu = 60, 100, and 300 kPa.

The Figure obtained for two parallel cavities show that the seismic bearing capacity Fy increases progressively with the spacing parameter S. For α = 1, the values of Fy are the lowest, indicating that the strong interaction between the two parallel cavities significantly impairs the behavior of the soil mass.

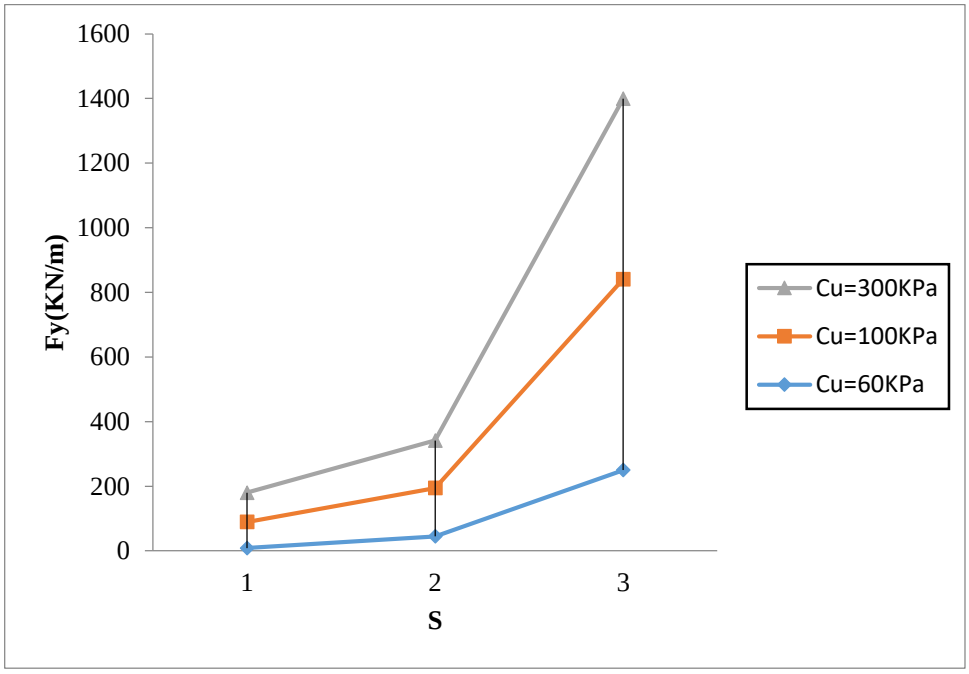


Figure IV.19: Effect of cavity spacing on seismic bearing capacity — two parallel cavities, α = 1, for Cu = 60, 100, and 300 kPa

Figure IV.20 shows the effect of cavity spacing on seismic bearing capacity with two parallel cavities, α = 2 and α = 3, for Cu = 60, 100, and 300 kPa. For α = 2, the curves exhibit higher values of Fy and a more pronounced increase with S, reflecting a significant reduction in the disturbing effect of cavities. For α = 3, the values of Fy reach their highest levels, especially for highly cohesive soils, and the curves progressively tend toward stabilization at large spacing. This means that for high spacing values and deep cavities, the influence of the parallel voids becomes weak when they are sufficiently separated. This evolution can be explained by the fact that increasing S improves the overall resistance of the system, reduces the interaction between the failure zones generated around the cavities, and allows the soil mass to better withstand seismic loads.

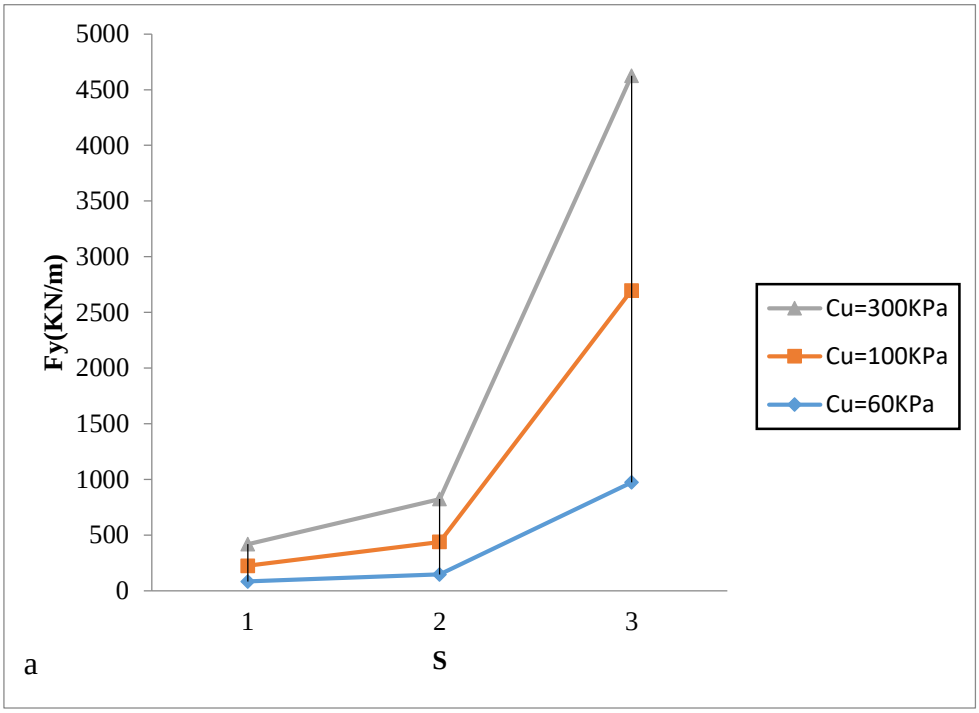


Figure IV.20: Effect of cavity spacing on seismic bearing capacity — two parallel cavities, α = 2 (a) and α = 3 (b), for Cu = 60, 100, and 300 kPa

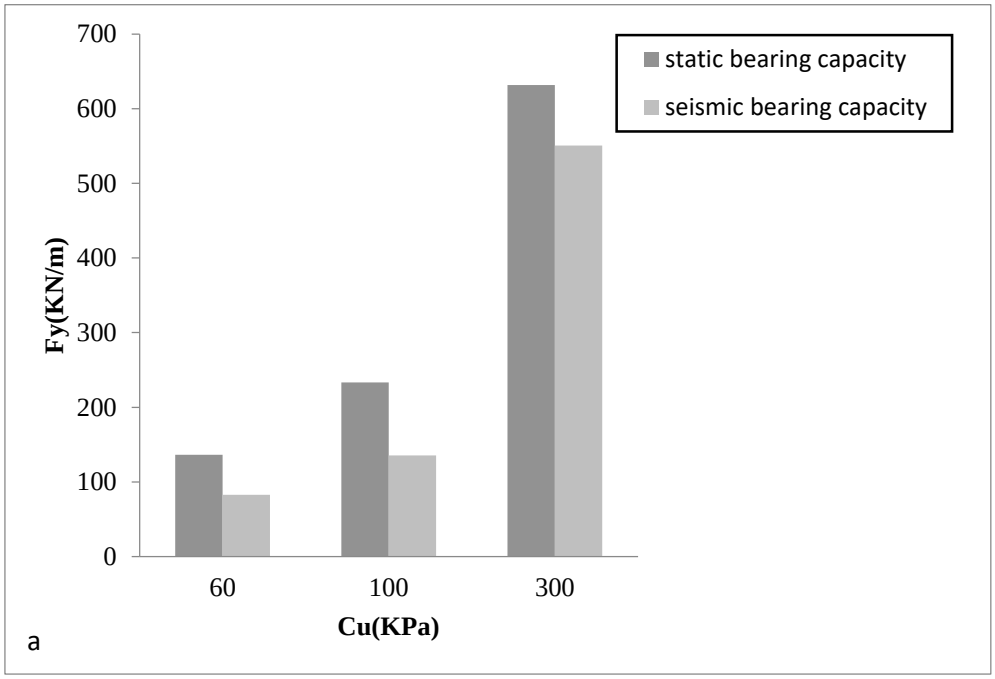
.

IV.4. Comparative Study: Static vs. Seismic Bearing Capacity

To evaluate the effect of seismic loading on the bearing capacity, a comparative study between the static and seismic bearing capacities was performed for a number of critical configurations.

Figure IV.21and 22 shows Comparison between static and seismic bearing capacities with single cavity, β = 0 and 1 about α = 1 and α = 2, for Cu = 60, 100, and 300 kPa. The analysis focused on the cases where the cavity is positioned directly beneath the footing (β = 0) and on the case of an eccentrically positioned cavity (β = 1), considering two shallow cavity depths (α = 1 and α = 2).

Figure IV.23 and 24 showthe comparison between static and seismic bearing capacities with two symmetrical and two parallel cavities, S = 1 m, α = 1 (a) and α = 2 (b), for Cu = 60, 100, and 300 kPa. In addition, the influence of two closely spaced cavities was examined for a relative spacing of S = 1 m in both the symmetrical and parallel configurations. These particular cases were selected because they correspond to the most critical situations, in which the effect of seismic loading on the degradation of bearing capacity is expected to be the most pronounced.



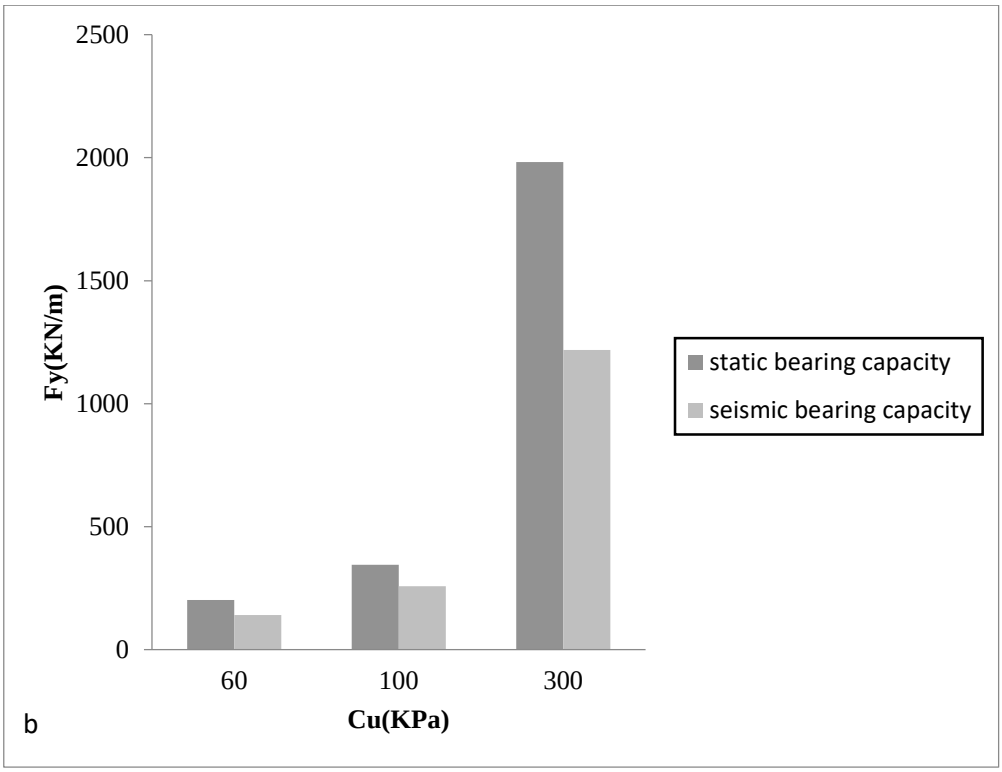
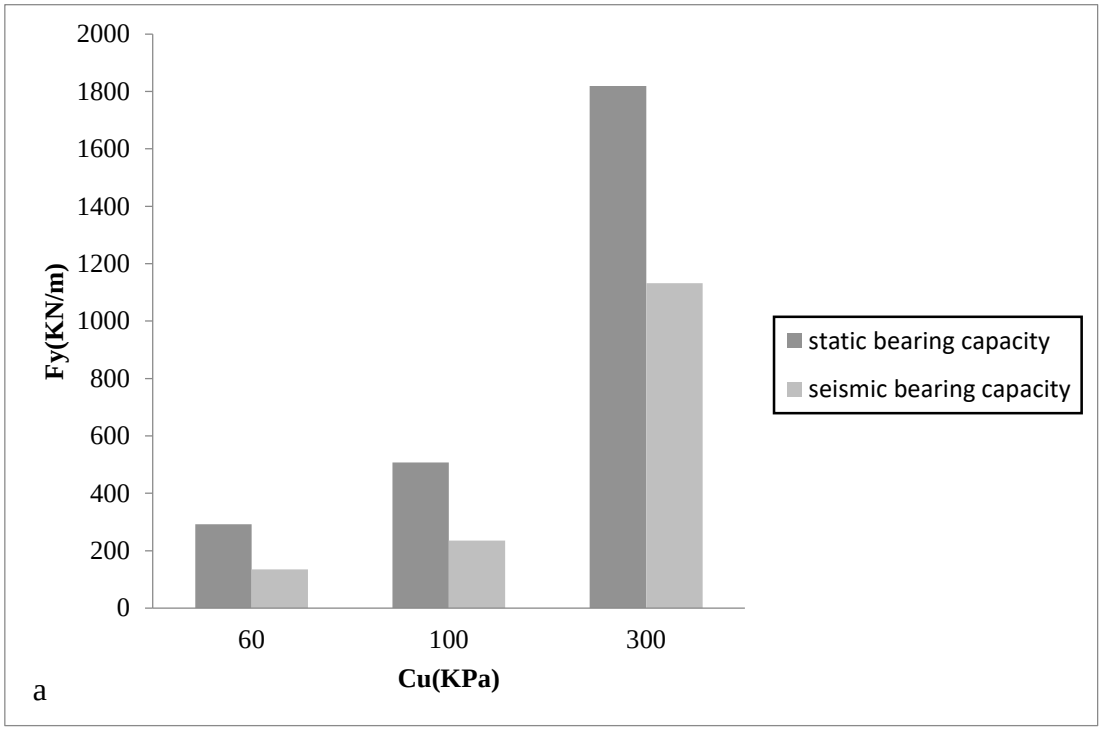


Figure IV.21: Comparison between static and seismic bearing capacities — single cavity, β = 0, α = 1 (a) and α = 2 (b), for Cu = 60, 100, and 300 kPa



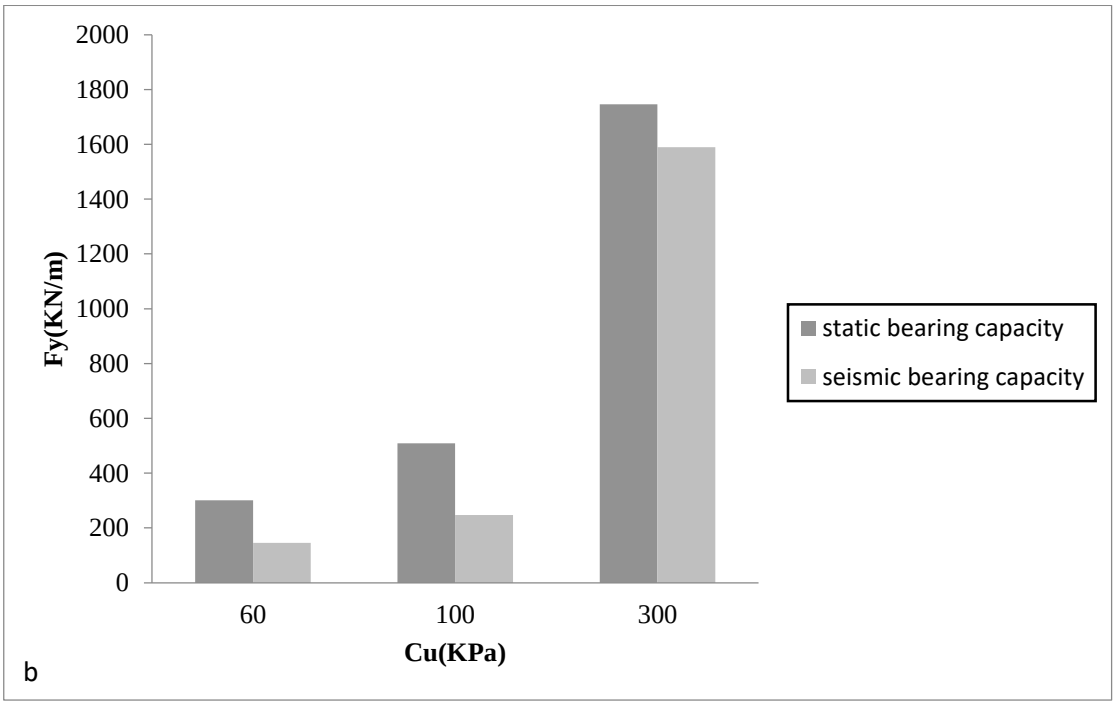


Figure IV.22: Comparison between static and seismic bearing capacities — single cavity, $\beta = 1$, $\alpha = 1$ (a) and $\alpha = 2$ (b), for Cu = 60, 100, and 300 kPa

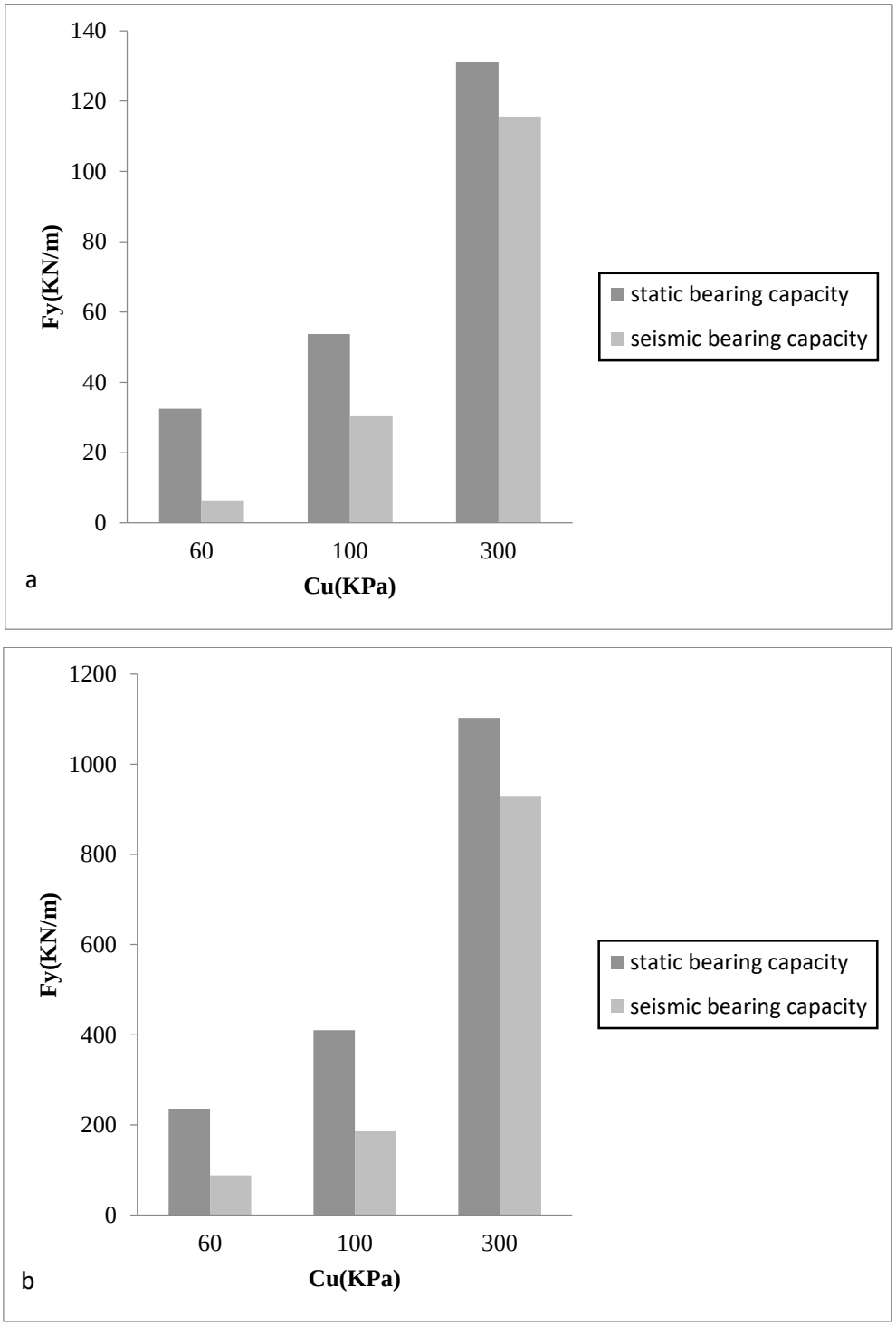


Figure IV.23: Comparison between static and seismic bearing capacities — two symmetrical cavities, S = 1 m, α = 1 (a) and α = 2 (b), for Cu = 60, 100, and 300 kPa

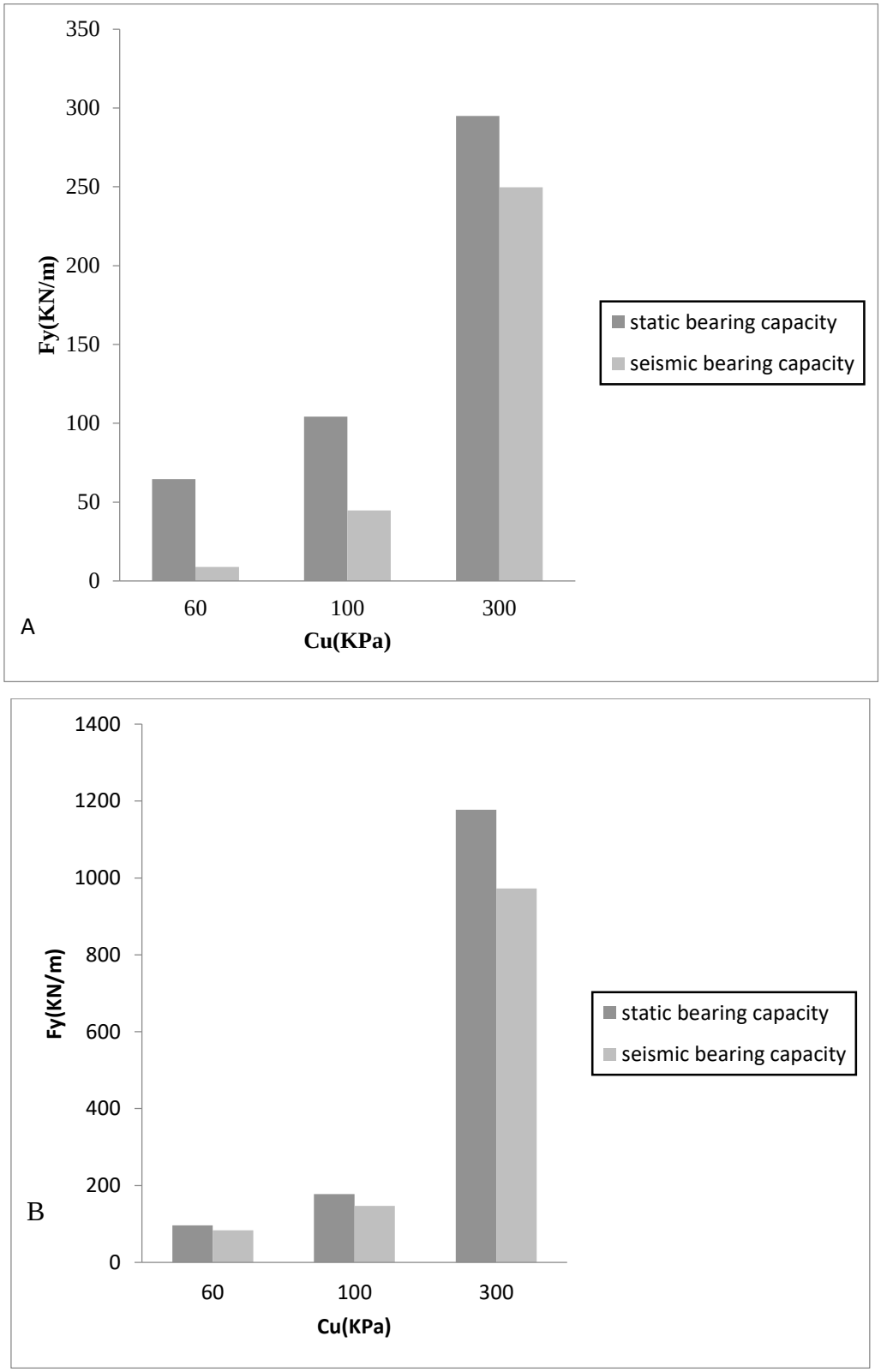


Figure IV.24: Comparison between static and seismic bearing capacities — two parallel cavities, S = 1 m, α = 1 (a) and α = 2 (b), for Cu = 60, 100, and 300 kPa

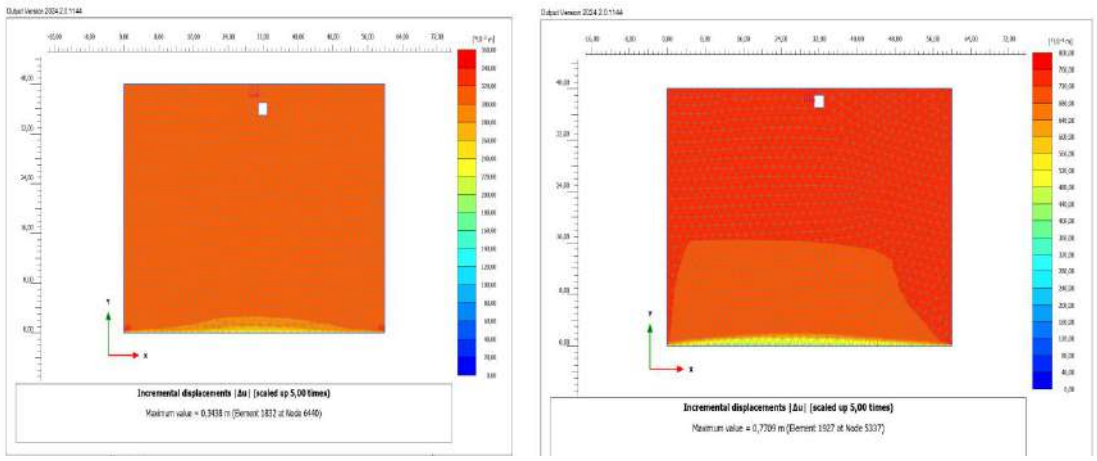
From the comparative analysis, it can be observed that in all cases, the seismic bearing capacity is lower than the static bearing capacity. This reduction indicates a degradation of the stability of the soil–foundation system under dynamic loading conditions. Indeed, seismic accelerations generate horizontal and vertical inertia forces within the soil mass, leading to a significant modification of the stress state and a faster mobilization of failure mechanisms.

Seismic action also causes an increase in displacements and plastic deformations in the soil, which reduces its shear strength and consequently its ability to support the loads transmitted by the foundation. As a result, the failure zone becomes more unstable, and the ultimate bearing capacity decreases compared to the static case.

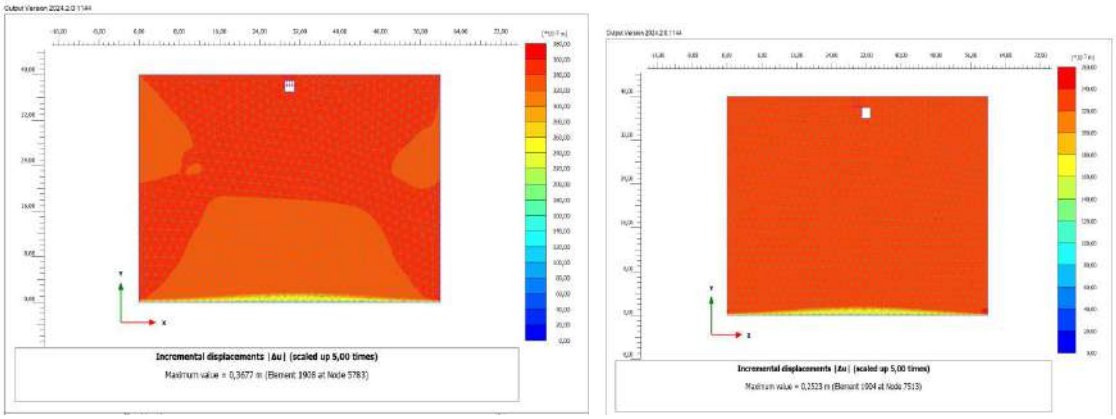
In the presence of a cavity, this reduction may be more pronounced, since seismic loading promotes stress concentration around the void and disturbs the stress distribution within the soil mass. The interaction between the cavity effect and the seismic inertia forces therefore leads to an additional decrease in the seismic bearing capacity.

IV.5.Failure mechanism:

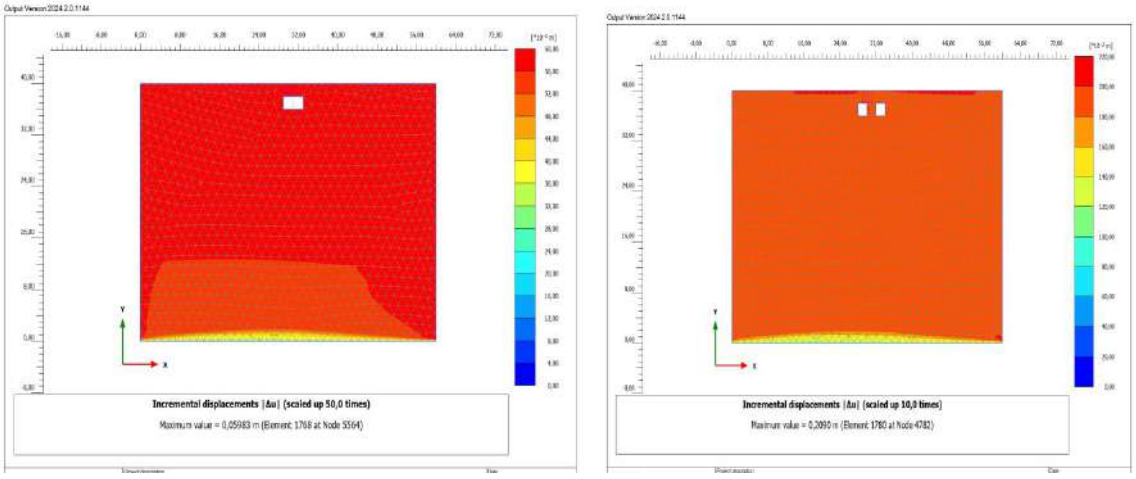
Under seismic loading, the failure mechanism becomes less distinct compared to the static case. The application of a strong earthquake motion with a duration of 20 s generates significant and repeated inertia forces within the soil mass. This dynamic loading leads to continuous stress redistribution and the propagation of plastic deformations over a large soil region. Consequently, shear zones are no longer localized along well-defined failure surfaces but spread throughout the soil layer, which explains the extensive red-colored zone observed in the results. This indicates an almost complete mobilization of the soil mass under the severe seismic excitation.



Sol 1 alpha=1 bata=1 Sol1 alpha2 beta1



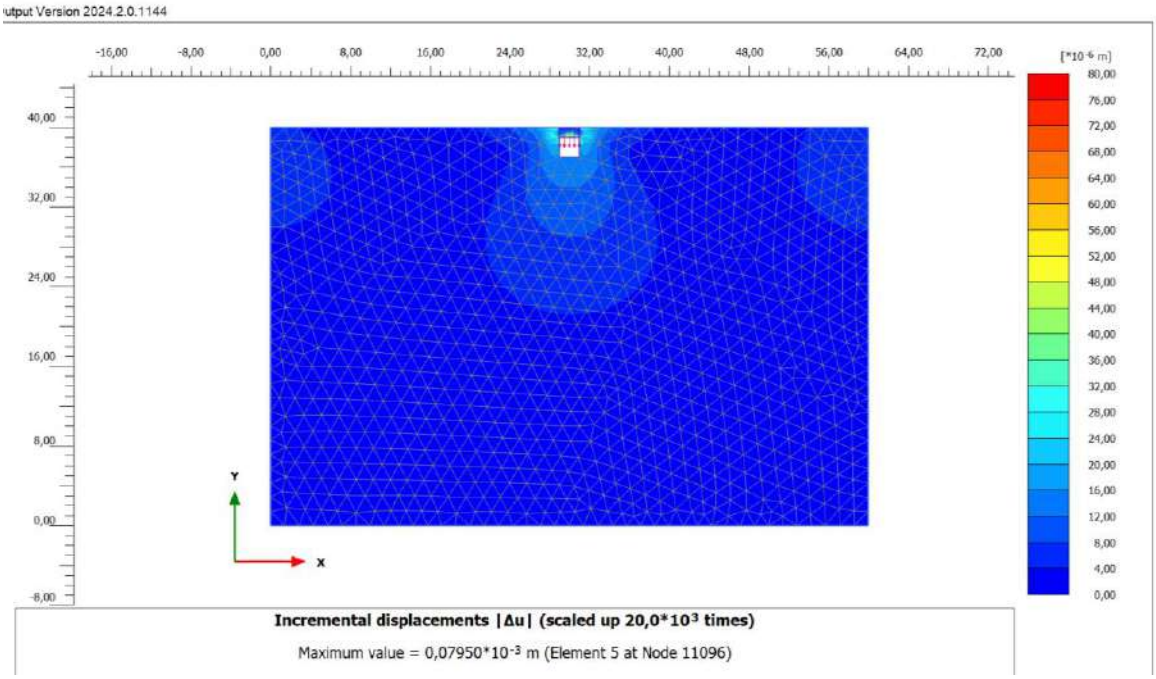
Sol 2 alpha1 beta1 **Sol2 alpha2 beta1**



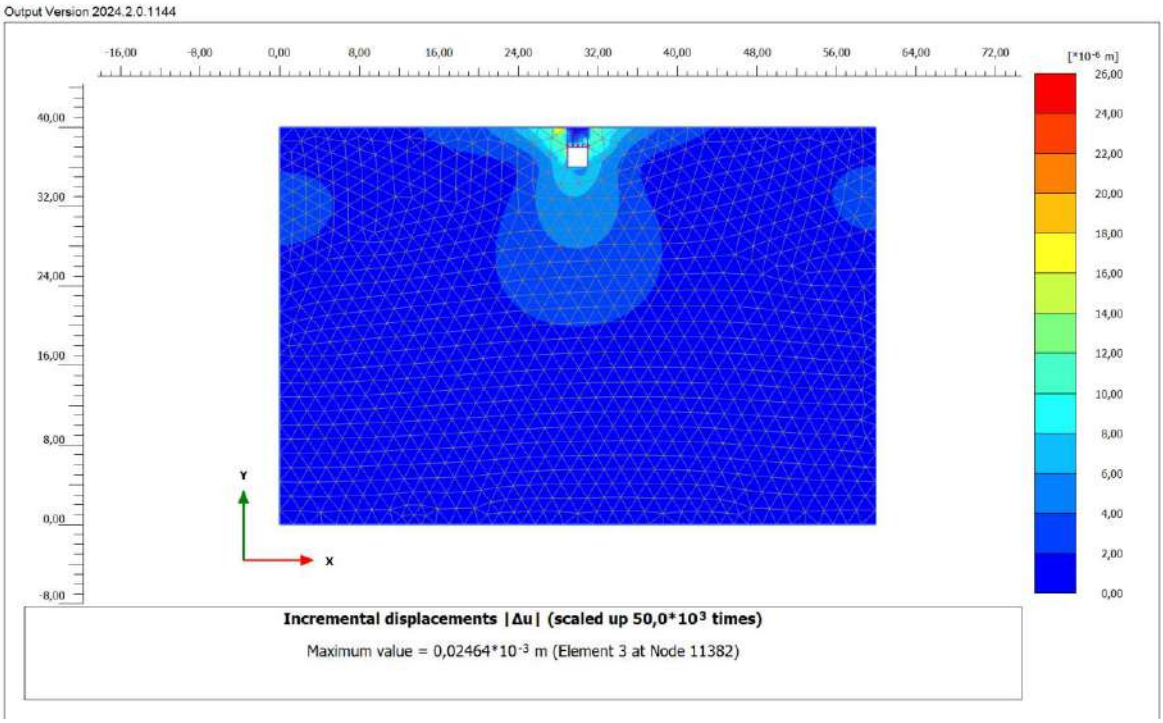
Sol3 alpha2 s=1 **sol3 alpha2 s=2**

Figure IV.25: Seismic failure mechanism

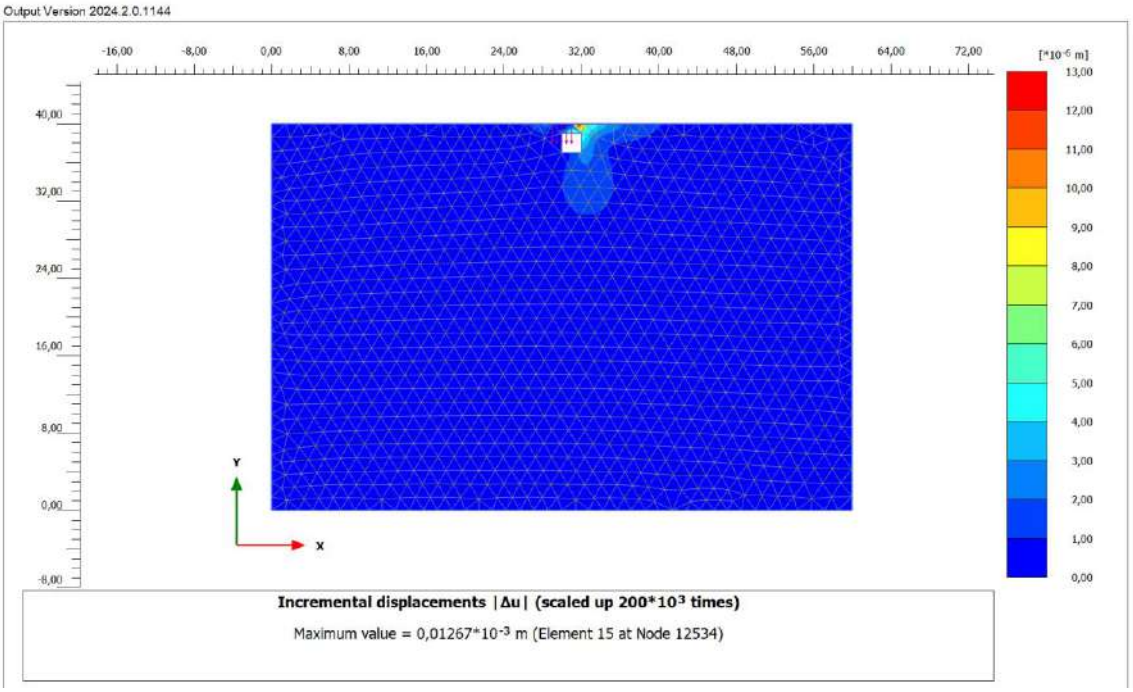
In the static case, when the cavity is located directly beneath the footing, stresses concentrate in the soil above the cavity, which may lead to punching failure followed by the collapse of the cavity roof. However, when the cavity is located away from the footing, the failure surface does not directly interact with the cavity. No cavity roof collapse is observed, and the failure mechanism develops mainly within the soil beneath the footing.



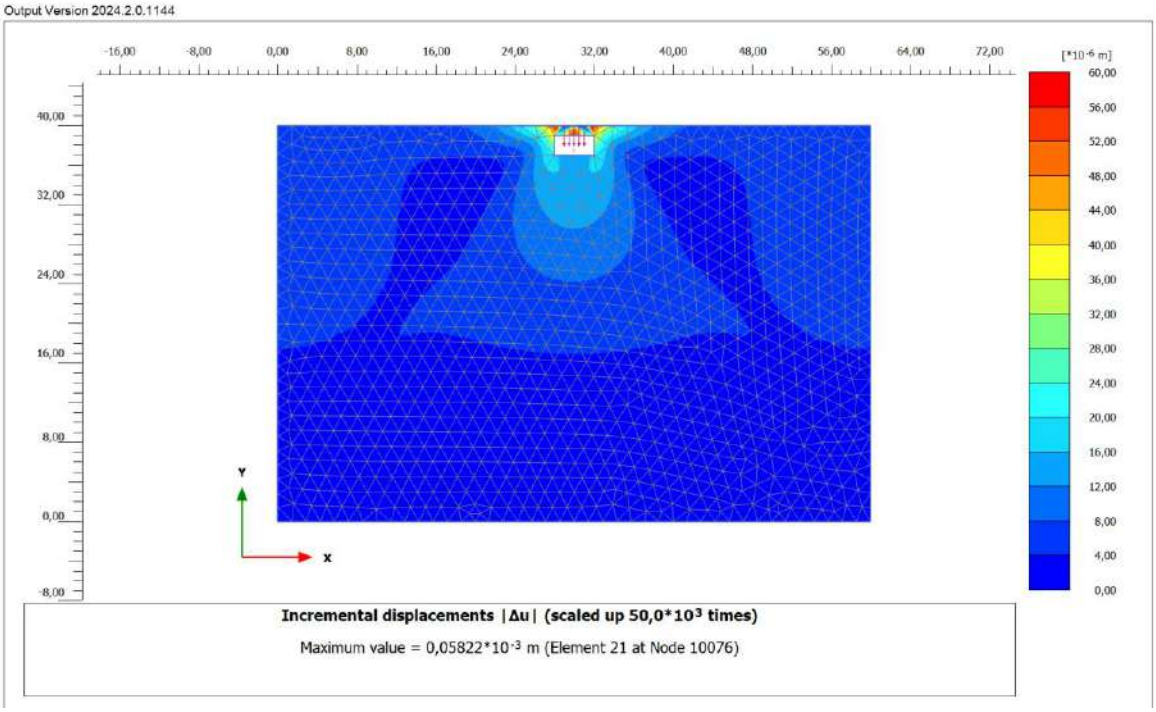
Sol 1 α=1,β=0



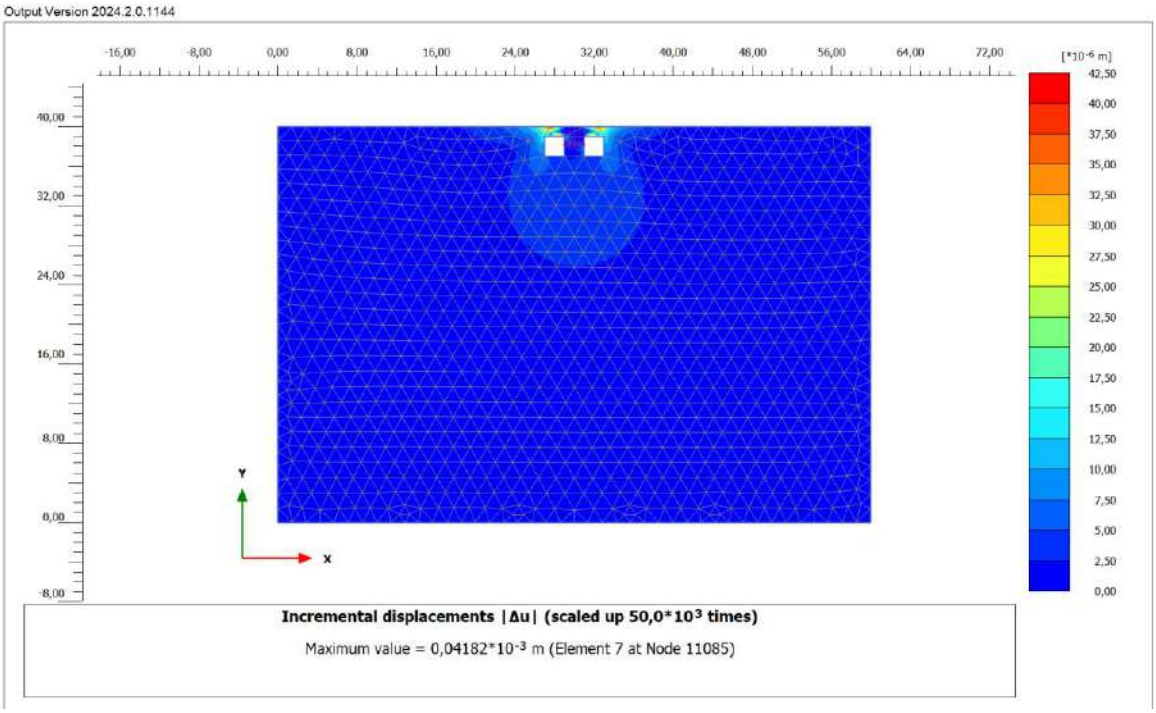
Sol 2 α=2,β=0



Sol3 α=1,β=1



Sol 1 α=1,S=1



Sol2 Sol 1 α=1,S=2

Figure IV.26: static failure mechanism

IV.6. Conclusion

This parametric study made it possible to highlight the influence of underground cavities on the seismic bearing capacity of shallow strip foundations on cohesive soil. The results demonstrate that the response of the soil–foundation system is strongly governed by the geometrical characteristics of the cavities as well as by the mechanical properties of the soil.

The following key conclusions can be drawn from the analyses:

- Soil cohesion is the dominant parameter: the seismic bearing capacity increases consistently with increasing Cu, regardless of the cavity configuration. Highly cohesive soils are significantly more resistant to the combined effects of underground voids and seismic loading.
- The presence of any underground cavity reduces the seismic bearing capacity compared to the cavity-free case. This reduction is most severe when the cavity is shallow ($\alpha = 1$) and positioned directly beneath the foundation ($\beta = 0$), as this configuration maximally disturbs the failure zone beneath the footing.
- Increasing the cavity depth α progressively reduces the interaction between the cavity and the foundation failure mechanism, improving the stability of the system. For

sufficiently deep cavities ($\alpha = 4$), the impact on the seismic bearing capacity becomes negligible.

- Increasing the cavity eccentricity β displaces the void away from the foundation loading axis, reducing its influence on the failure zone and thereby improving the seismic bearing capacity. This effect is most pronounced for shallow cavities and becomes negligible for deep cavities.
- In double-cavity configurations (symmetrical or parallel), increasing the inter-cavity spacing S reduces the interaction between the failure zones associated with each cavity. For S = 3 m, the cavities behave almost independently, and the bearing capacity approaches values comparable to those of isolated cavities at similar depths.
- The comparative study between static and seismic conditions confirms that seismic loading consistently reduces the bearing capacity. This reduction is amplified by the presence of cavities, particularly when they are shallow and closely spaced.

Finally, the results of this chapter provide an important quantitative contribution to the understanding of the behavior of shallow foundations in the presence of underground cavities under seismic loading. The findings can serve as a basis for the development of safety guidelines and design recommendations for foundations in karstic or cavity-prone ground in seismically active regions.

General Conclusion

The present study examined the effect of underground cavities on the static and seismic bearing capacity of strip footings founded on cohesive–frictional soils. Particular attention was given to understanding how cavity characteristics influence the response of the soil–foundation system when subjected to both static and earthquake loading. To achieve this objective, theoretical considerations were combined with numerical analyses performed using PLAXIS 2D, followed by an extensive parametric investigation based on the Kobe earthquake record.

The results clearly indicate that underground cavities cannot be neglected in foundation design. Their presence modifies the stress distribution within the soil mass and leads to a reduction in bearing capacity. In many cases, the cavities also alter the shape and extent of the failure mechanism that develops beneath the footing. These effects become more pronounced when the cavity is located close to the footing or within the zone where failure is likely to occur.

The study showed that cavity geometry has an important influence on foundation performance. Parameters such as depth, eccentricity, inclination, and spacing were found to significantly affect the behavior of the footing. Shallow cavities generally produced more severe consequences than deeper ones, while cavities located directly beneath the footing generated the greatest reduction in bearing capacity. The position and configuration of the cavities therefore, represent key factors that should be carefully evaluated during site investigations and design procedures.

The numerical results also revealed that increasing the spacing between cavities leads to an improvement in the load-carrying capacity of the foundation system. As the cavities become more separated, their interaction decreases and the adverse effects on the surrounding soil are reduced. Furthermore, soils characterized by higher cohesion exhibited a better ability to resist both static and seismic loading. This behavior highlights the beneficial role of soil strength in limiting the negative influence of underground voids.

Another important observation concerns the parameter α. The analyses demonstrated that larger values of this parameter contribute to improving system stability and reducing the impact of cavities on foundation behavior. Although the degree of improvement varies according to the cavity configuration and soil properties, the overall trend remained consistent throughout the different cases considered in this work.

Under seismic loading, the response of the soil–foundation system became considerably more complex. Earthquake-induced stresses amplified the effects of underground cavities and resulted in additional reductions in bearing capacity compared with static conditions. These findings emphasize the need to account for seismic actions when designing foundations in regions where subsurface cavities may exist.

Finally, this research provides a detailed assessment of the interaction between strip footings, cohesive–frictional soils, and underground cavities under both static and seismic conditions. The findings improve the current understanding of cavity-related geotechnical problems and offer useful guidance for engineering practice. It is hoped that the outcomes of this work will contribute to the development of safer and more reliable foundation designs in areas affected by natural or man-made underground cavities.

Future studies may extend the present research by considering three-dimensional numerical analyses, different types of foundations, and a wider range of seismic records. Experimental investigations and field observations would also be valuable for validating the numerical findings and further improving the understanding of soil–foundation–cavity interaction under realistic conditions.

References

CHAPTER I

[1] Bowles, J.E. (1996). Foundation Analysis and Design (5th ed.). McGraw-Hill, New York.

[2] Frank, R., Cuira, F., & Burlon, S. (1999). Guide technique de conception et de dimensionnement des fondations. MELT-LCPC, Paris.

[3] Vesic, A.S. (1973). Analysis of ultimate loads of shallow foundations. Journal of the Soil Mechanics and Foundations Division, ASCE, 99(SM1), 45–74.

[4] Terzaghi, K. (1943). Theoretical Soil Mechanics. John Wiley & Sons, New York.

[5] Richards, R., Elms, D.G., & Budhu, M. (1993). Seismic bearing capacity and settlements of foundations. Journal of Geotechnical Engineering, ASCE, 119(4), 662–674.

[6] Meyerhof, G.G. (1963). Some recent research on the bearing capacity of foundations. Canadian Geotechnical Journal, 1(1), 16–26.

[7] Brinch Hansen, J. (1970). A revised and extended formula for bearing capacity. Bulletin 28, Danish Geotechnical Institute, Copenhagen, 5–11.

[8] Lunne, T., Robertson, P.K., & Powell, J.J.M. (1997). Cone Penetration Testing in Geotechnical Practice. Blackie Academic & Professional, London.

[9] Liao, S.S.C., & Whitman, R.V. (1985). Overburden correction factors for SPT in sand. Journal of Geotechnical Engineering, ASCE, 112(3), 373–377.

[10] Kramer, S.L. (1996). Geotechnical Earthquake Engineering. Prentice Hall, Upper Saddle River, NJ.

[11] Towhata, I. (2008). Geotechnical Earthquake Engineering. Springer, Berlin.

[12] Paolucci, R., & Pecker, A. (1997). Seismic bearing capacity of shallow strip foundations on dry soils. Soils and Foundations, 37(3), 95–105.

[13] Choudhury, D., & Subba Rao, K.S. (2005). Seismic bearing capacity of shallow strip foundations. Geotechnical and Geological Engineering, 23(4), 403–418.

[14] Cascone, E., & Casablanca, O. (2016). Static and seismic bearing capacity of shallow strip footings. Soil Dynamics and Earthquake Engineering, 84, 204–223.

[15] Steedman, R.S., & Zeng, X. (1990). The influence of phase on the calculation of pseudo-static earth pressure on a retaining wall. Géotechnique, 40(1), 103–112.

[16] Choudhury, D., & Nimbalkar, S.S. (2005). Seismic passive resistance by pseudo-dynamic method. Géotechnique, 55(9), 699–702.

[17] Ghosh, P. (2008). Upper bound solutions of bearing capacity of strip footing by pseudo-dynamic approach. Acta Geotechnica, 3(2), 115–123.

[18] Bellezza, I. (2014). A new pseudo-dynamic approach for seismic active soil thrust. Geotechnical and Geological Engineering, 32(2), 561–576.

[19] Pain, A., Choudhury, D., & Bhatt, S.K. (2016). Seismic passive earth resistance using modified pseudo-dynamic method. Earthquake Engineering and Engineering Vibration, 15(2), 281–295.

[20] Gerolymos, N., & Gazetas, G. (2006). Development of Winkler model for static and dynamic response of caisson foundations with soil and interface nonlinearities. Soil Dynamics and Earthquake Engineering, 26(5), 363–376.

[21] Gazetas, G., Anastasopoulos, I., Adamidis, O., & Kontoroupi, T. (2013). Nonlinear rocking stiffness of foundations. Soil Dynamics and Earthquake Engineering, 47, 83–91.

[22] Conti, R., Rovithis, E., Tamagnini, C., Anastasopoulos, I., & Gazetas, G. (2013). Centrifuge modelling and FEM analysis of dynamic response of shallow foundations. Géotechnique, 63(11), 911–925.

[23] CEN (2004). Eurocode 8: Design of Structures for Earthquake Resistance — Part 5: Foundations, Retaining Structures and Geotechnical Aspects. EN 1998-5:2004. European Committee for Standardisation, Brussels.

[24] ASCE/SEI 7-22 (2022). Minimum Design Loads and Associated Criteria for Buildings and Other Structures. American Society of Civil Engineers, Reston, VA.

[25] CGS (2003). Algerian Seismic Regulations RPA 99 — Version 2003. Centre National de Recherche Appliquée en Génie Parasismique, Algiers.

CHAPTER II

[1] Azam, G., Hsieh, C.W. and Wang, M.C. (1991). Performance of strip footing on stratified soil deposit with void.

[2] Badie, A. and Wang, M.C. (1984). Stability of spread footing above void in clay.

[3] Baus, R.L. and Wang, M.C. (1983). Bearing capacity of strip footing above void.

[4] Bell, F.G. (1992). Engineering Geology.

[5] Ford, D.C. and Williams, P.D. (2007). Karst Hydrogeology and Geomorphology.

[6] Hoek, E. and Brown, E.T. (1980). Underground Excavations in Rock.

[7] Keawsawasvong, S. (2021). Limit analysis solutions for spherical cavities in sandy soils under overloading.

[8] Kiyosumi, M., Kusakabe, O., Ohuchi, M. and Le Peng, F. (2007). Yielding pressure of spread footing above multiple voids.

[9] Kiyosumi, M., Kusakabe, O. and Ohuchi, M. (2011). Model tests and analyses of bearing capacity of strip footing on stiff ground with voids.

[10] Lavasan, A.A., Talsaz, A., Ghazavi, M. and Schanz, T. (2016). Behavior of shallow strip footing on twin voids.

[11] Lee, J.K., Jeong, S. and Ko, J. (2014). Undrained stability of surface strip footings above voids.

[12] Parise, M. and Gunn, J. (2007). Natural and Anthropogenic Hazards in Karst Areas.

[13] Waltham, A.C., Bell, F.G. and Culshaw, M.G. (2005). Sinkholes and Subsidence.

[14] Wang, M.C. and Badie, A. (1985). Effect of underground void on foundation stability.

[15] Wang, M.C. and Hsieh, C.W. (1987). Collapse load of strip footing above circular void.

[16] Zhou, H., Zheng, G., He, X., Xu, X., Zhang, T. and Yang, X. (2018). Bearing capacity of strip footings on c–phi soils with square voids.

[17] Yongyao, L., Gang, L., Shuai, Z., Wenbo, Y. and Yiwen, G. (2023). Numerical investigation on the damage evolution of karst caves under internal water pressure.